Steiner, Gerard Royal

MULTIPATH DETECTION AND COMPENSATION IN REFLECTIONS FROM DISTRIBUTED TARGETS

University of Washington PH.D. 1981

MULTIPATH DETECTION AND COMPENSATION IN REFLECTIONS FROM DISTRIBUTED TARGETS

by

Gerard Royal Steiner

A dissertation submitted in partial fulfillment
of the requirements for the degree of

Doctor of Philosophy

University of Washington

1981

Approved by Dean W. Sytle
(Chairperson of Supervisory Committee)

Program Authorized
to Offer Degree Electrical Engineering

Date September 16, 1981

Doctoral Dissertation

In presenting this dissertation in partial fulfillment of the requirements for the Doctoral degree at the University of Washington, I agree that the Library shall make its copies freely available for inspection. I further agree that extensive copying of this dissertation is allowable only for scholarly purposes, consistent with "fair use" as prescribed in the U.S. Copyright Law. Requests for copying or reproduction of this dissertation may be referred to University Microfilms, 300 North Zeeb Road, Ann Arbor, Michigan 48106, to whom the author has granted, "the right to reproduce and sell (a) copies of the manuscript in microfilm and/or (b) printed copies of the manuscript made from microfilm."

Signature Donald A Stein

Date September 8, 1981

TABLE OF CONTENTS

TABLE OF CONTENTS (Continued)

LIST OF FIGURES

LIST OF TABLES

ACKNOWLEDGMENTS

The author wishes to express sincere appreciation to Professors Lytle, Ehrenberg, and Damborg for their assistance in the preparation of this manuscript. Thanks also go to Dr. Keith Gardner, Mr. Werner Hueber, and Mr. Leroy Marquardt for providing me the opportunity and encouragement to complete this endeavor. Special thanks go to my wife, Marilyn, and children, Craig, Julie, and Scott. Their encouragement, assistance, and patience were vital.

CHAPTER 1

INTRODUCTION

For the past three decades, the effects of multiple transmission paths on received signals have received considerable attention. This interest has arisen in a broad spectrum of applications including telecommunications, radar, sonar, and seismology as a result of the frequent encounters in these fields with multiple path environments. While the exact problems to be solved with respect to multipath are not identical, they have considerable commonality. In general they include the detection of multipath, estimation of path characteristics, and determining the processing of received signals to reduce or minimize the effects of the multipath.

In this work, these questions will be examined for the cases of a sonar or radar system with a known transmitted signal examining an unknown distributed target. Since neither the transfer function corresponding to the multipath transmission nor that of the target backscatter are known, methods to separate their effects are central to the study. The suitability of several types of possible interrogating signals are investigated. In particular, attention will be given to the effects of multipath on the power spectra of sonar or radar target signatures. This specific question is of interest in the field of automatic radar target classification and provides the central focus for this work.

1.1 Historical Background

Many of the questions involved in detecting the presence of multiple transmission paths and estimating their parameters are the same or closely

related to that of detecting closely spaced targets. When one speaks of point targets, the similarity is greatest. Consequently, much of the work that has served as the basis for recent studies in multipath effects have stemmed from the findings of earlier works on the detection of multiple targets. An early work by Root[1] examined this problem from the viewpoint of maximum likelihood estimation and signal design. Nillson[2] has discussed various systems to estimate the number and distribution of multiple targets using a least square error criterion and introducing an additional loss function to penalize for errors in the estimated number of targets. Extension of his findings to the case of distributed targets of unknown characteristics is considered briefly.

More recently, D. T. Mangano[3] has made a comparison of three filtering schemes for signals transmitted through multipath. These were a delay filter, matched filter, and a frequency-inverse filter. He provided a comparison of the coefficient of variation of the estimates derived from each system. No additive noise was included in the investigation. Ehrenberg, Ewart, and Morris[4] have examined the case where the multipath returns are closely enough spaced that matched filter processing (or the other two mentioned above) is not sufficient to resolve the paths with the signals used. They present a processing scheme that provides maximum likelihood estimates of the individual path delays and amplitudes, as well as a criterion for determining the number of paths present. Their analysis includes the presence of Gaussian noise and compares the performance of the maximum likelihood processing with the results obtainable by matched filtering and inverse filtering at various noise levels. A considerable improvement in parameter estimation is demonstrated using maximum likelihood estimate.

G. Turin[5] has examined the use of spread-spectrum techniques for combating the effect of multipath in digital radio communications. This study considered a model that included the presence of a large number of multipaths that varied slowly with time. An adaptive receiver processor was discussed.

A further processing technique that has been applied to the extraction of multipath information, as well as recovery of the original signal, has been that of cepstrum processing that was first introduced by Bogert, Healy, and Tukey[6]. This technique, which will be discussed in detail in Chapter 2, was first applied in the area of seismology with considerable success. Recent works by Hassab and Boucher[7] and Kemerait and Childers[8] have examined the application of cepsturm processing to signal detection and estimation, and time delay estimation in the presence of noise, respectively. Both investigations were limited to signals known except for amplitude and arrival time.

1.2 Preview

The method examined for recognizing multipath transmission in echoes from a distributed or multireflector target centers around the application of modified cepstrum analysis. Therefore, in Chapter 2, the derivation of the power and complex cepstrums and their properties are presented. A review of some earlier applications of these techniques are included to provide additional insight into the attributes of this processing technique.

Chapter 3 considers the application of cepstrum techniques to the present problem. In particular, the expected differences between the effects of a distributed target in producing multiple echos and the effects of multiple returns due to a multipath environment are discussed.

In Chapter 4, the models for the target and multipath are developed as well as the techniques employed for signal generation, addition of noise, and filtering techniques. Various results obtained using a continuous wave (CW) signal are presented along with a description of the modifications to standard cepstrum methods that were required. The effects of pulse length, noise, and ship motion are examined.

Chapter 5 is devoted to comparing the performance of several different signal types in the multipath situation. An extended discussion of operation with a multiple frequency regime is included due to the relatively recent introduction of this signal type into the radar community[9]. The simulation results for each are presented along with observations on their relative strengths and weaknesses.

Chapter 6 presents the methods used to obtain corrections for the effects of multipath as determined by the earlier techniques. In particular, the use of the cepstrum to improve target signature spectral estimates corrupted by multipath is discussed. Interest in this area is motivated by current use of these spectral estimates in algorithms developed to determine ship type from radar signatures.

Chapter 7 summarizes the major contributions of this research and indicates the areas for further study that appear most interesting and productive.

1.3 Scope of Application

As indicated at the beginning of the introduction, the problem examined in this work is of interest in both the fields of sonar and radar. While there are many specific differences in these two fields, the similarities make the findings

applicable to both. To allow consistent specific simulations throughout, frequencies and propogation speeds appropriate to the sonar scenario have been used exclusively. Ocean specific attributes, such as the variation of absorption with frequency have not been included, however, so the results are equally applicable to radar.

CHAPTER NOTES

1. W. L. Root, "Radar Resolution of Closely Spaced Targets," IRE Trans. on Military Electronics." MIL-6 (1962): 197-204.

2. N. J. Nilsson, "On the Optimum Range Resolution of Radar Signals in Noise," IRE Trans. on Information Theory, IT-111 (1961): 245-253.

3. D. T. Mangano, "A Comparison of Three Schemes for Filtering Signals which have Propogated through a Random Multipath Medium," JASA 67(3) (1980): 842-852.

4. J. E. Enrenberg, T. E. Ewart, and R. D. Morris, "Signal-Processing Techniques for Resolving Individual Pulses in a Multipath Signal," JASA 63 (6) (1978): 1861-1865.

5. George L. Turin, "Introduction to Spread-Spectrum Anti-Multipath Techniques and Their Application to Urban Digital Radio," Proceedings of the IEEE 68(3) (1980): 328-352.

6. B. Bogert, M. Healy, and J. Tukey, "The Quefrency Alanysis of Time Series for Echoes," Spectral Analysis ed. M. Rosenblatt, pp. 209-243.

7. Joseph C. Hassab and Ronald Boucher, "A Probabilistic Analysis of Time Delay Extraction by the Cepstrum in Stationary Gaussian Noise," IEEE Trans. on Information Theory IT-22(4) (1976): 444-453.

8. R. C. Kemerait and D. G. Childers, "Signal Detection and Extraction by Cepstrum Techniques," IEEE Trans. on Information Theory IT-18(6) (1972): 745-756.

9. M. Prickett and C. C. Chen, "Principles of Inverse Synthetic Aperture Radar (ISAR) Imaging," IEEE EASCON Record (1980).

CHAPTER 2

CEPSTRUM ANALYSIS

2.1 Power Cepstrum

In a paper[1] with a quite novel title ("The Quefrency Alanysis of Time Series for Echoes: Cepstrum, Pseudo-Autocovariance, Cross-Cepstrum, and Saphe Cracking"), Bogert, Healy, and Tukey introduced the concepts of cepstrum processing in 1962. Their methods include doing many things in the frequency domain that had been traditionally common to the time domain and vice versa. For this reason, and to emphasize the similarity and differences between their treatment and spectral analysis, they introduced a collection of new terms that were formed by reversing the first syllable of the corresponding term from spectral analysis. Hence such terms as cepstrum (spectrum), alanysis (analysis), and liftering (filtering) were used in their writing. Of these, only the term cepstrum has persisted in general usage. Accordingly, this is the only of their terms that will be used consistently here. Where the differences in the usage of other terms differs from their normal connotation due to the reversed domains, the difference will be explicitly noted when required to avoid confusion.

The power cepstrum was originally defined as the power spectrum of the log power spectrum of the original time series, i.e.,

$$\tilde{C}(t) \triangleq \left| F\{\log(\Phi(\omega))\} \right|^2 \qquad (1)$$

where

$$F(f(t)) = \int_{-\infty}^{\infty} f(t)e^{-j\omega t}\, dt \ . \tag{2}$$

$\Phi(\omega)$ is the power spectrum of the original time series and log is the natural logarithm. It is more convenient, however, to define the cepstrum as the square root of this quantity. That is

$$C(t) = | F\{\log(\Phi(\omega))\} | . \tag{3}$$

This might better be called the amplitude cepstrum, but the term power will be retained for consistency with the literature.

As will be seen, this function has a large value at times corresponding to the delay between multiple arrivals of a single signal.

To examine this property of the cepstrum and see its usefulness in determining the presence of multiple echos, it is most instructive, following the example of Bogert, et. al.[2], to analytically obtain the power cepstrum for a single signal with one, time delayed, attenuated replica added to it. If the original signal is y(t), and the replica is delayed τ, and has a relative amplitude α, then the total received signal z(t) is given by

$$z(t) = y(t) + \alpha y(t - \tau) \ . \tag{4}$$

Then if the power spectrum of the original signal, y(t), is $\Phi_y(\omega)$, then the power spectrum of the composite signal is

$$\begin{aligned}\Phi_z(\omega) &= | F(y(t)) + F(y(t))\alpha\exp(-j\omega\tau) |^2 \\ &= | F(y(t)) |^2 \cdot | 1 + \alpha\exp(-j\omega\tau) |^2 \\ &= \Phi_y(\omega) \cdot (1 + 2\alpha\cos\omega\tau + \alpha^2) \end{aligned} \tag{5}$$

Then, taking the natural logarithm of Φ_z, we have

$$\log\Phi_z(\omega) = \log\Phi_y(\omega) + \log(1 + 2\alpha\cos\omega\tau + \alpha^2). \tag{6}$$

For $|a| < 1$ we have the series expansion

$$\log(1+a) = a - \frac{a^2}{2} + \frac{a^3}{3} - \cdots , \tag{7}$$

so considering the case where $\alpha^2 << 1$ applying the expansion of equation (6) to the final log term in equation (5) and ignoring terms in α^2 we have

$$\log\Phi_z(\omega) = \log\Phi_y(\omega) + 2\alpha\cos\omega\tau \quad . \tag{8}$$

Then the cepstrum is obtained by taking the Fourier transform of this expression yielding

$$C(t) = |F\{\log\Phi(\omega)\}| + \alpha\delta(t-\tau) + \alpha\delta(t+\tau) \quad . \tag{9}$$

Thus the power cepstrum produces a function that consists of the cepstrum of the original signal ($|F \log \Phi(\omega)|$) and impulse functions at the times, $\pm\tau$, corresponding to the second arrival. Furthermore, the height of this spike is proportional to the relative amplitude of this second arrival.

If the second arrival has a magnitude, α , that is not sufficiently small to ignore the higher order terms, the log expansion can still be successfully employed. In this case, starting from equation (6), we have

$$\begin{aligned}
\log\Phi_z(\omega) &= \log\Phi(\omega) + \log\{(1+\alpha^2)(1+\tfrac{2\alpha}{1+\alpha^2}\cos\omega\tau)\} \\
&= \log\Phi(\omega) + \log(1+\alpha^2) + \tfrac{2\alpha}{1+\alpha^2}\cos\omega\tau - \left(\tfrac{2\alpha}{1+\alpha^2}\right)^2 \tfrac{1}{2}\cos^2\omega\tau \cdots \\
&\approx \log\Phi(\omega) + \log(1+\alpha^2) + \tfrac{2\alpha}{1+\alpha^2}\cos\omega\tau - \tfrac{1}{4}\left(\tfrac{2\alpha}{1+\alpha^2}\right)^2 \\
&\quad + \tfrac{1}{4}\left(\tfrac{2\alpha}{1+\alpha^2}\right)^2 \cos 2\omega\tau + \cdots
\end{aligned} \tag{10}$$

Therefore, it is seen that increasing the amplitude of the second return raises the average level of the cepstrum peak at τ and adds peaks that are of lesser amplitudes at multiples of τ. While this diminishes the simplicity associated with a low level second return ($\alpha << 1$), the power cepstrum can, nonetheless, be clearly interpreted since the multiple peaks produced are simply related in their respective delay times.

As additional returns are added to the received signal, the complexity of interpreting the cepstrum is increased, but the position of the peaks is still related to the relative delays of the individual returns. A look at the case of three returns demonstrates the relative positioning. Here the received signal is

$$z(t) = y(t) + \alpha_1 y(t-\tau_1) + \alpha_2 y(t-\tau_2) \; ; \tag{11}$$

if $(\alpha_1^2 + \alpha_2^2) << 1$, then

$$\begin{aligned} |\Phi_z(\omega)|^2 \simeq |\Phi(\omega)|^2 (1 &+ \alpha_1^2 + \alpha_2^2 + 2\alpha_1 \cos\omega\tau_1 \\ &+ 2\alpha_2 \cos\omega\tau + 2\alpha_1\alpha_2 \cos(\tau_1 - \tau_2)) \\ &+ 2\alpha_2 \cos\omega\tau_2 + 2\alpha_1\alpha_2 \cos\omega(\tau_1 - \tau_2)). \end{aligned} \tag{12}$$

This produces peaks in the cepstrum that correspond to the difference betweeen delay times, as well as to the individual delay times themselves. As the amplitude of the echoes increases and higher order terms must be retained, peaks in the cepstrum are introduced at multiples of the various delays and delay differences.

Increasing the number of discrete arrivals further produces no further qualitative differences in the composition of the cepstrum. The output contains an increased number of peaks. As the number of arrivals increases, the amplitude of individual peaks is, in general, reduced.

2.2 Complex Cepstrum

The complex cepstrum, as described by Kemerait and Childers[3], is analogous to the power cepstrum with the phase information retained. This, as will be shown, allows inverse processing to return to the original time domain after filtering of the cepstrum. The relations and effects of the processes are most clearly presented by examining the simple two return case, with second arrival low amplitude, that was discussed in the preceding section. This parallels the analysis presented by Kemerait and Childers[3] and that of Oppenheim, Schafer, and Stockham[4].

Returning to the simple reflection model, we have

$$z(t) = y(t) + \alpha y(t-\tau) \ . \tag{4}$$

Taking the Fourier transform yields

$$Z(\omega) = Y(\omega)(1 + \alpha e^{-j\omega\tau}) \ . \tag{13}$$

Instead of taking the logarithm of the power spectrum as was done previously, here the logarithm is taken of the Fourier transform as given by (13). Since the argument of the logarithm is complex, care will be required throughout the processing to properly maintain the phase relations. Taking the logarithm

$$\log(Z(\omega)) = \log(Y(\omega)) + \log(1+\alpha e^{-j\omega\tau}) \ , \tag{14}$$

then applying the expansion for log (1 + a) and retaining the higher order terms gives

$$\log(Z(\omega)) = \log(Y(\omega)) + e^{-j\omega\tau} - \frac{\alpha^2}{2} e^{-j\omega 2\tau} + \frac{\alpha^3}{3} e^{-j\omega 3\tau} - \cdots \ . \tag{15}$$

The complex cepstrum is then the inverse Fourier transform,

$$\hat{C}(z(t)) = F^{-1}(\log(z(t))) = \hat{C}(y(t)) + \alpha\delta(t-\tau) - \frac{\alpha^2}{2}\delta(t-2\tau) + \frac{\alpha^3}{3}\delta(t-3\ ) - \cdots \ . \tag{16}$$

Thus, the resulting complex cepstrum of z(t) consists of the complex cepstrum of the original signal, y(t), plus a decaying series of spikes occurring at multiples of the second return delay time. This is seen, then, to provide information equivalent to that available from the power cepstrum. Its relation to the power cepstrum is the same as that of the Fourier transform to the normal power spectrum in that it retains phase information. All the information of the original signal remains in the complex cepstrum and may be recaptured by following an inverse sequence of operations.

Before discussing the filtering operations on the complex cepstrum and subsequent inverse operations to return to the original time domain (the cepstrum is also a time series, but will be referred to as the cepstral domain to distinguish it from the normal time domain), one aspect of obtaining the complex cepstrum requires mention. Since the Fourier transform of the original time series will be complex, the logarithm of equation (14) is a complex logarithm. Unless corrected, the resulting phase of the logarithm will be given as a principal value, i.e., multiples of 2π will be removed. As a result, the phase of the logarithm will be discontinuous because of possible 2π "errors" between consecutive samples. This, in turn, would produce incorrect results when taking the inverse Fourier transform that yields the complex cepstrum. Since the phase is actually varying in a continuous manner, the discontinuities, introduced by the 2π jumps resulting from using the principal value, would produce false high frequency (quefrency) components into the cepstrum. To avoid this error, the phase of the complex logarithm must be "unwrapped" prior to the final transformation. This is done by adding or subtracting multiples of 2π to the originally modulo 2π phase values. The addition is done so as to

make the phase a continuous function, i.e., to remove the 2 discontinuities. As long as the phase varies relatively slowly between consecutive samples in a digital implementation, the "unwrapping" is straightforward.

Figures 1, 2, and 3 illustrate the process. Figure 1 shows the original phase values for the first 21 samples of the logarithm of a hypothetical signal. Discontinuities can be seen between values 5 and 6 and between values 14 and 15. Figure 2 shows the unwrapped phase values. To prevent the complex cepstrum from being dominated by the phase term of the logarithm, The linear trend present in the values of Figure 2, is then removed by adjusting the phase values to lie the same distances above and below a zero-mean line that they lay above the solid line of Figure 2. This line could be generated as a least squares linear fit to the "unwrapped" phase values. The final phase sequence is shown in Figure 3. This last step of removing the linear phase trend is required only if the phase has a large slope. Since the phase is the imaginary portion of the complex logarithm, it would control the magnitude of the logarithm in this case. This creates a problem in a system with finite computational accuracy. It should be noted that zeroes in the spectrum introduce unremovable discontinuities.

The primary purpose of using the complex cepstrum is that it may be filtered to allow recovery of a particular portion of the original time series through the inverse transformations. Three filters ("lifters" in the transposed terminology of Bogert, Healy, and Tukey) have received frequent application[5]. They are the "comb," "short-pass," and "long-pass" filters. Comb filtering is achieved by zeroing the cepstrum at the points that are due to the echo(es) arrival(s). Usually the location of these points is first determined from the power cepstrum due to its superior performance in this regard. These zeroed

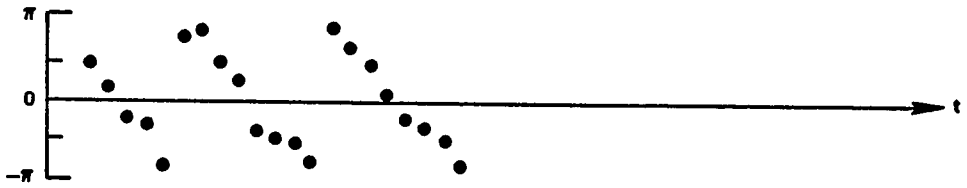

Figure 1. Example of Original Phase of Complex Logarithm.

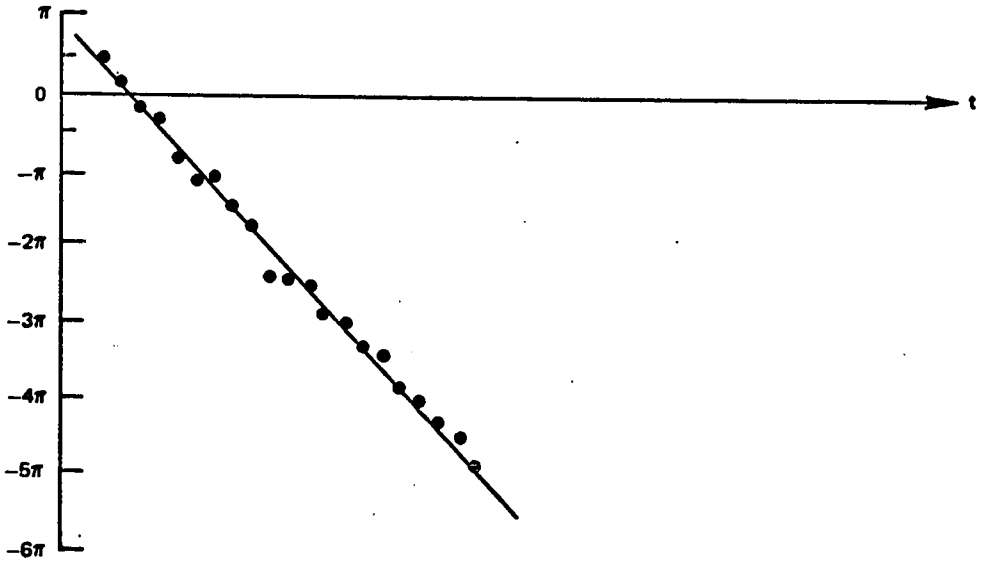

Figure 2. Unwrapped Phase of Complex Logarithm.

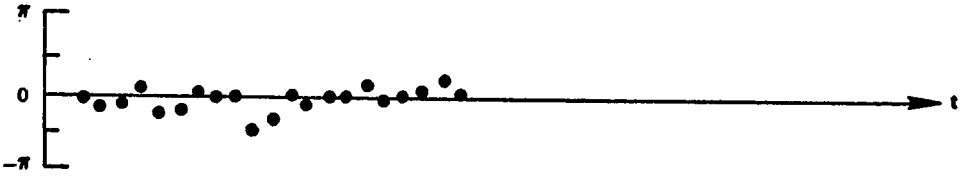

Figure 3. Unwrapped Phase of Complex Logarithm with Linear Trend Removed.

values are then replaced by averaging the adjacent points in the complex cepstrum. This procedure substantially removes the echo when the inverse transformation is applied.

A second filtering, short-pass filtering (cf. normal low-pass filtering), also removes the effects of the echoes. Here the values of the complex cepstrum greater than that of the shortest delay are set to zero. This method can only be applied when the delays are great enough that substantial portions of the cepstrum due to the first arrival are not also zeroed. If this is not the case, the original signal can be substantially distorted. This procedure is essentially an extension of the comb filter in that the portion of zeroing that actually affects the desired echo removal is precisely the zeroing at those points where the comb filter acted. An advantage of the short-pass filter is that, with multiple echoes, all but the first arrival will be removed with a single operation.

The third filter, the long-pass, is just the reverse of the short-pass and has the opposite effect. Here the values of the complex cepstrum before the second arrival spike are zeroed. This has the effect of removing the original arrival and leaving only the echoes. As was the case with the "short-pass," its success without excessive distortion requires that the first and second arrivals be well separated.

The complex cepstrum has not been used in this investigation. Suggestions for its application in future work will be discussed briefly.

2.3 Effects of Noise

Much of the early modeling work in cepstrum analysis has been done in a noise-free environment. This was the case for the derivation of the cepstrum characteristics in the preceeding section. A brief comment on the effects of

noise on the performance of the cepstrum will provide the background for subsequent discussions.

Hassab and Boucher have conducted a detailed analysis[6] on the effects of stationary Gaussian noise. They demonstrate that the performance cannot be predicted by the total signal-to-noise ratio across the whole bandwidth processed. Kenerait and Childers[7] have reported an 18 dB signal-to-noise threshold for successful signal extraction. With certain signals and certain forms to the noise spectrum, Hassab and Boucher have shown considerably better performance possible without smoothing.

The effects of the noise are two-fold. First, the noise statistically reduces the amplitude of the echo peak at the delay time in the cepstrum. Secondly, the noise tends to introduce additional cepstrum outputs that obscure the delay spike, especially with the reduced level of this spike. Since the magnitude of the delay spike depends on the relative amplitude of the second arrival signal; the performance of the cepstrum at any particular signal-to-noise ratio will be affected by this relative amplitude. This will be discussed in greater detail in Chapter 4.

CHAPTER NOTES

1. B. Bogert, M. Healy, and J. Tukey, "The Quefrency Alanysis of Time Series for Echoes," Spectral Analysis ed. M. Rosenblatt, pp 209-243.

2. Ibid.

3. R. C. Kemerait and D. B. Childers, "Signal Detection and Extraction by Cepstrum Techniques," IEEE Trans. on Information Theory IT-18(6) (1972): 745-756.

4. Ibid.

5. Alan V. Oppenheim and Ronald W. Schafer, Digital Signal Processing, pp. 490-527.

6. Kemerait and Childers, 745-756.

7. Joseph C. Hassab and Ronald Boucher, "A Probabilistic Analysis of Time Delay Extraction by the Cepstrum in Stationary Gaussian Noise," IEEE Trans. on Information Theory IT-22(4) (1976): 444-453.

8. Kemerait and Childers, 745-756.

CHAPTER 3

CEPSTRUM PROCESSING WITH DISTRIBUTED TARGET AND MULTIPATH

The salient feature of the problem being considered, detecting and estimating multipath parameters in the reflected signal from a distributed target, is the similarity between the effects of the distributed or multireflector target and the effects of multipath. Both of these processes are characterized as producing weighted sums of delayed replicas of the transmitted signal. The effects on the successful processing of real data that deviates from this modeling will be discussed in Chapter 4. It is noteworthy at this point, however, to note the most apparent simplifications incorporated in the characterization. The total target may well have a more complex transfer function than can be accurately depicted as the composite of displaced point reflectors. Similarly, it is not clear that the nondispersive characterization of the multipath channels is adequate for all applications of interest. These two factors, however, are not expected to greatly affect the results obtained.

3.1 Target Model

The target has been modeled as a one-dimensional array of point reflectors of various cross-sections, i.e., producing various amplitude reflections. No distortion of the pulse is generated during the reflection process in this model. (Target motion will be mentioned briefly in Chapter 4.) With a transmitted pulse x(t), the composite reflected signature is then given by

$$y(t) = \sum_{i=1}^{N} \alpha_i x(t-\tau_i) \tag{17}$$

where α_i and τ_i are the amplitude and delay, respectively, associated with the ith reflector. Throughout the study forty and fifty point reflectors have been used.

By appropriate selection of the α_i's and τ_i's, signals were obtained that resembled actual radar and sonar signatures of various vessels. No attempt was made to actually characterize any specific target. However, care was taken to insure that the target models portrayed the variety of signatures found in real reflections. For example, targets were generated having single and multiple major scattering centers.

3.2 Multipath Model

The multipath model closely parallels that of the distributed target in that it too is a weighted, delayed summing process. If the single path return from a target is y(t), then the multipath echo is given by

$$z(t) = \sum_{j=1}^{M} \beta_j y(t-\sigma_j) \tag{18}$$

where β_j and σ_j are the amplitudes and delays associated with each path. As with the target model, no dispersive effects have been introduced.

3.3 Combined Model

When both a multipoint target and multipath transmission are present, the resulting signal is obtained by combining equations (17) and (18) to give

$$z(t) = \sum_{j=1}^{M} \sum_{i=1}^{N} \alpha_i \beta_j \, x(t-\tau_i-\sigma_j) \qquad (19)$$

The signals studied have been limited to the frequency range of zero to eight kilohertz to allow sampling at 20 kilohertz without aliasing. The received signals have been generated using equation (18) directly, computing the value of z(t) analytically at each sampling time. Pulse lengths greater than or equal to four milliseconds were used.

3.4 Differences Between the Target and Multipath Effects

The key to the method applied to separate target and multipath effects, through the power cepstrum, rests on the differences in the values of N and M in equation (19). As stated in the preceeding section, the targets considered have been modeled as forty or fifty point reflectors. Modeling efforts for actual targets indicate that even larger numbers of reflectors are often essential to faithfully reproduce real target signatures. In contrast, in many scenarios of interest in active target recognition systems, the presence of only two or three paths of significant energy is typical. It is clear that, in the two way transmission case under consideration, only certain values for the number of paths are possible. In the case that there are two paths to the target, there will be three arrivals present: one going and returning by the direct path, the second--one way direct, one way refracted (this represents two indistinguishable cases), and the third--going and returning by the refracted path. (The changes in target signature with vertical aspect have been ignored in this one-dimensional model. This simplification is a good approximation in many cases of interest where the difference in vertical arrival angle between the paths is

small.) Similarly, the case where there are three separate paths leads to six arrival times.

In section 2.1, it was shown (equation (12)) that adding a third arrival increased the number of spikes in the cepstrum (speaking of the low amplitude case) from one to three. To understand the cepstrum's ability to distinguish between the contributions to the received signal (equation 19) that are due to the multireflector target and those due to multipath, it is necessary to examine, in greater detail, the cepstrum of the target (without multipath) as a function of the number of reflectors.

The target reflection is (equation 19)

$$y(t) = \sum_{i=1}^{N} \alpha_i x(t-\tau_i)$$

Then the power spectrum is

$$\Phi_y(\omega) = \Phi(\omega) \left| \sum_{i=1}^{N} \alpha_i \exp(j\omega\tau_i) \right|^2 \tag{20}$$

Expanding the last factor,

$$\Phi_y(\omega)=\Phi(\omega)\left(\sum_{i=1}^{N} \alpha_i \exp(j\omega\tau_i)\right)\left(\sum_{k=1}^{N-1} \alpha_k \exp(-j\omega\tau_k)\right) . \tag{21}$$

Regrouping and applying a trigonometric identity yields

$$\Phi_y(\omega)=\Phi(\omega) \sum_{i=1}^{N} \alpha_i^2+\left(\sum_{i=k+1}^{N} \sum_{k=1}^{N-1} 2\alpha_i\alpha_k \cos(\tau_i-\tau_k)\right) . \tag{22}$$

Then

$$\log\Phi_y(\omega)=\log\Phi(\omega)+\log\left(\sum_{i=1}^{N}\alpha_i^2+\sum_{i=k+1}^{N}\sum_{k=1}^{N-1}2\alpha_i\alpha_k\cos\omega(\tau_i-\tau_k)\right) \quad (23)$$

Factoring the argument of the last logarithm yields

$$\log\Phi_y(\omega)=\log\Phi(\omega)+\log\left(\sum_{i=1}^{N}\alpha_i^2\left(1+\frac{\sum_{i=k+1}^{N}\sum_{k=1}^{N-1}2\alpha_i\alpha_k\cos\omega(\tau_i-\tau_k)}{\sum_{i=1}^{N}\alpha_i}\right)\right) \quad (24)$$

$$=\log\Phi(\omega)+\log\sum_{i=1}^{N}\alpha_i^2+\log(1+q)$$

where

$$q=\frac{\sum_{i=k+1}^{N}\sum_{k=1}^{N-1}2\alpha_i\alpha_k\cos\omega(\tau_i-\tau_k)}{\sum_{i=1}^{N}\alpha_i} \quad (25)$$

In order to proceed with a series expansion of log (1 + q), it is necessary for $|q| < 1$. To examine the expectation of this requirement being met, assume that the α_i are independent, identically distributed random variables with unspecified probability density function, $p(\alpha)$. Furthermore, let

$$\sigma_{ik} = (\omega(\tau_i-\tau_k)) \text{ modulo } 2\pi \quad (26)$$

and assume that σ_{ik} has a uniform distribution from zero to 2π. Since $\omega(\tau_i - \tau_K)$ is, in general, much greater than one and there is no reason to expect any relation between the spacing of reflectors and the frequency of the signal; this is a very reasonable assumption.

In this case, the following is true for q.

$$E(q)=E\left\{\frac{\sum_{i=k+1}^{N}\sum_{k=1}^{N-1}2\alpha_i\alpha_k\cos\omega(\tau_i-\tau_k)}{\sum_{j=1}^{N}\alpha_j^2}\right\} , \tag{27}$$

where E is the expected value. Since α_i, α_k, and σ_{ik} are independent, (25) may be factored and the summations brought outside the expected value giving

$$E(q)=\sum_{i=k+1}^{N}\sum_{k=1}^{N-1}E\left\{\frac{2\alpha_i\alpha_k}{\sum_{j=1}^{N}\alpha_j^2}\right\}E(\cos\sigma_{ik}) . \tag{28}$$

Since

$$E(\cos\sigma_{ik}) = \int_0^{2\pi}\cos\sigma d\sigma=0 , \tag{29}$$

the expected value of q is also zero.

Since each is zero mean, the variance is given simply by the second moment.

$$\mathrm{Var}(q)=E(q^2)$$

$$=E\left\{4\sum_{m=1}^{N-1}\sum_{n=m+1}^{N}\sum_{i=1}^{N-1}\sum_{k=i+1}^{N}\left[\frac{\alpha_i\alpha_k\alpha_m\alpha_n}{\sum_{n=1}^{N}\sum_{l=1}^{N}\alpha_l^2\alpha_n^2}\right]\cos\sigma_{ik}\cos\sigma_{mn}\right\} \tag{30}$$

Since the α's and σ's are independent, the expectation of the product may be factored into the product of the two expectations yielding

$$\mathrm{Var}(q)=4\sum_{m=1}^{N-1}\sum_{n=m+1}^{N}\sum_{i=1}^{N-1}\sum_{k=i+1}^{N}E\left\{\frac{\alpha_i\alpha_k\alpha_m\alpha_n}{\sum_{n=1}^{N}\sum_{l=1}^{N}\alpha_l^2\alpha_n^2}\right\}\cdot \tag{31}$$

$$\cdot E(\cos\sigma_{ik}\cos\sigma_{mn})\ .$$

For $i \neq m$ or $k \neq n$, σ_{ik} and σ_{mn} are independent. In this case

$$E(\cos\sigma_{ik}\cos\sigma_{mn})=0\ . \tag{32}$$

For $i = m$ and $k = n$,

$$E(\cos\sigma_{ik}\cos\sigma_{mn})=E(\cos^2\sigma_{ik})=\frac{1}{2}\ . \tag{33}$$

Consequently, using equations (32) and (33) to simplify equation (31)

$$\mathrm{Var}(q)=2\sum_{i=1}^{N-1}\sum_{k=i+1}^{N}E\left[\frac{\alpha_i^2\alpha_k^2}{\sum_{l=1}^{N}\sum_{n=1}^{N}\alpha_l^2\alpha_n^2}\right] \tag{34}$$

For N large,

$$E\left[\frac{\alpha_i^2\alpha_k^2}{\sum_{l=1}^{N}\sum_{h=1}^{N}\alpha_l^2\alpha_h^2}\right]\cong\frac{\left[E(\alpha_i^2)\right]^2}{E\left\{\sum_{l=1}^{N}\sum_{h=1}^{N}\alpha_l^2\alpha_h^2\right\}}=\frac{\alpha^{2\,2}}{\sum_{l=1}^{N}\sum_{h=1}^{N}\overline{\alpha^{2\,2}}}=\frac{1}{N^2} \tag{35}$$

Then

$$\mathrm{Var}(q)=2\sum_{i=1}^{N}\sum_{k=i+1}^{N-1}\frac{1}{N^2}=2N\frac{N-1}{2}\frac{1}{N^2}\cong 1 \tag{36}$$

Then by the central limit theorem, q will approach a normal distribution with zero mean and variance one as n increases. This result, which was independent of the actual distribution of the target reflection coefficients (to the accuracy of the approximation made), indicates that the series expansion for logarithm may be applied in approximately seventy percent of the cases. The results obtained throughout this work indicate that, with the target reflector distributions used, the expansion is valid in essentially all cases.

When the condition on q is met, applying the series expansion for log (1 + q) to equation (23) yields

$$\log \Phi_y(\omega)=\log \Phi(\omega)+\log \sum_{i=1}^{N} \alpha_i^2 + \frac{\sum_{k=1}^{N} \sum_{i=k+1}^{N} 2\alpha_i \alpha_k \cos\omega(\tau_i-\tau_k)}{\sum_{i=1}^{N} \alpha_i^2} \tag{37}$$

The higher order terms that have been omitted must be retained for accurate representation when the $\alpha_i \alpha_k / \Sigma \alpha_i^2$ are not sufficiently small as might be the case if there were only two strong reflections and the rest weak. The effect of these terms will be mentioned shortly, but, they will be omitted in the present discussion with no effects on the conclusions reached.

The cepstrum may now be calculated as

$$C(\Phi_z)=C(\Phi)+C_0+\frac{\sum_{k=1}^{N} \sum_{i=k+1}^{N} 2\alpha_i \alpha_k \delta(t-(\tau_i-\tau_k))}{\sum_{i=1}^{N} \alpha_i^2} \tag{38}$$

where

$$C_0 = \log \sum_{j=1}^{N} \alpha_j^2 \tag{39}$$

The first term in equation (38) is the cepstrum of the transmitted signal; the second is the result of the $\log \sum_{j=1}^{N} \alpha_j^2$ term in equation (37) and produces a spike at time zero in the cepstrum. The third term provides the desired result.

As additional echoes are added, new peaks are introduced into the cepstrum as previously stated. More significantly, equation (38) shows that as new reflections are added, the amplitude of existing peaks is reduced. This is a result of the $1/\sum_{j=1}^{N} \alpha_j^2$ factor. The reduction will be greatest if the magnitude of the additional reflection is comparable or greater to that of the earlier reflections. (The reduction will actually constantly increase with an increase in the added reflection. If it is much larger than earlier reflections, however, the new peak that it introduces will become the largest and further increases will lead to an increase in the height of the largest cepstral peak.) In the case where all the reflections are of the same amplitude, the height of individual peaks in the cepstrum will vary inversely with n.

Figure 4 demonstrates this characteristic of the cepstrum for one series of target models. The ordinate on this and subsequent plots of cepstral values is a unitless quantity obtained from the evaluation of equation (3). The computation was done digitally using a 1024 point Fast Fourier Transform with the International Mathematics and Statistics Library subroutine FFT 2C and the natural logarithm. From the definition of the cepstrum, it is seen that the magnitude scaling of the input does not affect the results since the logarithmic operator reduces this scaling to an additive constant. The final Fourier Transform is affected only in its first, or constant amplitude value which is of no interest in the present study.

A fifty point target was generated; power cepsta were then computed for the various number of reflections indicated in the figure. This was done by selecting that number of points from the original fifty and then generating the corresponding echo. As additional reflectors were added, all reflectors used previously were retained. This allowed individual peaks to be followed from

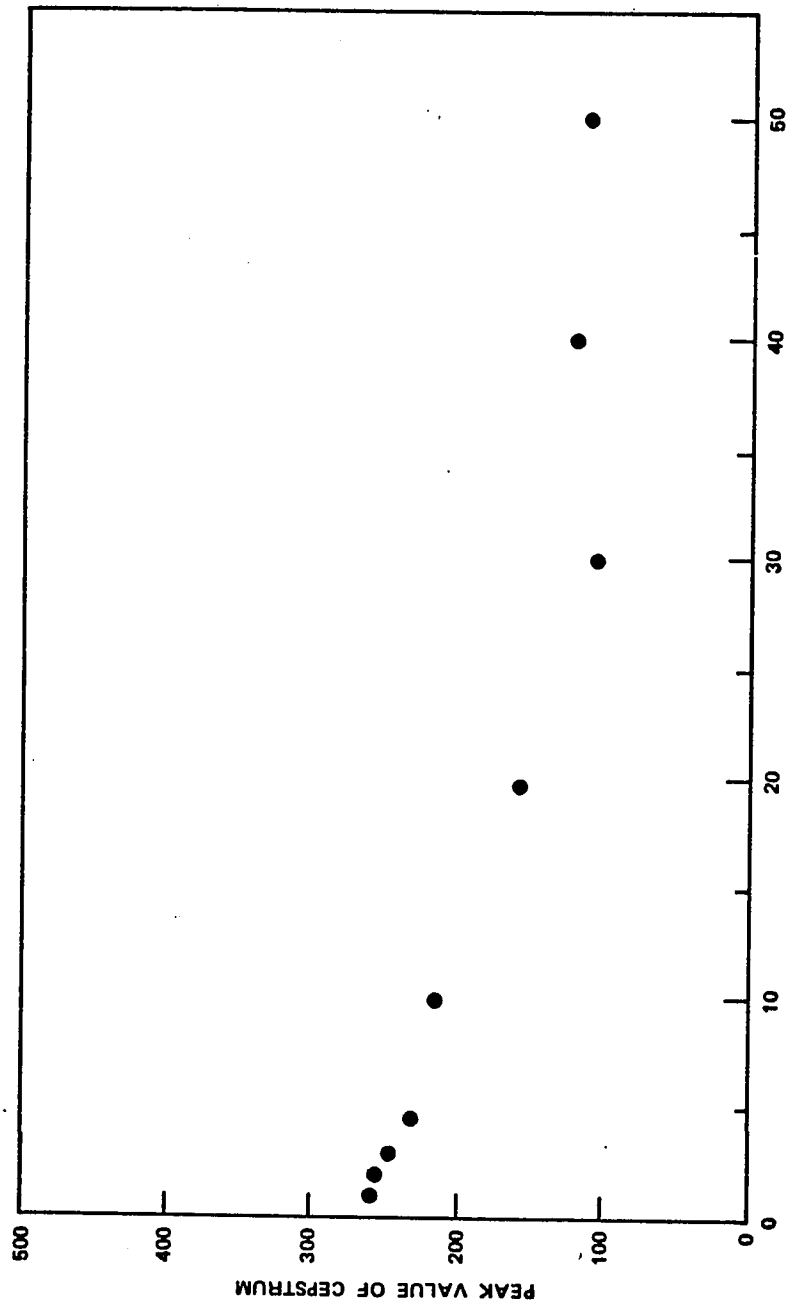

Figure 4. Peak Value of a Target's Cepstrum as it Varies with the Number of Reflectors.

cepstrum to cepstrum. The figure shows the peak value of the cepstrum for each number of reflectors computed. The decrease with n is clearly evident. Note that there is a slight increase in the peak cepstrum going from thirty to forty reflectors. Equation (38) indicates that this is possible only if the forty point peak is a new one. This was indeed the case. The peak that provided the 110.2 maximum in the thirty point target cepstrum was reduced to 97.5 when the ten new points were added to the reflector.

Figures 5 and 6 show the first 160 points of the cepstrum for the case of ten and fifty point reflectors, respectively. The transition from a small number of relatively large peaks to a larger number of smaller peaks is readily apparent. The reduction of the peak at 98 (4.9 millisecond delay) is most noticeable. As expected, the number of distinct peaks is less than the n(n - 1)/2 indicated by equation (36). This results from the relative magnitude of the actual α_i used in the model and the possibility of several peaks either coinciding or being sufficiently close to each other. Another constrinuating factor is that many of the time differences are greater than that plotted in these figures.

Before proceeding to introduce multipath into the echo examined by the cepstrum, a brief return to the question of higher order terms in equation (37) is needed to close the target cepstrum discussion. Comparing equations (10) and (38) it is clear that the next group of terms in equation (38) will be

$$-\sum_{i=k+1}^{N}\sum_{k=1}^{N}\frac{1}{2}\frac{4\alpha_i^2\alpha_k^2}{\left(\sum_{j=1}^{N}\alpha_j^2\right)^2}\cos^2\omega(\tau_i-\tau_k)$$

$$=-\sum_{i=k+1}^{N}\sum_{k=1}^{N}\frac{1}{2}\left\{\frac{2\alpha_i\alpha_k}{\sum_{j=1}^{N}\alpha_j^2}+\frac{4\alpha_i\alpha_k}{\sum_{j=1}^{N}\alpha_j^2}\cos(\omega(\tau_i-\tau_k))\right\} \qquad (40)$$

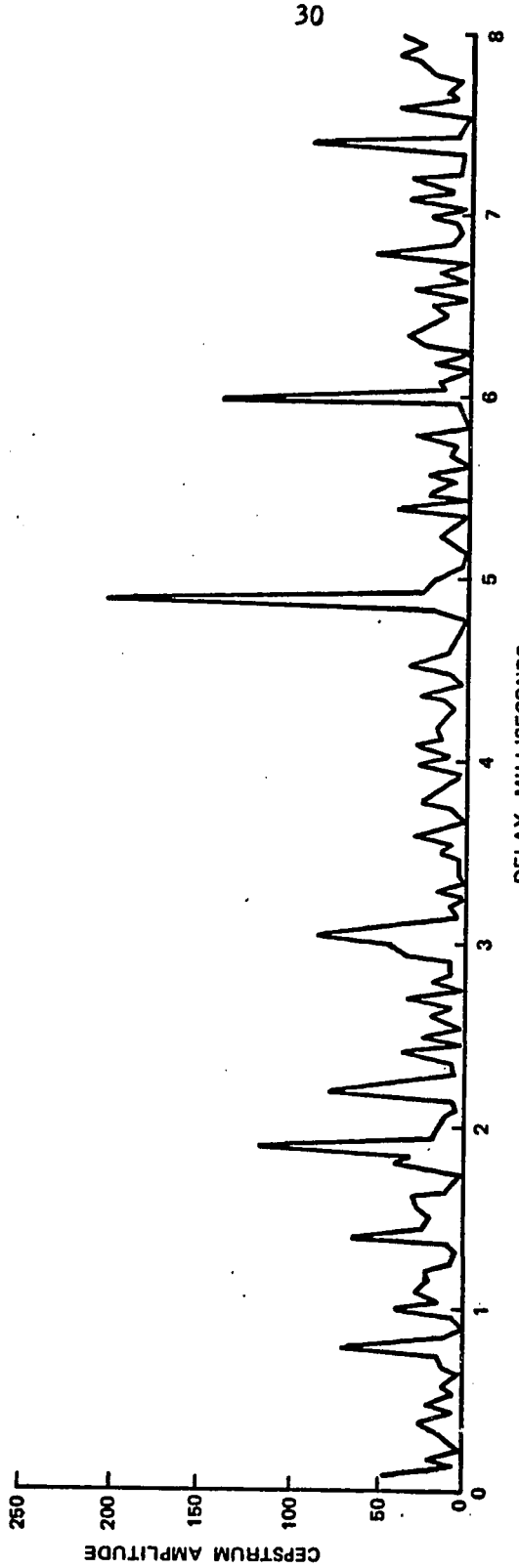

Figure 5. Target Cepstrum with a Ten Point Target.

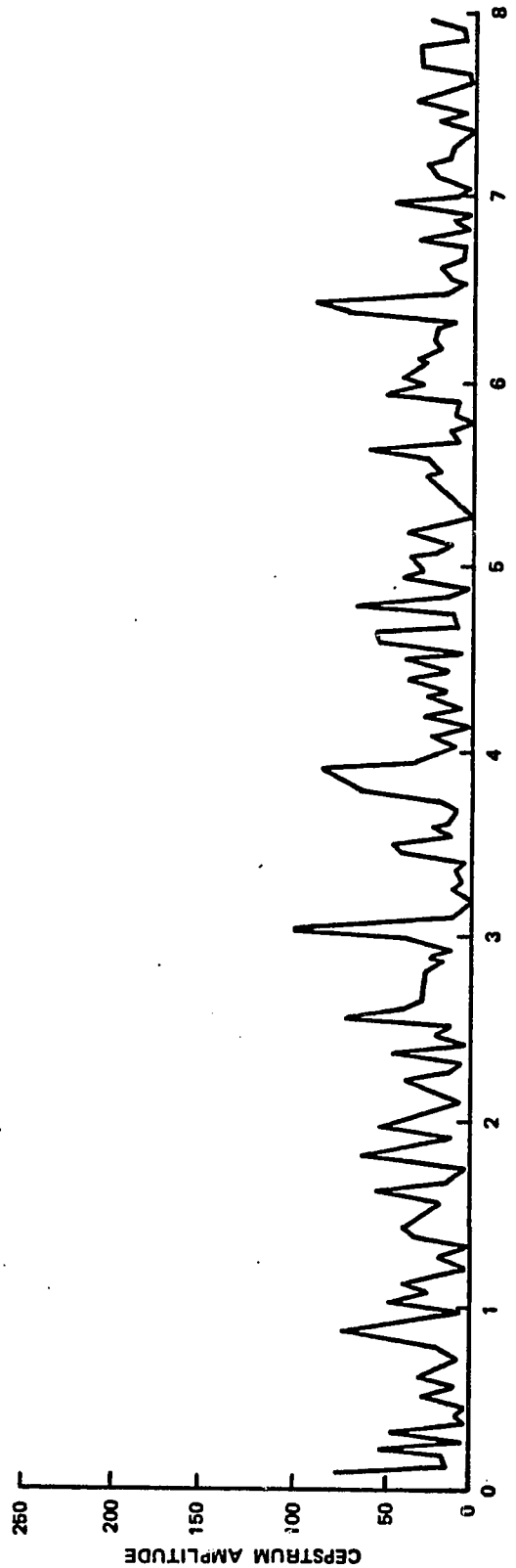

Figure 6. Target Cepstrum with a Fifty Point Target.

This increases the value of the cepstrum at time zero and produces additional spikes at times twice the original time differences. These spikes will have a lower amplitude than the spikes at the original time differences and, therefore, will not change any of the peak amplitude conclusions.

Although no bounds have been obtained on the height of the cepstral peaks for a multipoint target reflection, it has been shown that adding reflectors increases the number of peaks and reduces their individual magnitudes. This provides the basis for looking at the effects of multipath on the cepstrum and a comparison with the distributed target effects.

As stated at the beginning of the chapter, the characteristic that distinguishes the multipath from target effects is the much lower number of replications that result from multipath. In the case of the target signature, the number of repeated arrivals (N) is conservatively modeled as being fifty. As seen from the denominator of equation (39), the large number of arrivals reduces the corresponding cepstrum peak associated with each. The smaller number (M) of arrivals of the entire target signature due to multipath results in a smaller value for the denominator of equation (39). This leads to a much smaller reduction in peak heights in peaks due to multipath. Using the expression for the multipath distortion, equation (18),

$$z(t) = \sum_{j=1}^{M} \beta_j y(t-\sigma_j) \ , \tag{18}$$

consider the case where M = 3. This will be referred to as the two path case, although it leads to three arrivals in the bi-directional transmission scenario as previously discussed.

This provides a power cepstrum

$$C(\Phi_z)=C(\Phi_y)+C_0+\beta_1\beta_2\delta(t-(\sigma_2-\sigma_1))$$
$$+\beta_1\beta_3\delta(t-(\sigma_3-\sigma_1))+\beta_2\beta_3\delta(t-(\sigma_3-\sigma_2)) \tag{41}$$

for β_1, β_2, β_3 the total transmission coefficient for each round trip circuit. Then with γ_1 and γ_2 the one-way coefficients for the one-way paths with delays τ_1 and τ_2, respectively, then β_1, β_2, β_3, σ_1, σ_2, and σ_3 may be expressed in terms of the former quantities as

$$\begin{aligned}
\beta_1 &= \gamma_1^2 \\
\beta_2 &= 2\gamma_1\gamma_2 \\
\beta_3 &= \gamma_2^2 \\
\sigma_1 &= 2\tau_1 \\
\sigma_2 &= \tau_1+\tau_2 \\
\sigma_3 &= 2\tau_2 \,.
\end{aligned} \tag{42}$$

Then substituting equations (42) into equation (41) gives for the multipath cepstrum:

$$C(\Phi_z)=C(\Phi_y)+C_0+2\gamma_1^2\gamma_2^2\delta(t-(\tau_1+\tau_2))$$
$$+\gamma_1^2\gamma_2^2\delta(t-2(\tau_2-\tau_1))+2\gamma_1\gamma_2^3\delta(t-(\tau_2-\tau_1)) \,. \tag{43}$$

Again, with no loss of generality, consider the transmission coefficient of the direct path to be unity, i.e., $\gamma_1 = 1$, and its arrival delay zero, i.e., $\tau_1 = 0$. This is simply a scale change and an axis translation. The equation (43) becomes

$$C(\Phi_z)=C(\Phi_y)+C_0+2\gamma_2\delta(t-\tau_2)+\gamma_2^2\delta(t-2\tau_2)+2\gamma_2^3\delta(t-\tau_2)$$
$$=C(\Phi_y)+C_0+2\gamma_2(1+\gamma_2^2)\delta(t-\tau_2)+\gamma_2^2(t-2\tau_2) \quad . \qquad (44)$$

It has already been shown that the peaks of $C(\Phi y)$ have been reduced by a factor $1/\sum_{i=1}^{N}\alpha_i^2$. Therefore, for appropriate values of γ_2^2, it is expected that the cepstral peak at τ_2 will be larger than the peaks of $C(\Phi y)$. This assertion will be examined quantitatively in the next two chapters. This will be done by examining cepstra from modeled signatures with and without multipath to determine appropriate thresholds to separate the two. Figure 7 shows a typical resultant cepstrum. The peak at 4.5 milliseconds delay corresponds to the actual multipath arrival time.

3.5 Additional Comments on Processing

In the preceding section, one observed aspect of the cepstrum from a multipoint target with multipath has not been discussed. This term occurs explicitly or implicitly in every cepstral expression presented. It is the cepstrum of the transmitted pulse. This is $C(\Phi)$ in equation (39) and is thereby included in equations (5) and (43) through $C(\Phi y)$.

If nothing is done to remove this term, it, in fact, dominates the cepstrum in the case of the ideal, square continuous wave pulse thus far considered. This is demonstrated in Figure 8. Here the transmitted pulse is two milliseconds long and the primary multipath delay is three milliseconds. The large peaks at four, eight, and twelve milliseconds are at multiples of the pulse length and are

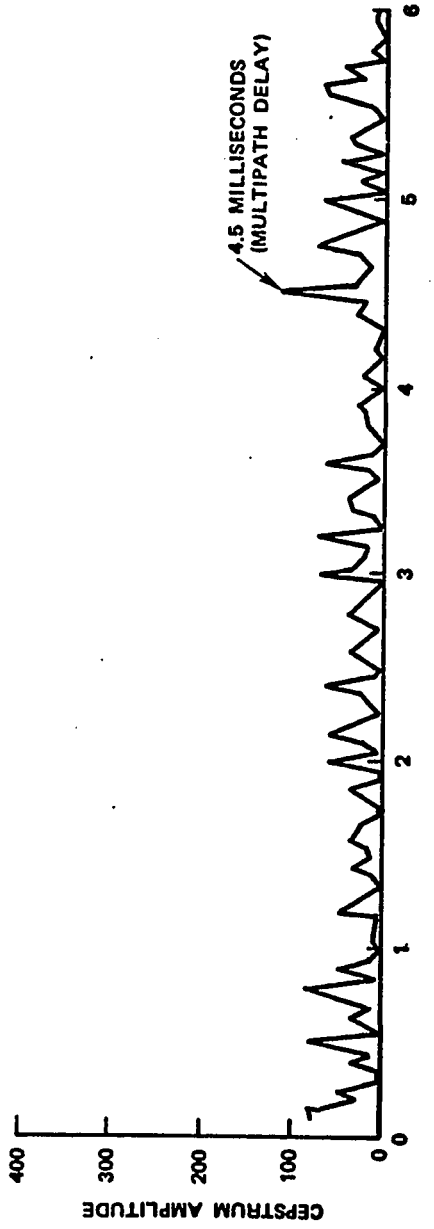

Figure 7. Signature Cepstrum with Multipath.

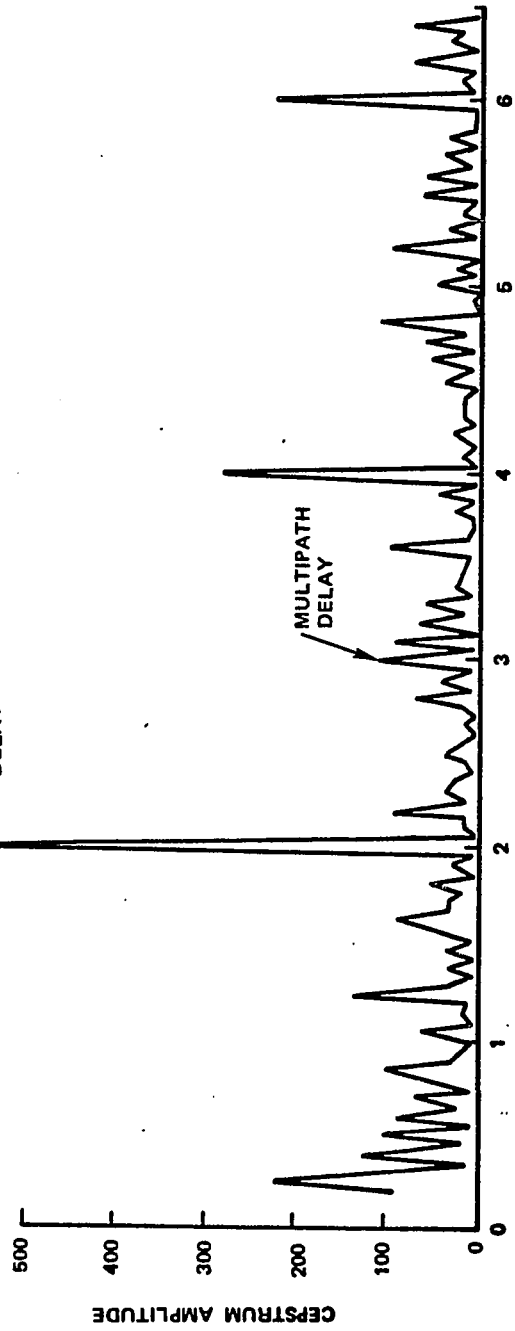

Figure 8. Cepstrum with Pulse Length Peaks.

seen to completely dominate the cepstrum. The small peak corresponding to the multipath delay at three milliseconds is much smaller that the peaks associated with the pulse length and is, in fact, less than the peak at 1.25 milliseconds. This peak, as well as the other low peaks present, are presumably due to the cepstrum of the target signature.

The origin of these large peaks from the transmitted pulse length may be understood by considering the pulse as the sum of two continuous waves with a phase difference of π and modulated by step functions at $t = 0$ and $t = \tau$pulse length, respectively. Thus, the transmitted pulse is the sum of two time delayed replicas of the same signal. The previous discussions indicate that since the two signals are of equal energy, their cepstral spikes will be of large magnitude. As well, this equal energy predicts the slow decay in amplitudes of peaks at multiples of the delay (pulse length).

This aspect of the cepstrum has entered into earlier uses of the cepstrum, although generally in less dramatic ways. In their original paper, Bogert, Healy, and Tukey discussed it[1]. In their simulations they used colored noise for the basic signal. The effects of the basic signal spectrum were virtually removed by "long-pass" filtering of the spectrum (the cepstral equivalent of normal high-pass filtering). Since in the present application, the transmitted signal is known, its effects may be more completely removed. This is done by subtracting the log spectrum of the transmitted signal from the log spectrum of the received signal before taking the final Fourier transform. This is directly analogous to the pre-whitening filter.

The effects of the operation are seen in Figure 9. This shows the cepstrum for the same received signal used in Figure 8, but this time with the

Figure 9. Cepstrum with Pulse Spectrum Removed

filtering included. Not only have the peaks associated with the pulse length been removed, but the multipath spike has been greatly enhanced.

This filtering of the received spectrum has been included in all power cepstrum analysis that is presented.

CHAPTER NOTES

1. B. Bogert, M. Healy, and J. Tukey, "The Quefrency Alanysis of Time Series for Echoes," Spectral Analysis ed M. Rosenblatt, pp. 209-243.

CHAPTER 4

PERFORMANCE IN MULTIPATH DETECTION

In Section 3.2, the distinction between the effects of a multiple reflector target and those of a multipath transmission media was derived and illustrated. As indicated there, a bound cannot be obtained on the values in the cepstrum introduced by each process. On the other hand, the results indicate that the peak cepstral value can be expected to be greater in those cases where a small number of multipaths are present. In this chapter, further results are presented to quantify this expectation. Where it is possible and productive to do so, analytic relations are presented to establish aspects of the distinction; however, a major portion of the findings are the result of a simulation study. Consequently, the universality of the conclusions is dependent on the accuracy of the simulation. The attributes of the simulation which result from the previously described target and multipath models, as well as the particular signals and processing are described in the next section.

4.1 Simulation Characteristics

The numerical model used for the targets was given by equation (17) and consists of a spatially distributed collection of ideal point reflectors. This introduces several approximations that deviate from reality. The first of these is that the actual process producing the reflection from a physical target is not ideal in the sense that one would not expect its transfer function (for a single reflector) to be completely uniform over the frequency range of interest. Related to this is the probability that many reflecting objects are not

adequately modeled as occurring at a point, but are actually distributed over a region. Both of these deviations, however, tend to make the model more demanding than reality. Each will cause the target reflection to look more like the sum of time delayed versions of the same signal than it actually is. Thus, from these considerations, it is reasonable to expect that the cepstral peaks from an actual measured single path target echo will be less than those obtained in the model.

A third drawback of the modeling stems from the adequacy of the selected distribution of reflectors in the model targets to resemble ship or submarine reflectors. Having allowed the target to consist of many point reflectors are the particular distributions in location and amplitude suitable to model actual targets encountered with sonar and radar? Although a relatively small number of targets (15) have been examined, an attempt has been made to cover a wide range of possibilities. Some were selected with only a few major scatterers and many smaller ones. Others have a larger number of strong scatterers. Still others consist of a fairly low range of individual point scattering strengths. The cepstral peak values, on the other hand, show a rather small variation from target to target, as will be seen in following sections. The modeled targets are plotted in Figure 10 by magnitude and location of their reflectors.

Another criticism that has been raised against cepstral analysis of modeled data is that of not sufficiently band limiting the modeled echo[1]. This is somewhat the case here in that the transmitted pulse was strictly time limited, i.e., set identically to zero outside the pulse length time windows. Consequently, the signal is not band limited and some aliasing occurs with the sampling. This aliasing is quite small, however, and should not greatly affect

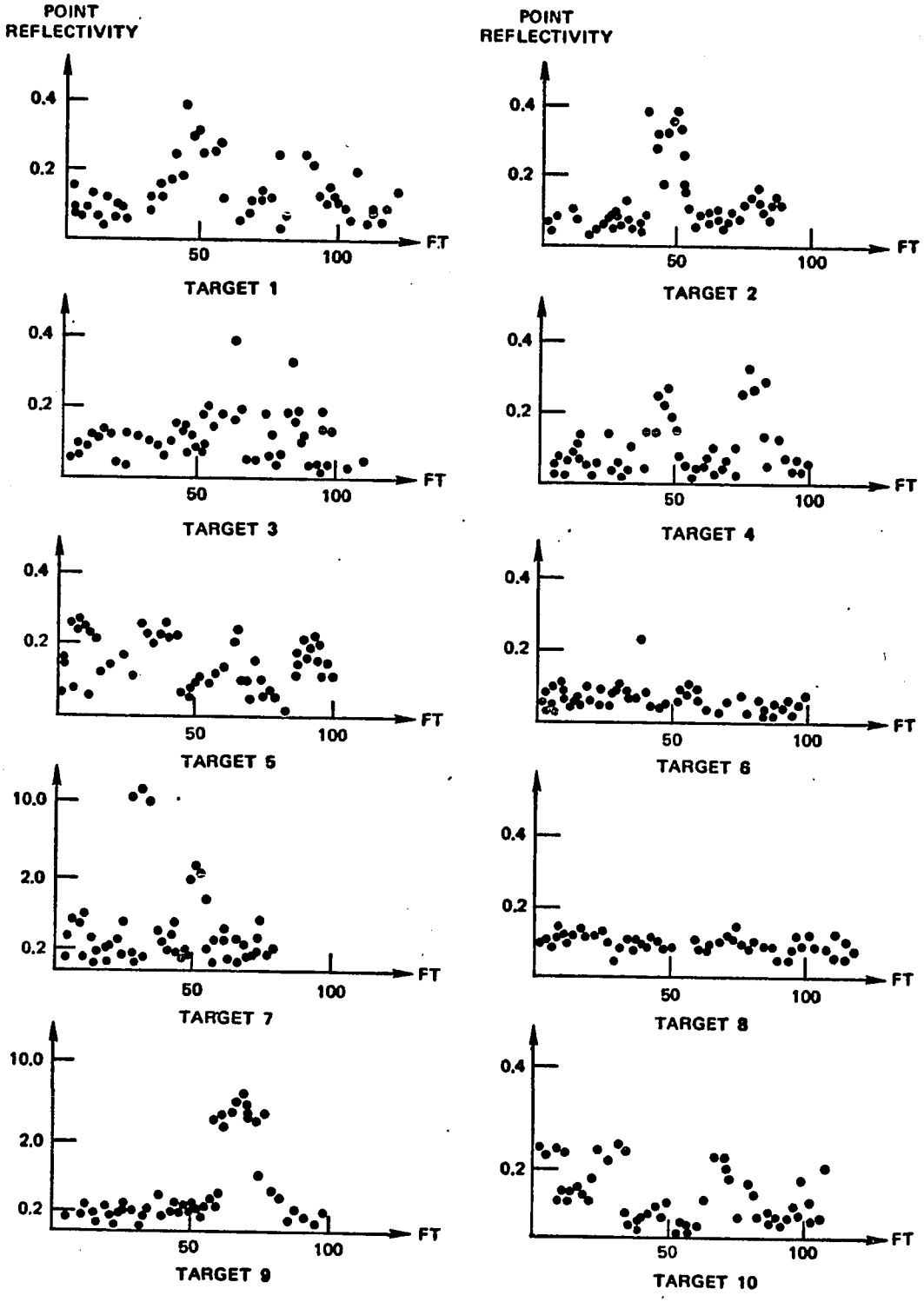

Figure 10. Amplitude and Location of Target Reflectors.

the results. A further consideration that diminishes the effects of time limiting the pulse is that additive noise was included in all simulated echoes. The results obtained with varying noise levels again reduce concern that significant artifacts have been introduced by time limiting the signal.

The first two approximations of the target model have counterparts in the multipath model. No dispersion nor frequency variation of the transmissivity via a single path have been included. This is quite realistic in radar applications where the total spectrum of a given signal is generally quite narrow in comparison to its center frequency. In the sonar signal this is less justified since the 3 dB bandwidth of many signals considered here exceeds an octave. On the other hand, if the transfer function along each of multiple paths has nearly the same shape, their effects will tend to cancel in the final cepstral result.

4.2 Theoretical Expectations for the Cepstral Behavior as a Function of Pulse Length

In Chapters 2 and 3, the fundamental relations of the cepstrum of a distributed target's echo and the received signal with multipath were derived. In this section, these relations are examined in greater detail with particular attention to the effects of the signal pulse length (or bandwidth) in the case of a modulated continuous wave (CW) pulse and the amount of noise present. Other signal types will be considered in the following chapter.

The interest of this work is in identifying the presence of multipath in a sonar or radar target echo and reducing its effects on the power spectrum of the received signal. The investigation is, therefore, centered around determining thresholds that will adequately separate cepstral peaks due to multipath

from those due to the multireflector target or noise and the performance of these thresholds with multipath strength. The basis for expecting such a threshold to exist has been established in Section 3.4. As indicated in that discussion, the exact thresholds, appropriate to a practical problem, will be dependent on the true character of the targets of interest. As will be seen, however, a wide variation in target characteristics produces sufficiently limited variations in the peak cepstrum value (when no multipath occurs) to make this investigation meaningful.

First consider the effects of pulse length on the multipath cepstrum. The resolution of individual returns of a signal is traditionally related to the reciprocal of the signal bandwidth. In the case of a CW pulse, this resolution is simply the pulse length of the signal. The resolution is best obtained by matched filtering when the events are separated by more than a pulse length. Ehrenberg, et. al.[2], have shown that when the events are not distinct in the sense of having this minimum separation, then matched filtering is no longer optimal. They have obtained substantially improved resolution by application of maximum likelihood estimators.

In the present context of a multireflector target, such a technique could be applied to determine each reflector echo by each path. In the absence of noise and with sufficient processing bandwidth, this approach could distinguish each arrival to any desired accuracy, although the computational demands would quickly become excessive (e.g., with a 50 reflector target and two paths, there would be 150 arrivals - requiring a search in 150-dimensional space).

As has been illustrated in Chapter 3, the cepstrum produces the desired delays in a single iteration. From equation (9), the cepstrum, in the case of a weak multipath, is

$$C(t) = F\log\Phi(\omega) + \alpha\delta(t-\tau)+\alpha\delta(t+\tau) \qquad (9)$$

While this expression contains an approximation resulting from the truncation of the log (1 + a) expansion, the dissociation of the cepstral multipath peak at from the spectrum of the transmitted pulse is complete. That is, the position of the multipath (delay) peak is seen to be located precisely at τ regardless of the form of $\Phi(\omega)$, the spectrum of the basic signal. This is equally true in the case of the echo from a distributed target. If the $\Phi(\omega)$ in the equation is the spectrum of the target reflection, the position and magnitude of the peak due to the multipath arrival is independent of the spectrum of the target echo. Since the cepstrum of the target reflection may be non-zero at this delay, the actual peak height at the multipath delay will be affected by the target.

There is, of course, no guarantee that the cepstrum of the reflected signal itself does not have a significant magnitude at the delay time corresponding to this peak. The computed cepstrum will be the sum of these two values. Thus, the height of the cepstral peak will vary from target to target and with the magnitude of the multipath arrival. The contributions due to a specific target and multipath configuration will be independent of the signal characteristics as seen from equations (38) and (41). The signal characteristics appear only in the additive term $C(\Phi)$ which has been removed in processing. By the same token, however, the cepstrum of the target echo can be seen to be the sum of the contributions of the multiple reflector echoes and the cepstrum of the transmitted signal itself. As was indicated earlier, since this is a known

component of the cepstrum, it has been subtracted from the cepstrum in the present calculations. Thus, the results are expected to be independent of pulse length in the case where there is no noise in the signal. Some results from the model study are shown below in Table 1.

Note that in the digital evaluation the infinite height of a delta-function is reduced to N/2 where N is the number of points in the discrete Fourier transform. In the cases presented in this work, 1024 point transforms were used so the delta function height is 512.

	Multipath Strength = .2, = 2.3 msec.			Multipath Strength = .3, = 5.7 sec.		
Pulse length	4 ms	8 ms	16 ms	4 ms	8 ms	16 ms
Targ 4	183	183	182	291	346	318
Ave of targets 4, 5, 6 & 9	205	210	213	291	292	313

Table 1. Cepstrum Values Corresponding to Multipath Delay for Two Multiple Cases and Three Pulse Lengths.

While these values show some variation, they are consistent with the conclusions drawn above. There is a slight increase in the average amplitude with pulse length, but it is less than the standard deviation of the results at each pulse length. Note also that the average heights of the multipath cepstral peak for the two multipath amplitudes have approximately the same value as predicted by equation (9).

One effect of pulse length on cepstral processing that has not been discussed above is the presence of noise. As one would expect, the perform ance, indeed the very capability, of the power cepstrum in detecting multipath,

is affected by the signal-to-noise ratio. As Hassab and Boucher (10) have shown this is dependent not only on the total signal-to-noise ratio, but by the signal-to-noise ratio across the spectrum. With the use of a longer CW pulse, and consequently a narrower bandwidth, the received signal may be more narrowly band pass filtered. This provides a higher signal-to-noise ratio for the resulting signal and, consequently improvement in performance. It should be noted that this does not increase the expected height of the multipath cepstral peak, but rather decreases the probability of the peak being destroyed by noise as will be seen in the subsequent section.

4.3 Multipath Detection in the Presence of Noise

Noise has several related effects on the ability of the power cepstrum to locate the time of multiple signal arrivals and to provide an estimate of their relative amplitudes. These effects have been extensively investigated by Hassab and Boucher in the case of multiple arrivals of a simple, known signal. Their analysis and findings will be summarized here for completeness. The analysis will then be adapted to apply to the case of a distributed target and the particular CW signals being used in this investigation. The model results will then be compared with the theoretical predictions and the noise effects examined quantitatively.

The following derivations closely follow the work of Hassab and Boucher.[3] Starting with the two arrival signal of equation (4) and adding a noise signal, n(t), the total received signal becomes

$$z(t) = y(t)+ay(t-\tau)+n(t) \tag{45}$$

from which follows the power spectrum

$$\Phi_z(\omega)=|Z(\omega)|^2=(1+a^2)\Phi y(\omega)+2a\Phi y(\omega)\cos\omega\tau+\phi_n(\omega)+\phi_c(\omega) \qquad (46)$$

where

$$\phi_n(\omega) = |N(\omega)|^2 \qquad (47)$$

and

$$\phi_c(\omega)=(1+\alpha e^{-j\omega\tau})Y(\omega)N^*(\omega)+(1+\alpha e^{j\omega\tau})Y^*(\omega)N(\omega) \ , \qquad (48)$$

which includes the cross terms in $Y(\omega)$ and $N(\omega)$.

For future convenience let

$$\phi_c(\omega) = 2(\alpha_1 N_r+\alpha_2 N_i) \ , \qquad (49)$$

where

$$\alpha_1 = Y_r+a(\cos\omega\tau)Y_r+a(\sin\omega\tau)Y_i \qquad (50)$$

and

$$\alpha_2 = Y_i + a(\cos\omega\tau)Y_i - a(\sin\omega\tau)Y_r \quad . \tag{51}$$

The subscripts r and i denote the real and imaginary parts, respectively. Then equation (48) may be rewritten

$$\begin{aligned}\phi_c(\omega) = 2\{&(Y_r + a\cos(\omega\tau)Y_r + a\sin(\omega\tau)Y_i)N_r \\ &+ (Y_i + a\cos(\omega\tau)Y_i - a\sin(\omega\tau)Y_r)N_i\} \quad .\end{aligned} \tag{52}$$

Equation (46), after considerable manipulation, may be expressed as

$$\begin{aligned}\Phi_z(\omega) = \left[(1+a^2)\,\Phi_y(\omega)\right]\left[1+\frac{\phi_n(\omega)}{(1+a^2)\,\Phi_y(\omega)}\right]\cdot \\ \cdot\left[1+\gamma B(\omega)\cos\omega\tau\right]\left[1+\Psi_c(\omega)\right] \quad ,\end{aligned} \tag{53}$$

where

$$\gamma = \frac{2a}{1+a^2} \quad , \tag{54}$$

$$B(\omega) = \frac{1}{1+\dfrac{\phi_n(\omega)}{(1+a^2)\Phi_y(\omega)}} \quad , \tag{55}$$

$$\Psi_c(\omega) = \frac{\phi_c(\omega)}{\alpha_1^2+\alpha_2^2+\phi_n(\omega)} \quad , \tag{56}$$

and

$$\alpha_1^2+\alpha_2^2 = \Phi_y(\omega)(1+a^2+2a\cos\omega\tau) \quad . \tag{57}$$

Continuing in the evaluation of the cepstrum, the log of equation (53) yields

$$\log\Phi_z(\omega) = \log\{(1+a^2)\Phi_y(\omega)\}+\hat{\phi}(\omega) + \log\{1+\gamma B(\omega)\cos\omega\tau\}+\hat{\Psi}(\omega), \tag{58}$$

where

$$\hat{\phi}(\omega) = \log\left\{1+\frac{\phi_n(\omega)}{(1+a^2)\Phi_y(\omega)}\right\}, \tag{59}$$

$$\hat{\Psi}(\omega) = \log\{1+\Psi_c(\omega)\} \, , \tag{60}$$

and

$$B(\omega) = e^{-\hat{\phi}(\omega)} \quad . \tag{61}$$

The effects of the additive noise are imbedded in $\hat{\phi}(\omega)$, $B(\omega)$, and $\Psi(\omega)$ and at this point, due to the nonlinear operations applied, are both additive and multiplicative. In particular, note that the information carrying $\cos \omega t$ is modulated by $B(\omega)$, a noise related factor.

Continuing, the series expansion for log (1 + x) is applied to the last two terms of equation (58) yielding

$$\log\Phi_z(\omega)=\log\{(1+a^2)\Phi_y(\omega)\}+\hat{\phi}(\omega)+\sum_{k=0}^{\infty}(-1)^{k-1}M_k(\omega)\cos k\omega\tau + \sum_{n=1}^{\infty}\frac{(-1)^{n+1}}{n}\{\Psi_c(\omega)\}^n \tag{62}$$

with

$$\begin{aligned} M_0(\omega) &= \frac{(\gamma B(\omega))^2}{4}+\frac{3(\gamma B(\omega))^4}{32}+\frac{5(\gamma B(\omega))^6}{96}+ \ldots \\ M_1(\omega) &= \gamma B(\omega)\pm\frac{(\gamma B(\omega))^3}{4}+\frac{(\gamma B(\omega))^5}{8}+ \ldots . \\ &\ldots\ldots \end{aligned} \tag{63}$$

These coefficients M_i are obtained by converting the $\cos^n \omega\tau$'s to expressions of the form $a_1 \cos \omega\tau + a_2 \cos 2\omega\tau \ldots + \cos n\omega\tau$ by standard trigonometric identities.

Next, as in Chapter 2, the power cepstrum is obtained by taking the Fourier transform of equation (62).

Consider the interesting (and limiting) case where there is low signal-to-noise and the echo is weak. In this case, simplification of equation (63) is achieved by ignoring the higher order terms. Then the transform of equation (62) is given by

$$C(t) = F\{\log\Phi_z(\omega)\} = F\{\log(1+a^2)\Phi_y(\omega)\} + F\{\hat{\phi}(\omega)\} + \frac{\gamma b(t-\ )}{2} + \Psi_c(t) \quad , \tag{64}$$

where

$$b(t) = F\{B(\omega)\cos\omega\tau\} \tag{65}$$

To proceed, consider, as previously modeled, the case of stationary, gaussian noise,

$$p\{n(t)\} = \frac{1}{\sqrt{2\pi}\,\sigma}\exp\{-n^2(t)/2\sigma^2\} \quad . \tag{66}$$

Then with $N_r(\omega)$ and $N_i(\omega)$ the real and imaginary parts of $N(\omega)$, their joint

probability density function is

$$p\{N_r(\omega),N_i(\omega);\omega \text{ fixed}\} \tag{67}$$
$$=\exp\{-[\Phi_n(\omega)]^{-1}(N_r^2(\omega)+N_i^2(\omega))\}/\pi\Phi_n(\omega)$$

and

$$\phi_N(\omega) = N_r^2(\omega)+N_i^2(\omega) \tag{68}$$

is chi-square distributed so

$$p\{\phi_n(\omega)\} = \begin{cases} \frac{1}{\Phi_n(\omega)}\exp(-\phi_n(\omega)/\Phi_n(\omega)) & \phi_n \geq 0 \\ 0 & \phi_n < 0 \end{cases} \tag{69}$$

The noise is passed through the logarithmic operation (see equation (59)) so that

$$\phi_n(\omega) = (1+a^2)\Phi_y(\omega)\{e^{\hat{\phi}(\omega)}-1\} \quad . \tag{70}$$

The probability density function for $\hat{\phi}(\omega)$ is[4]

$$p\{\hat{\phi}(\omega)\} = \begin{cases} \chi(\omega)\exp\{\hat{\phi}(\omega)-\chi(\omega)(\exp\hat{\phi}(\omega)-1)\} & \hat{\phi}(\omega)\geq 0 \\ 0 & \hat{\phi}(\omega)<0 \end{cases} \tag{71}$$

where

$$\chi(\omega) = (1+a^2)\frac{\Phi_y(\omega)}{\Phi_n(\omega)} \quad , \tag{72}$$

which is the spectral signal-to-noise ratio scaled by $(1 + a^2)$.

Similarly, the probability distribution function of $B(\omega)$ may be derived from the transformation

$$\phi_n(\omega) = (1+a^2)\Phi_y(\omega)\left\{\frac{1}{B(\omega)} - 1\right\} \tag{73}$$

This yields[5]

$$p\{B(\omega)\} = \begin{cases} \frac{\chi(\omega)}{B^2(\omega)} \exp -\chi(\omega)\left(\frac{1}{B(\omega)}-1\right) & 0 \leq B \leq 1 \\ 0 & 0 \not\leq B \not\leq 1 \end{cases} \quad . \tag{74}$$

The above results provide an understanding of the effects of noise on the cepstrum of a double path echo with a simple signal (e.g. the case of a short continuous wave pulse with a single point reflector). These can be assessed with the aid of plots of the expected value of $B(\omega)$ and $\hat{\phi}(\omega)$ and their variances as a function of the signal-to-noise ratio. These are shown below in Figure 11[6]. While these curves describe the behavior of B and $\hat{\phi}$ at each frequency as a function of the signal-to-noise ratio, they provide insight into the overall expected effects of noise on the cepstrum.

The expected value of $B(\omega)$ decreases with $\chi(\omega)$, the signal-to-noise ratio multiplied by $(1 + a^2)$. The expected value of the peak is reduced to 63% of the

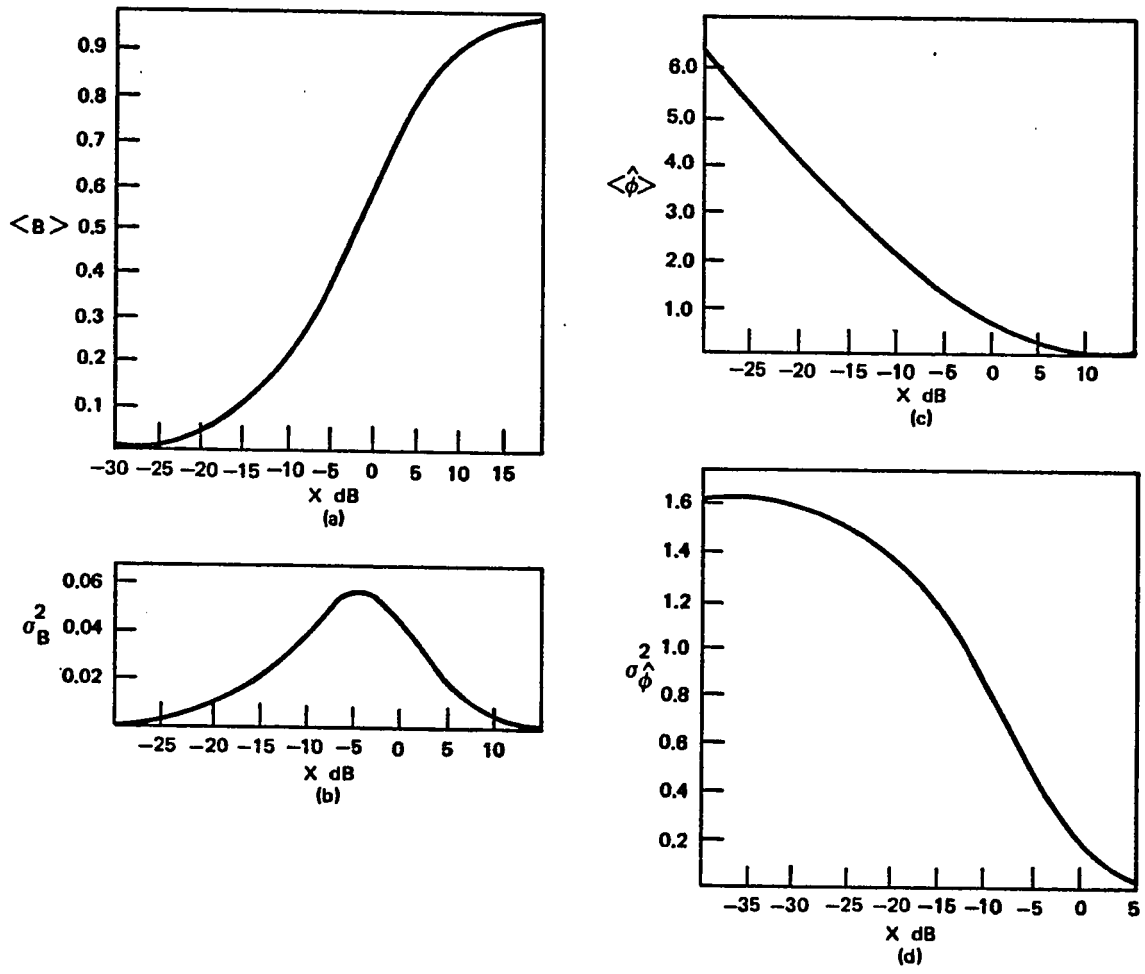

Figure 11. Expected Values of Noise Parameters.

noise free value when $X(\omega)$ is zero dB. At 10 dB, it is 91% of the noise free expectation. Low level noise has a very little affect on the cepstrum. As the zero dB value for the ratio is approached, however, the cepstral peak decreases rapidly. The variance of the modulation value is highest in this region.

As shown in Figure 11c, the expected value of $\hat{\phi}$, on the other hand, remains quite low until the signal-to-noise parameter, X, is reduced to zero dB or lower. The additive noise terms in the power cepstrum increases logarithmically with further reduction in the ratio. Recall that these curves are for $B(\omega)$ and $\hat{\phi}(\omega)$, i.e., they apply at each frequency. These conclusions about the cepstral peak heights only apply when the signal-to-noise ratio is essentially constant across the frequency band being processed. They nonetheless provide useful insight into the effects of noise on the cepstrum, even when the ratio is not constant.

The expected effects of noise may then be summarized as follows. The introduction of a small amount of noise into the signal leaves the cepstrum essentially unchanged. As the noise level increases with respect to the signal level, the noise produces an ensemble decrease in the cepstral value associated with the multipath return. This occurs due to a modulation effect between the noise and the information carrying $\cos \omega\tau$ term in equation (40). The expected additive value to the cepstrum due to the noise also increases with the noise level. This increases logarithmically with the noise level as the noise becomes much greater than the signal.

In the present study, the signal of interest is not the simple known signal of the above summary, but rather the unknown signature of a multireflector target. An examination of the previous analysis, however, will reveal that most of the conclusions are still valid. In the foregoing, in equation (64), it was

assumed that $F\{(1+a^2)\,\Phi_y(\omega)$ did not produce appreciable contributions to the cepstrum at the delay times of potential interest. Consequently, the effects of noise on the interaction between this term and the information carrying cos $\omega\tau$ term were not considered. As discussed in Chapter 3, with a typical multipoint target signature this is not the case. Furthermore, in order to correctly detect the multipath, not only must the associated cepstral value exceed a level not exceeded by noise related values, it must also exceed a level not attained by distributed target cepstral peaks.

Consider the cepstrum of the signal from the multipoint target with noise, but without multipath. Combining equations (22) and (46) gives

$$\Phi_z(\omega)=\Phi_x(\omega)\sum_{i=1}^{N}\alpha_i^2+\sum_{i=1}^{N-1}\sum_{k=i+1}^{N}2\alpha_i\alpha_k\cos\omega(\tau_i-\tau_k)+\phi_n(\omega)+\phi_{cn}(\omega) \tag{75}$$

where

$$\phi_n(\omega) = |N(\omega)|^2 \tag{76}$$

and

$$\phi_{cn} = \left[\sum_{i=1}^{N}\alpha_i e^{-j\omega\tau_i}\right]Y(\omega)N^*(\omega)+\left[\sum_{i=1}^{N}\alpha_i e^{j\omega\tau_i}\right]Y^*N(\omega) \tag{77}$$

For convenience, as in equation (43) let

$$\phi_{cn}(\omega) = 2\{\alpha_a N_r + \alpha_b N_i\} \quad , \tag{78}$$

where now

$$\alpha_a = \left(\sum_{i=1}^{N-1}\sum_{j=i+1}^{N} 2\alpha_i\alpha_j \cos\omega(\tau_j-\tau_i)\right)Y_r + \left(\sum_{i=1}^{N-1}\sum_{j=i+1}^{N} 2\alpha_i\alpha_j \sin\omega(\tau_j-\tau_i)\right)Y_i \tag{79}$$

and

$$\alpha_b = \left(\sum_{i=1}^{N-1}\sum_{j=i+1}^{N} 2\alpha_i\alpha_j \cos\omega(\tau_j-\tau_i)\right)Y_i - \left(\sum_{i=1}^{N-1}\sum_{j=i+1}^{N} 2\alpha_i\alpha_j \sin(\tau_j-\tau_i)\right)Y_r \quad , \tag{80}$$

then

$$\phi_{cn}(\omega) = 2\left\{\left[\left(\sum_{i=1}^{N-1}\sum_{j=i+1}^{N}\alpha_i\alpha_j\cos\omega(\tau_j-\tau_i)\right)Y_r + \left(\sum_{i=1}^{N-1}\sum_{j=i+1}^{N}\alpha_i\alpha_j\sin(\tau_j-\tau_i)\right)Y_i\right]N_r + \left[\left(\sum_{i=1}^{N-1}\sum_{j=i+1}^{N}\alpha_i\alpha_j\cos\omega(\tau_j-\tau_i)\right)Y_i - \left(\sum_{i=1}^{N-1}\sum_{j=i+1}^{N}\alpha_i\alpha_j\sin\omega(\tau_j-\tau_i)\right)Y_i\right]N_i\right\} \quad . \tag{81}$$

With these changes, equation (46) becomes

$$\Phi_z(\omega) = \left[\sum_{i=1}^{N}\alpha_i^2\Phi_x(\omega)\right]\left[1+\frac{\phi_n(\omega)}{\sum_{i=1}^{N}\alpha_i^2\,\Phi_x(\omega)}\right]\left[1+B_N(\omega)\sum_{i=1}^{N-1}\sum_{j=i+1}^{N}2\gamma_{ik}\cos\omega(\tau_i-\tau_k)\right]\left[1+\Psi_c(\omega)\right] \tag{82}$$

where

$$\gamma_{ik} = \frac{\alpha_i \alpha_k}{\sum_{j=1}^{N} \alpha_j^2} \quad , \tag{83}$$

$$B_N(\omega) = \frac{1}{1 + \frac{\phi_n(\omega)}{\left(\sum_{j=1}^{N} \alpha_j^2\right)\Phi_x(\omega)}} \tag{84}$$

and

$$\Psi_c(\omega) = \frac{\phi_c(\omega)}{\alpha_a^2 + \alpha_b^2 + \phi_n(\omega)} \quad . \tag{85}$$

Equation (82) is of the same form as equation (58) and the consequent behavior of the cepstrum combines the features of a distributed target as discussed in Chapter 3 and the effects of noise as presented earlier in this section. As indicated in equation (84), the modulation caused by the noise is the same across the multiple returns and will reduce their height as indicated in Figure 11. A difference is expected, however, on the final behavior of the cepstrum. Since there are numerous peaks in the cepstrum due to the various arrival delay differences from the multiple reflectors, the probability of a sizeable contribution to the cepsturm from the additive noise term, ($\hat{F\phi}(\omega)$) in equation (64) coinciding with a substantial peak due to one of these time

differences is increased. Consequently, it is expected that the variance of the heights of peaks resulting from multiple reflector spacing will increase.

When the actual case of interest, that of a multiple reflector target with multipath is considered, no new phenomena appear. As in Chapter 3, the multiple reflector signature may be treated as the basic signal and the multipath as the delay to be detected. The discussion of the preceeding paragraphs describe the noise effects on the cepstral contributions of $\Phi y(\omega)$ in equation (43). In turn, the same performance effects of noise equally apply to the multipath cepstrum itself, $C(\Phi_Z)$ in equation (43).

Qualitatively, noise will compound the problem of detecting multipath in observing the signature of a multi-reflector target in two ways. First it will introduce a modulation of the cepstrum at the corresponding delay. Second, it will add to the cepstrum by the $F\{\phi(\omega)\}$ term with magnitude and variance as indicated in Figure 11. This will tend to increase the variance of peaks associated with the multiple reflector nature of the target.

4.4 Model Results With Noise

In order to further examine the noise effects on the cepstrum's detection of multipath, a series of modeled results were investigated. The target signatures with and without multipath were generated as described in section 4.1. White Gaussian noise was introduced across the band by the addition of a signal generated by the International Mathematics and Statistics Library (IMSL) routine GGNML[7]. This routine supplies independent, zero mean, unit variance, normally distributed values. The proper level was obtained by scaling. Three different multipath strengths were used: .4, .25, and .2. The actual signal strength in the return, as measured by the total energy of the single path echo,

varied from target to target, but by less than 2 dB. The strength of the single path return was used in defining the signal-to-noise ratios.

The results for the single path case are shown in Figure 12. Each point plotted represents an individual run. Each point at a given signal-to-noise ratio corresponds to a separate target. Each target is plotted in the same relative position for each signal-to-noise ratio. Thus, the leftmost point plotted at 36 dB, 16 dB, and 10 dB each corresponds to the same target. The variation at each high signal-to-noise ratio is due entirely to the differences between targets.

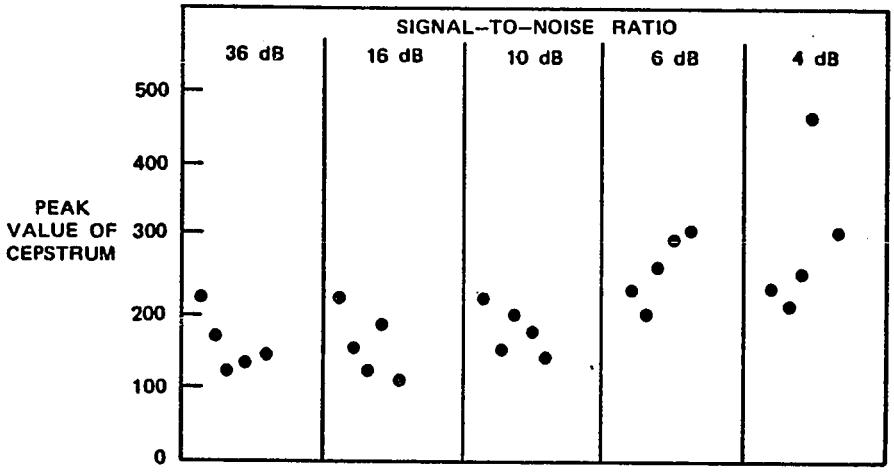

Figure 12. Peak Cepstrum Value with Single Path.

It can be seen that, while differences occur in the peak cepstrum value for individual targets, the peak levels remained relatively unchanged while the signal-to-noise ratio was greater than 10 dB. Some increase is seen in the lower peak values at the 10 dB signal-to-noise level. These increases between the 16 dB and 10 dB cases result from the additive noise term and the higher peak in

the noisier case occurs at different delay times than it did in the purer 12 dB case. In contrast, the peak values that show a decrease with increased noise occur at the same delay times and the reduction results from the modulation term.

As the signal-to-noise ratio is reduced further, the additive cepstral effects predominate in determining the peak cepstral values. This will result in increased false detection of multipath at increased noise levels or, as will be shown, increase the relative strength required of multipaths in order to allow detection. Note the increased spread in the peak values with low signal-to-noise ratios in agreement with the predicted performance indicated in Figure 11b.

These trends are further illustrated in Figure 13 where the peak values for two of the targets are plotted individually as a function of signal-to-noise ratio. Again, each of the plotted points represents only one simulation run and,

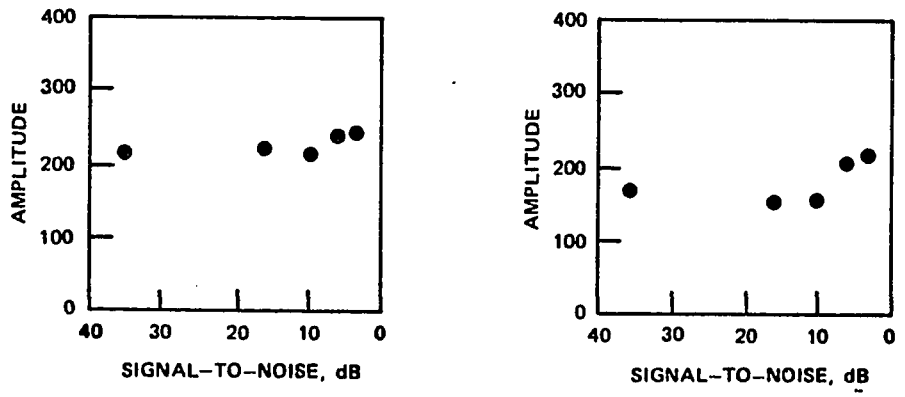

Figure 13. Two Examples of Single Path Maximum Cepstral Strength as it Varies with Noise.

therefore, only one realization of the additive noise. The noise attributes described are nonetheless evident. While the signal-to-noise is above 10 dB, adding noise has almost no discernable effect in one case and causes a slight decrease in the other. As the noise level is increased more, the additive cepstral effects dominate, especially in the second case.

Figure 14 shows the simulation results with noise and multipaths of various relative amplitudes at a variety of signal-to-noise ratios. Whether or not the peak value of the cepstrum occurs at the time of the multipath delay is indicated by the plotting symbol key identified in the figure. As long as the signal-to-noise ratio exceeds 10 dB, the peak cepstral values without multipath are all less than 225, have an average value of 164, and a standard deviation of 37. This indicates that values in excess of 250 will almost always result from multipath rather than the multireflector target nature when the noise is below this level.

In the next section of the figure it is seen that with this same 10 dB signal-to-noise criterion and with the relative transmission by the second path 40% that of the primary path, the peak cepstral value always corresponded to the multipath delay. As well, its amplitude always exceeds 300; for the cases examined the average peak value is 405. As the transmission via the second path becomes less, the amplitudes of the cepstral peaks diminish. This approximately follows the linear relation indicated by equation (9). This is verified by the average peak value of 257 in the case of a 25% second path amplitude and 203 in the case of the 20% multipath amplitude.

Since the multipath peaks in the cepstrum are lower when the multipath amplitude is less, the effects of noise in obscuring the multipath delay peak occur sooner. In the particular scenarios that were modeled, there is 20%

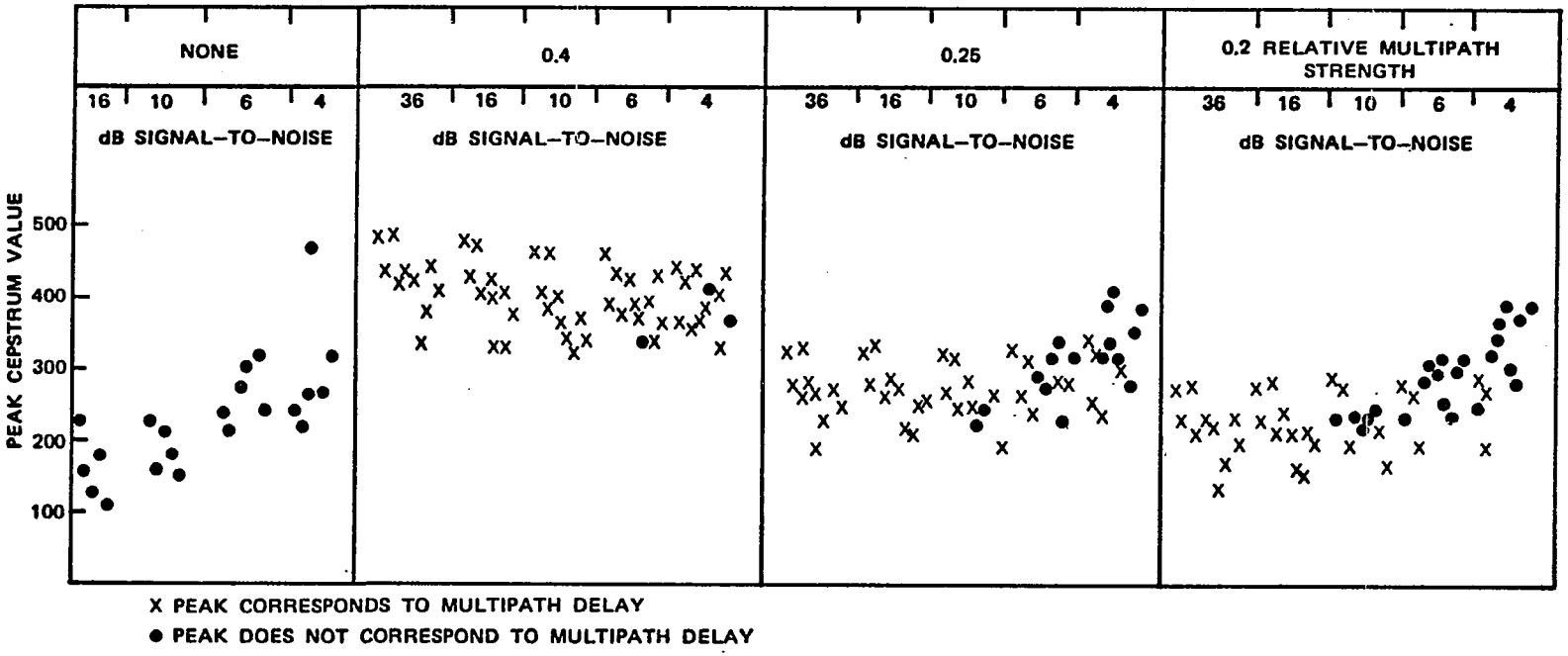

Figure 14. Peak Cepstrum Values for Various Targets, Multipath Strengths and Signal-to-Noise Ratios with 4500 Hz, 4 millisecond Continuous Wave Pulse.

incorrect multipath identification with the 25% path strength and 50% incorrect with a 20% path strength.

At higher noise levels, the percent of incorrect multipath identifications increases as does the average peak value. At the point where the noise and signal levels are the same, the cepstral values obtained from the model without multipath completely overlap the corresponding values with multipath. At this point detection and estimation of multipath at the indicated strengths appears to become impossible in the sense of maintaining both a good probability of detection and at the same time a low false alarm rate.

The average peak value and its standard deviation for each signal-to-noise ratio and each relative path strength are shown in Figure 15. The values are also tabulated at the bottom of the figure. Each of these values is based on ten samples from the simulation. These values will be used in the following section where detection thresholds are discussed further.

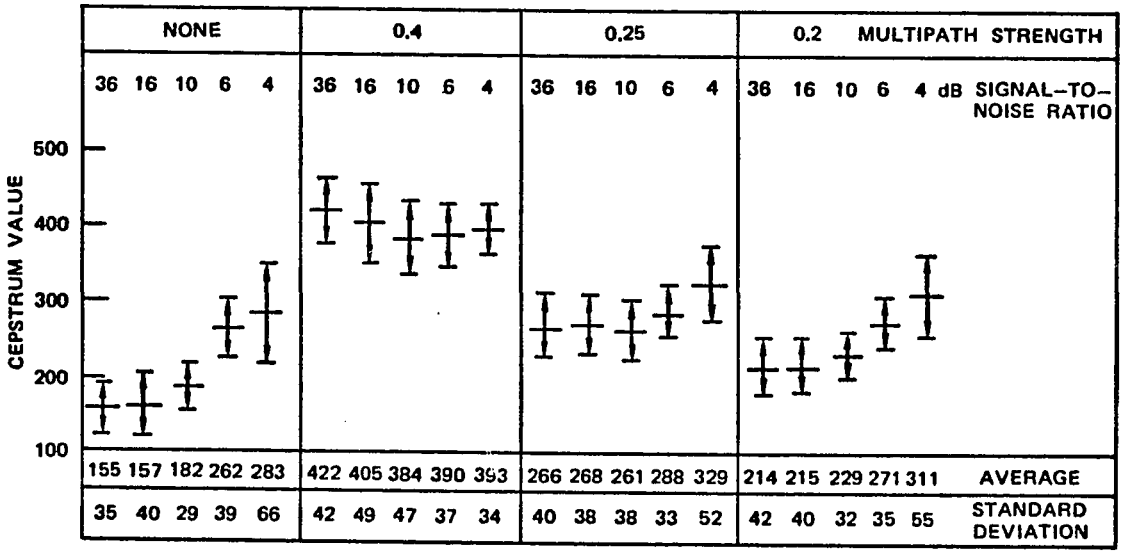

Figure 15. Average Peak Cepstrum Values.

The behavior of the multipath cepstral peak for a single target with two multipath cases is shown in Figure 16. These particular cases were included in Figure 15. Their repetition here allows examination without the distraction of target-to-target variations. The behavior noted above is quite evident. In these cases, both corresponding to a .4 relative multipath strength, the peaks are high enough that the peak reducing effect of the noise dominates. The reduction is greatest in the second case at the high noise (low signal-to-noise) values.

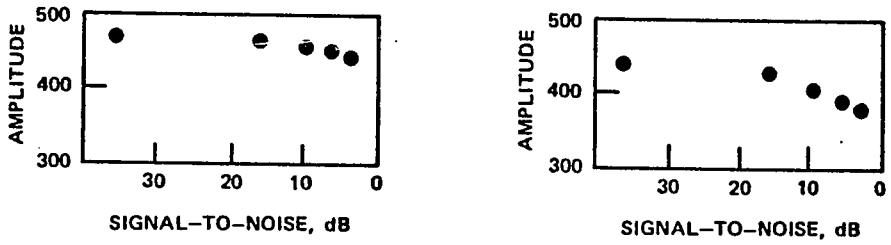

Figure 16. Multipath Cepstrum Values with Increasing Noise.

The different cepstrum values for the same path strength seen here and elsewhere is due to the differences in the target cepstral value at the different delays. In the low noise case, the peak value is 479 for the 1.3 millisecond delay; 436 for the 3.7 millisecond delay multipath. The predicted value for both is 410. The differences, 69 and 26, respectively, are the values of the target cepstrum at those delays. Thus, in the low noise case, the cepstrum levels at the multipath delays are in complete agreement with the theoretical values.

In detecting multipath with an unknown target signature, it would not be possible to remove the target's contribution from the measured cepstrum. It is, in fact, the target's contribution that is sought as will be examined in Chapter 6. Consequently, analysis separating target and multipath contributions to

individual peaks will not be included in subsequent sections on detection. Only the known contribution from the transmitted waveform has been removed.

4.5 Multipath Detection Thresholds

The purpose of this section is to explore the existence of thresholds for the cepstrum in order to detect multipath with a usefully high probability while at the same time keeping the rate of false multipath detection low. From Figures 14 and 15, there is indication that such thresholds exist if the multipath is strong enough and the signal-to-noise ratio is high enough. The low noise case will be examined first.

Figure 17 presents the results obtained from more than one hundred simulations run with a 32 dB signal-to-noise ratio. The average peak value for the cepstrum for the cases where there was no multipath is 209. The sample standard deviation is 33.3 and the total spread is 140. The highest value obtained is 290. This particular value occurred with target number five which had two very major, narrow reflecting areas (Figure 10). This target was specifically included to represent an extreme case in terms of having a target reflector distribution that would produce a large cepstral value. It is anticipated, therefore, that actual targets would seldom, if ever, produce peaks this high. It is, nonetheless, included in the following analysis.

In the cases where the second path had a one-way strength 40% the direct path, the second arrival always produced a cepstral spike at the correct time and it was the largest value for that cepstrum. These peaks had an average value of 398 and a standard deviation of 26. The lowest peak value for this multipath strength was 333, significantly greater than the largest value obtained from a single path reflection. Thus, with these particular model

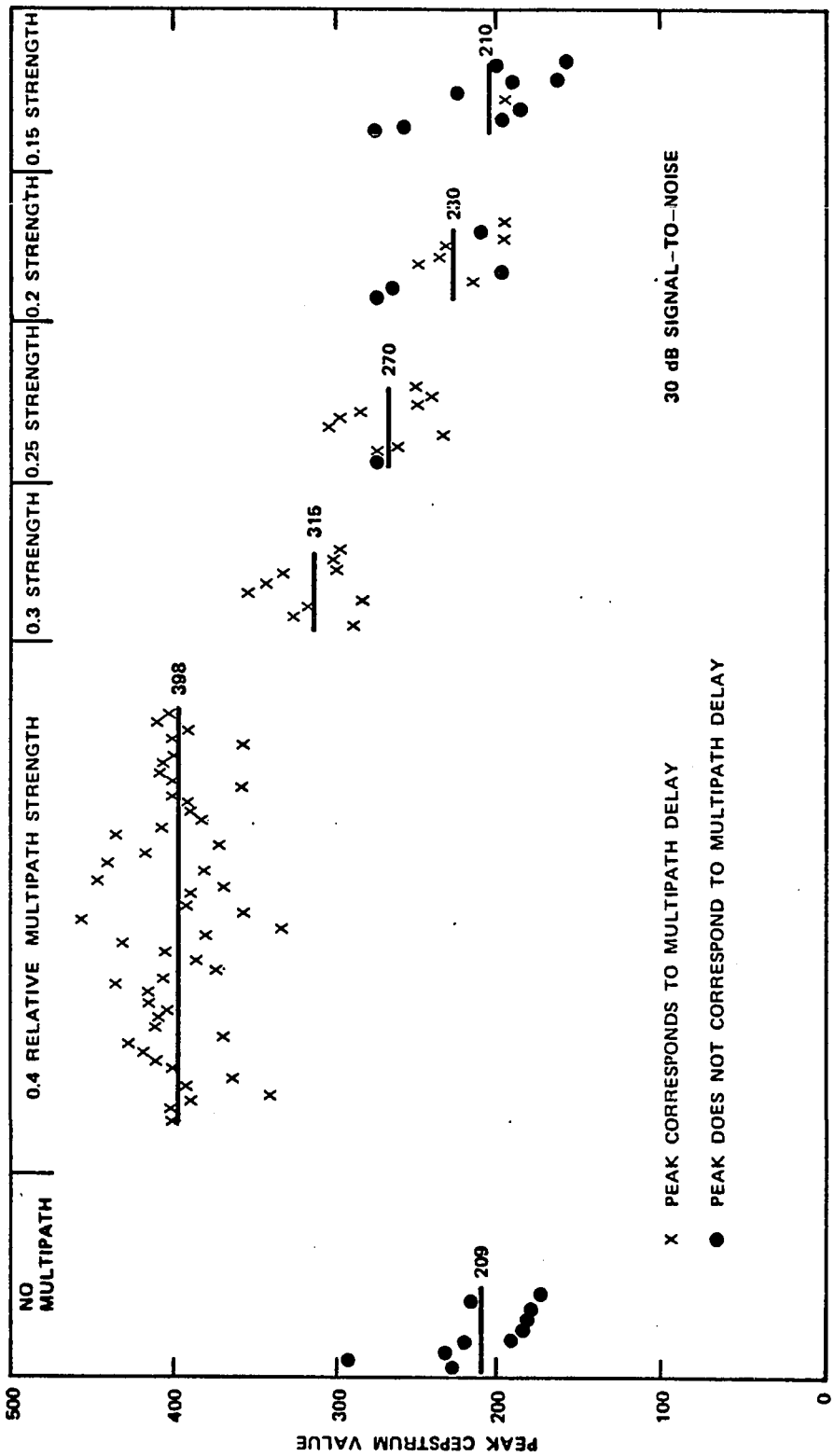

Figure 17. Peak Cepstrum Values for Various Multipath Strengths 4500 Hertz Continuous Wave Pulse.

targets it appears possible to detect multipath, of this magnitude, with very high probability and without significant possibility of false detection. A threshold of 300, e.g., completely separate the data.

As the strength of the multipath decreases, so does the height of the corresponding cepstral peak. As long as the peak value corresponds to the multipath delay, the average of the peak is very close to 1024 times the relative path strength as predicted by equation (9). The average peak values from Figure 17 are plotted below in Figure 18 retaining only those values where the peak corresponds to the multipath delay. The relation is linear as predicted, except at the lowest multipath .strength (.15). This deviation is expected since only one correct peak occurred at this multipath strength (Figure 17). If the values of the correct delay peaks at this return strength are averaged, the value is 164, in much closer agreement with theoretical value.

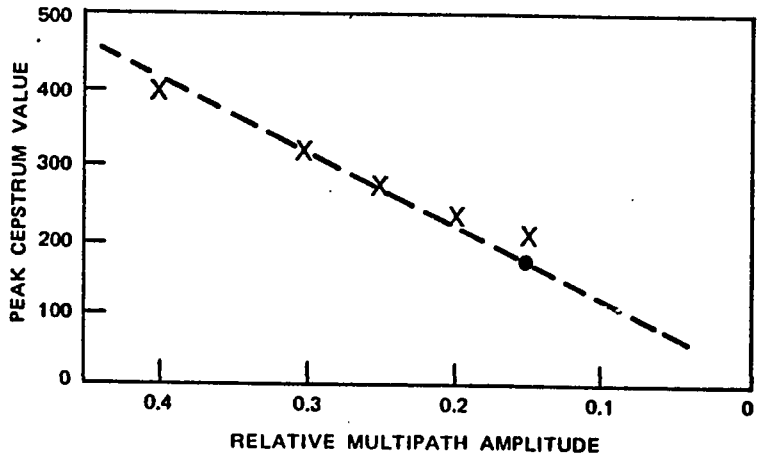

Figure 18. Variation of Cepstrum with Path Strength.

Returning to Figure 17, the model results indicate that as long as the multipath cepstral peaks are greater than the values without multipath, the

peak value correctly identifies the multipath delay. As the multipath strength decreases, the cepstrum peak decreases and a detection threshold becomes impossible at the same level where the highest peak no longer corresponds to the multipath delay. For example, a threshold level of 280 correctly detects all the 40% path strength cases and all of the 30% strength cases. At 20% delay path strength, the peaks do not exceed this threshold and 44% of the peaks do not correspond to the delay time. On the basis of the limited data, a threshold between 240 and 300 is indicated for multipath detection in high signal-to-noise conditions.

In section 4.4, it was shown that the cepstrum performance changed little due to noise as long as the signal-to-noise ratio exceeded 10 dB. Figure 19 gives the results using the same targets and multipath scenarios that produced the values shown in Figure 17. Here, however, the signal-to-noise ratio has been reduced to the 10 dB level. The performance is very similar, especially at the higher multipath strengths. At the lower relative multipath strengths (.25, .2, and .15) there is a more noticeable decrease in the cepstral values. With the threshold at 240, the number of false detections is doubled and detection at the .25 path strength is greatly reduced. With the 300 threshold, the false detection is still zero, but detection at the .3 path strength becomes very poor.

Figure 20 summarizes the multipath detection probabilities for three different signal-to-noise ratios (36 dB, 10 dB, and 4 dB) and various multipath strengths as identified in the individual plots. These values were obtained by using the sample variances from Figure 15 and assuming a Gaussian distribution. The cepstrum value at each delay is the sum of several contributions: target, multipath, and noise. With fifty target reflectors and two paths, there are one hundred fifty arrivals. This leads to over twenty two thousand arrival delay combinations, i.e., differences in the time of individual arrivals. Consequently,

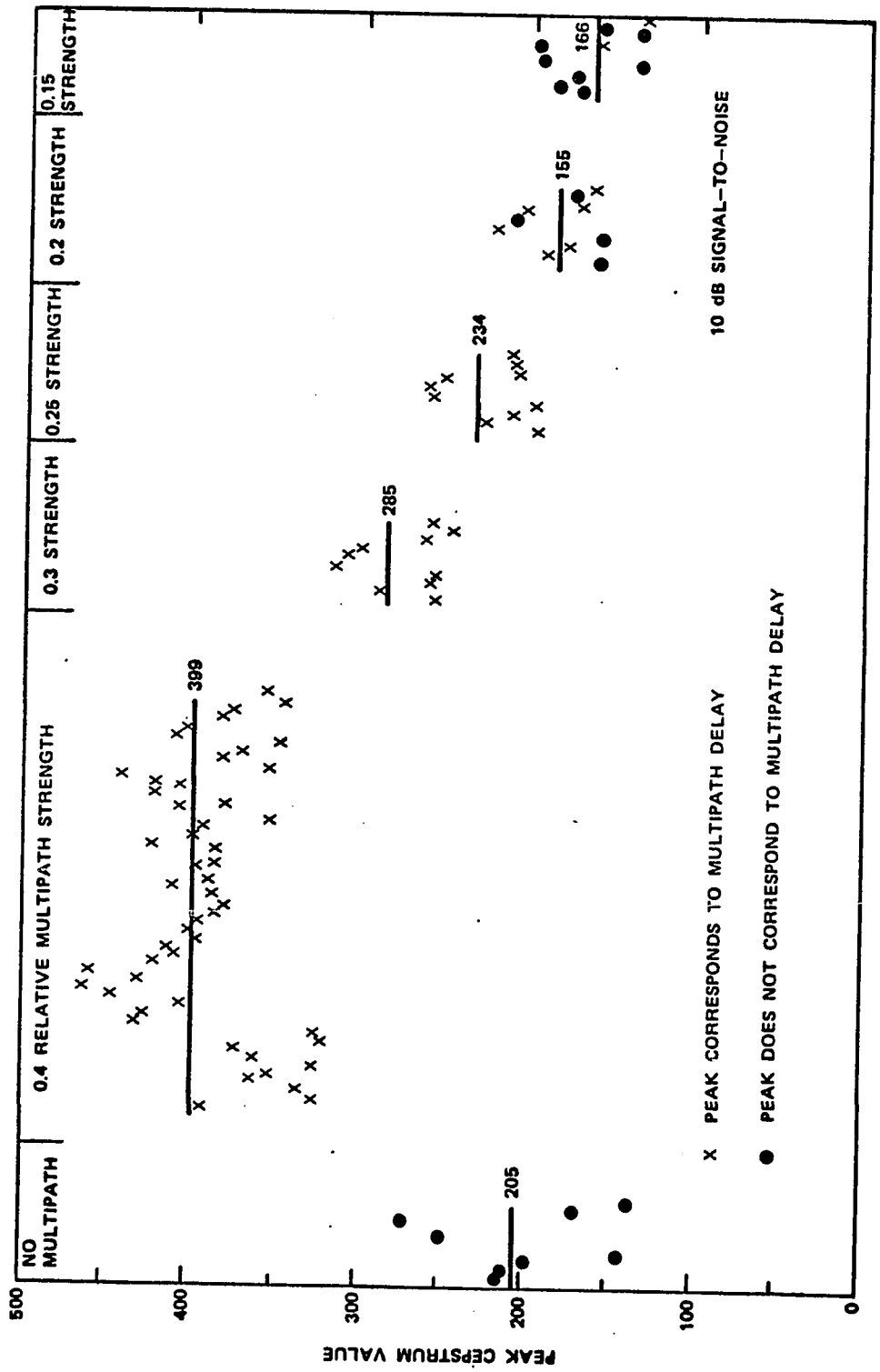

Figure 19. Peak Cepstrum Values with 10 dB Signal-to-Noise.

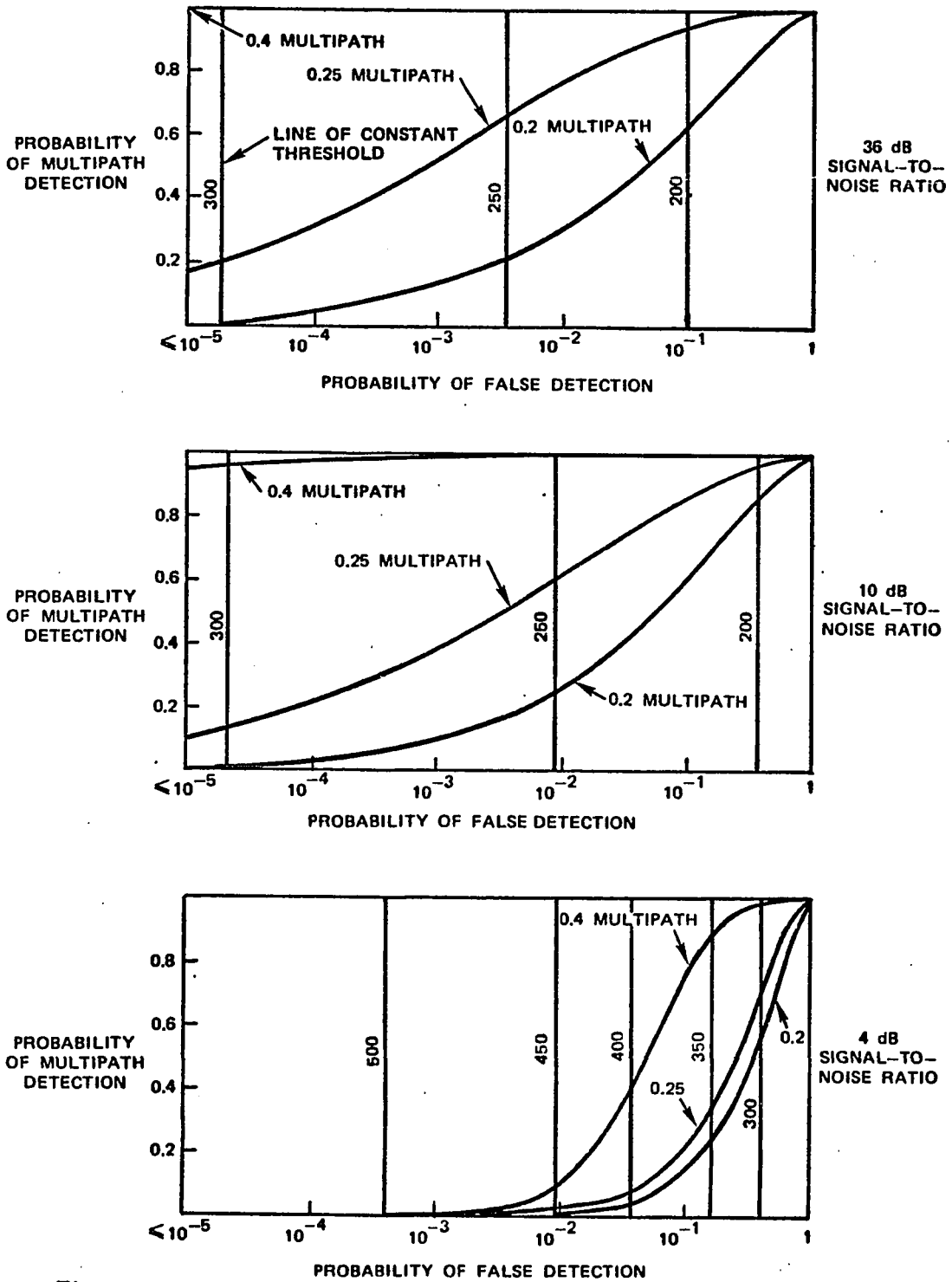

Figure 20. Multipath Detector Performance for Three Noise Levels and Three Multipath Strengths with a Continuous Wave Pulse.

there will be many of those delay combinations adding to produce each value of the cepstrum. This will make the final distribution of the amplitude trend toward Gaussian by the Central Limit Theorem.

Several portions of the data were examined to test this Gaussian hypothesis. The results of both the Kolmogorov-Smirnoff and chi-square goodness of fit tests support the Gaussian assumption.[8] The chi-square test, for example, showed that deviations from the Gaussian distribution of the magnitude seen in the data distribution are to be expected in sixty percent of the cases.

Even with the Gaussian assumption, there remains the question of how good an estimate of the mean and variance of the population is provided by the sample mean and variance with the sample size used. The false detection statistics are based on ten samples each; the probability of detection on ten to forty cases, a restriction imposed by financial constraints. This indicates that the sample variance should be within 25% of the population variance 70% of the time. The consistency of the results tends to lend greater credance.

Increased noise then increases the false detection rate and decreases the ability to detect weaker mutipaths. Referring back to Figure 14, further noise increases continue this trend. At sufficiently low signal-to-noise only the stronger multipaths remain detectable and then only upon settling for a significant false detection incidence.

4.6 Effects of Motion

In the discussion and modeling results presented thus far, it has been assumed that there is no relative motion between the transponder (or antenna)

and the target. Since this is almost never the actual case, a discussion of the effects of the targets relative motion is appropriate.

The motion of the target will have two effects on the returned signal. The first of these is the familiar Doppler shift that changes the frequency of the signal in proportion to the ratio of the relative velocity of the target and the speed of propogation of the signal. Since nothing in the computation of the cepstrum is coupled to the transmitted frequency, this net shift in the signal frequency will not affect the performance of the cepstrum.

The second effect of the motion is illustrated in Figure 21. As pointed out in section 3.4 and illustrated in Figure 4, in the stationary case two transmission paths lead to three reflected arrivals. With motion, the second arrival is split into two separate arrivals. Referring to the figure, a signal transiting to the reflector by path "a" may return by path "b." The signal going to the target by the longer path will not travel by path "b" but rather by path "b'" since the reflector will have moved from x to x_1 between the time the signal reached the reflector by the direct path and the time it arrived by the longer path. Thus the two way time via "ab" and via "b'a" will be different. The final arrival from "bb" transit and return remains a single arrival as it was without motion. There will, then, be four arrivals at the receiver rather than three.

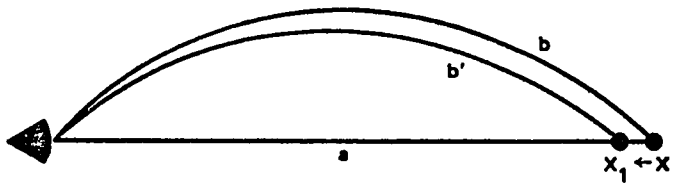

Figure 21. Two Path Geometry with Motion.

Simulations were run with parameters corresponding to 10, 20, and 30 kts in the sonar scenario, with a stationary second arrival delay of four milliseconds. The total cepstral area in the peak associated with the multipath remained within the interval indicated in the stationary case (Figure 14). At the higher speeds (20 and 30 knots), however, the difference between "ab" and "b'a" became on the order of the range increment in the cepstrum. This caused the associated peak to be spread over two range cells rather than one. Thus, while motion has some effect on the performance of the cepstrum, it appears that it will require only slight modifications in the processing for multipath detection. This would consist of summing adjacent cepstrum values to remove the effects of arrival splitting.

4.7 Effects of Additional Paths

In Chapter 3, the effects of increasing the number of returns were examined in detail to provide insight into the behavior of the target signatures cepstrum. Equation 39 gives the final result showing that additional returns lower the height of all the cepstrum peaks. From this equation, individual peak height A_{ij}, is given by

$$A_{ij} = \frac{2\alpha_i\alpha_j}{\sum_{m=1}^{N}\alpha_m^2} \tag{86}$$

where A_{ij} is the height coefficient for the peak associated with the delay between the ith and the jth returns, and α_i is the amplitude of the ith return.

Thus, additional multipaths will make the detection of each more difficult. The reduction in peak heights will be greatest when all paths are of about

the same strength. If there are two major arrivals and several weak ones, the detection of the major multipath will not be greatly affected and the weak multipaths will remain difficult or impossible to detect as was the case with a single weak path. The path strength required for detectability will, in general, be raised.

Table 2 provides the simulation results for one three path case that is illustrated in Figure 22. Here the relative one way transmission strengths of the three paths are 1, 0.5, and 0.4, respectively. This provides six arrivals at the integrating transponder. As predicted by equation (86), the two strongest delayed returns (at $2\tau_o + \Delta\tau_1$ and $2\tau_o + \Delta\tau_2$) predominate the cepstrum.

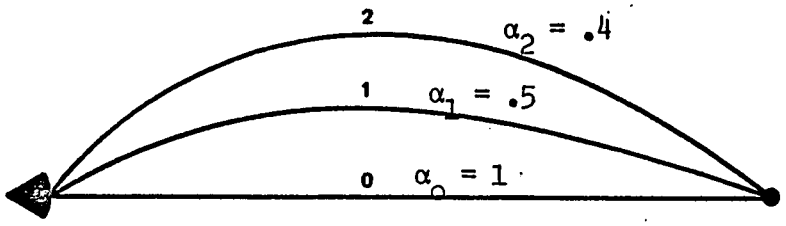

Paths	Arrivals Delay	Strength
00	$2\tau_o$	1.00
01, 10	$2\tau_o + \Delta\tau_1$	1.00
02, 20	$2\tau_o + \Delta\tau_2$	0.80
11	$2\tau_o + 2\Delta\tau_1$	0.25
22	$2\tau_o + 2\Delta\tau_2$	0.16
12, 21	$2\tau_o + \Delta\tau_1 + \Delta\tau_2$	0.40

Figure 22. Three Path Example.

Delay (msec)	Relative Path Strength (2 Way)	Predicted Cepstrum Value with 2 Paths	Predicted Cepstrum Value with 3 Paths	Cepstrum Value in Model Targets with 3 Paths 1	2	3	Ave 3 Path Value
1.5	1.0	512.	378	372	379	375	375
2.4	.8	410.	310	326	306	306	312

Table 2. Three Path Results.

The observed values are lower than the values that would have occurred with only two paths and agree very well with the predicted values.

CHAPTER NOTES

1. Joseph C. Hassab and Ronald Boucher, "A Probabilistic Analysis of Time Delay Extraction by the Cepstrum in Stationary Gaussian Noise," IEEE Trans. on Information Theory IT-22(4) (1976): 444.

2. J. E. Ehrenberg, T. E. Ewart, and R. D. Morris, "Signal-Processing Techniques for Resolving Individual Pulses in a Multipath Signal," JASA 63(6) (1978): 1861-1895.

3. Hassab and Boucher, pp. 444-453.

4. Ibid., p. 447.

5. Ibid.

6. Ibid., p. 450.

7. International Mathematics and Statistics Library Reference Manual (Houston: IMSL, 1979).

8. W. J. Conover, Practical Nonparametric Statistics, pp. 293-326.

CHAPTER 5

CEPSTRAL PERFORMANCE WITH VARIOUS SIGNAL TYPES

In the preceeding chapter, the effects of pulse length and noise on cepstral multipath detection were discussed. In this chapter, the relative performance with various waveforms, or signal spectra, will be examined. While the signals chosen are not exhaustive, they cover a representative sampling of signals presently used or under study for use in radar or sonar applications. Specifically linear frequency modulated pulses, linear period modulated pulses, bionic signals, and discrete stepped frequency pulses are discussed.

As concluded in Chapter 4, the pulse length, in the low noise case, has no effect on the ability of the cepstrum to detect and estimate multipath delays and amplitudes. This leads to the expectation that varying the waveform used will also have little, if any, effect in the low noise case. On the other hand, Hassab and Boucher's work has demonstrated the cepstral dependence on the pointwise signal-to-noise ratio across the frequency band being processed. Consequently, it is to be expected that the performance of the different signals may vary when noise becomes a significant factor.

5.1 Linear Frequency Modulation

Linear frequency modulated signals are of the form

$$x(t) = \cos(\omega_o t + \alpha t^2) \tag{87}$$

where ω_o and α are parameters that determine the initial frequency and rate at which the frequency changes, respectively. When compared with a continuous wave pulse, a linear frequency modulated pulse has the energy spread over more of the spectrum. Consequently, for a fixed total signal energy, the peak power spectral density will be lower than for a continuous wave pulse. As indicated previously (section 4.3) the effects of noise depend on the pointwise signal-to-noise ratio across the spectrum. On the other hand, the results with varying continuous wave pulse lengths in the low noise case suggest that low noise performance with the linear frequency modulated signal will largely parallel that of the continuous wave.

In the study, cepstral processing was done using the unprocessed received signal, i.e., without previous matched filtering or pulse compression. The same cases that were examined for the four millisecond continuous wave were repeated using a linear frequency modulated signal. This signal was a four millisecond chirp going from one kilohertz to four kilohertz. The signal-to-noise ratio of 32 dB was maintained. The peak cepstrum values are plotted in Figure 23. The results are quantitatively very similar to those obtained with a continuous wave pulse. The two major differences are in the no multipath values and in the weak multipath cases. Especially in the no multipath case, the peak values are generally significantly lower. With the frequency modulated signal, the highest single path value is 259 compared to 290 with the CW. The average value is 160, fifty lower than in the CW case. With some risk of false detections, a detection threshold of 200, for example, provides complete detection down through a 25% multipath strength and 60% detection for a 20% path strength with the frequency modulated pulse.

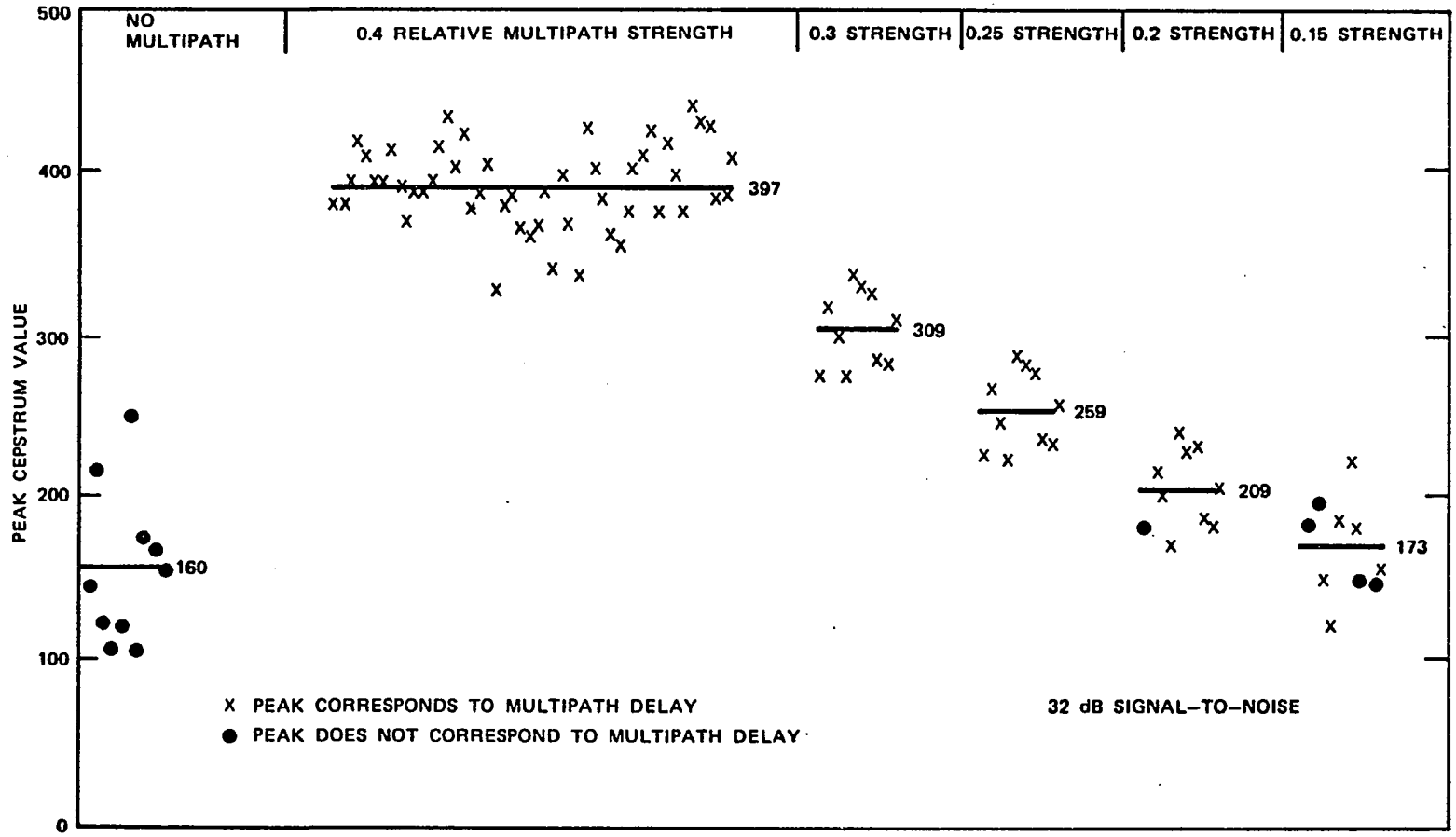

Figure 23. Peak Cepstrum Values for Various Multipath Strengths with Four Millisecond Frequency Modulated Pulse.

The percentage of correct multipath delay estimations is also higher than in the CW case. With the frequency modulated pulse all delays were correctly estimated at 25% multipath strength, 90% at 20% multipath strength, and 60% at 15% multipath strength. In the later instance, however, the cepstrum values are for the most part, below the suggested threshold value. The higher correct percentage seems directly related to the lower values obtained with no multipath. Since the cepstrum peak magnitudes are lower than in the CW case for no multipath, lower multipath peaks can be accurately detected and their delays estimated.

Figure 24 summarizes the results shown in detail in Figure 25 for the performance of the frequency modulated signal in noise. As was noted in the 32 dB case, the single path maximum remains lower than in the continuous wave case even at the lower signal-to-noise ratios. As well, the additive noise effects on the cepstrum do not appear as great in the 40% path strength case.

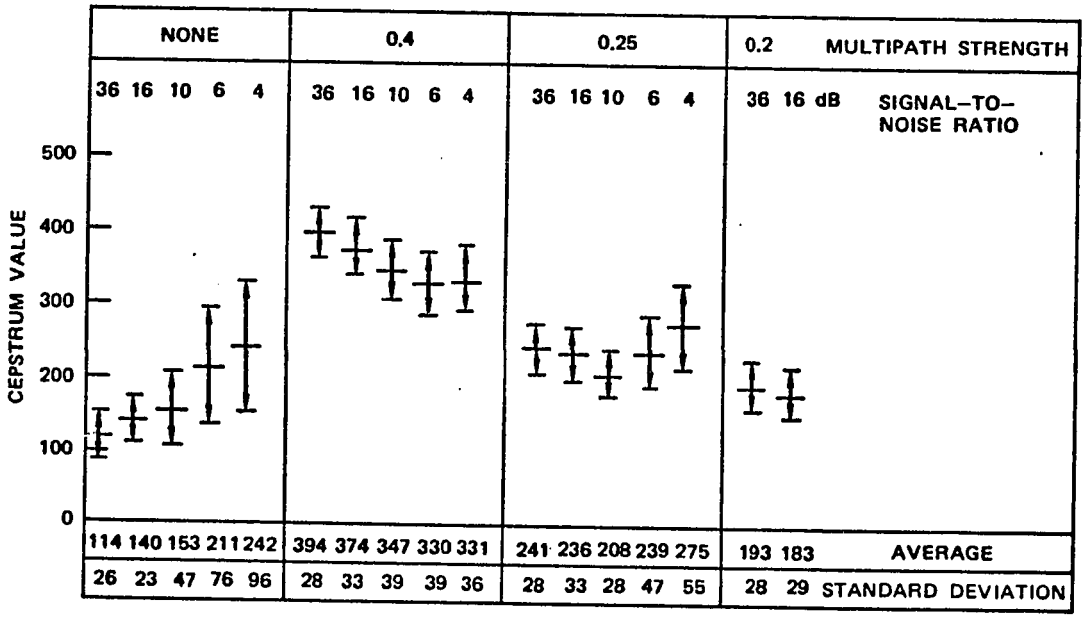

Figure 24. Average Peak Cepstrum Values - Frequency Modulated Pulse.

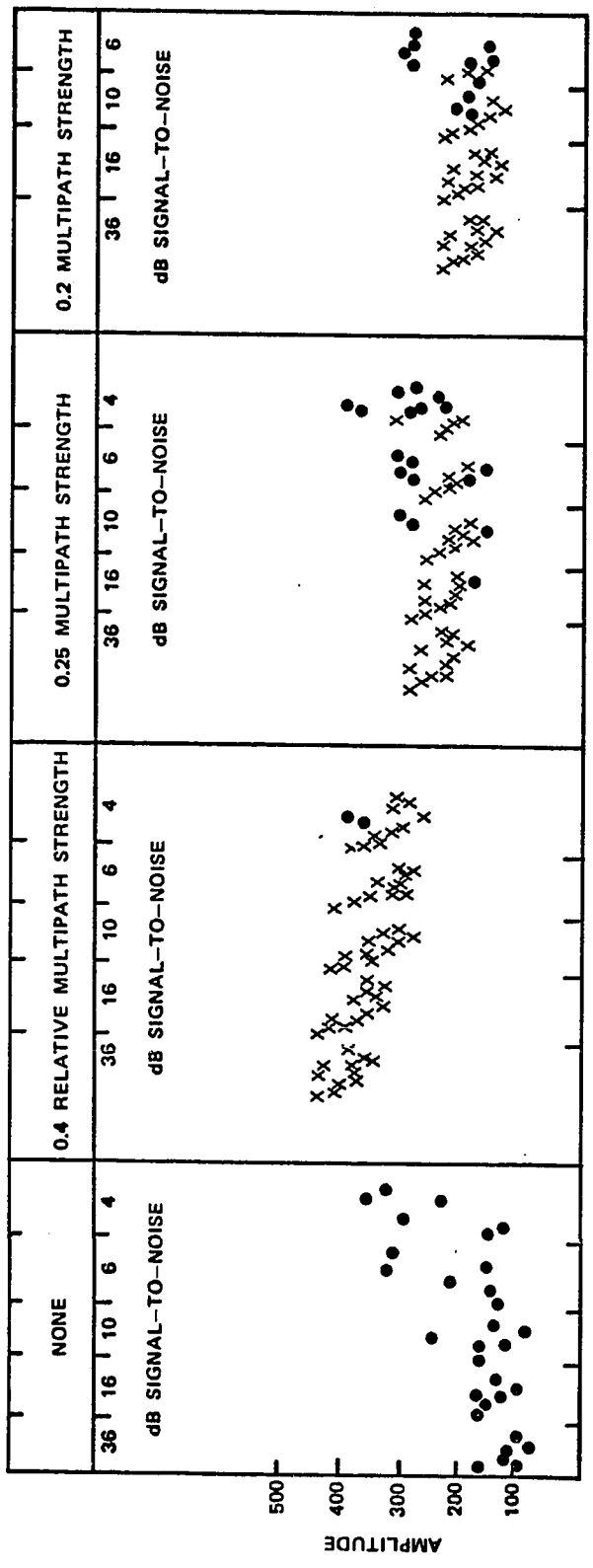

Figure 25. Peak Cepstrum Values for Various Targets, Multipath Strengths and Signal-to-Noise Ratios with Frequency Modulated Pulse.

Both of these effects probably stem from maintaining the signal-to-noise ratio higher over more of the spectrum. The correct identification of the multipath delay is no better for the linear frequency modulated signal at the higher noise levels. The differences present in the simulation are not statistically significant.

Figure 26 provides a summary of the probability of detection and false alarm rates for several multipath strengths and signal-to-noise ratios. These are presented in the same manner as was the continuous wave results in Figure 20. The same assumptions also apply.

5.2 Bionic Sonar Signal

A family of waveforms, termed bionic as a result of their similarity to bat and dolphin signals, have received considerable attention in the sonar classification community (1, 2, 3, 4). These signals are of the form

$$x(t) = A\exp\{-\rho(\log|t_o-t|)^2\cos\beta\log|t_o-t|\}. \qquad (88)$$

These signals have, among other attributes, the property of being Doppler tolerant in that their form is invariant under Doppler shift. While typically wideband, these signals do not have the property of the linear frequency modulation pulses in spreading their energy evenly across their nominal bandwidth. The spectrum of the signal used in this study (with $\rho = .17$, $\beta = 31.4$) is shown in Figure 27. The skewed form of the signal spectrum is apparent.

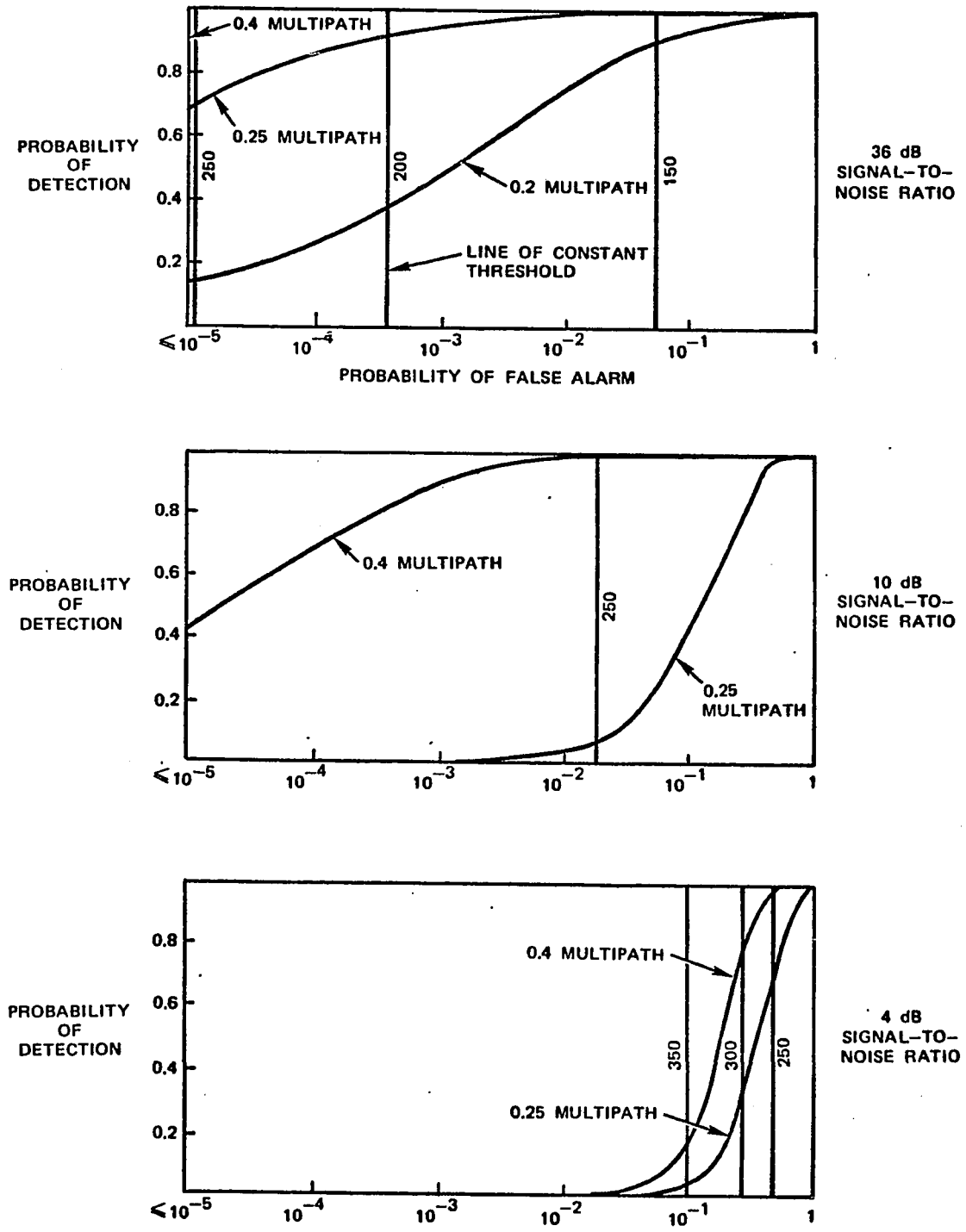

Figure 26. Multipath Detector Performance for Three Noise Levels and Three Multipath Strengths with a Frequency Modulated Pulse.

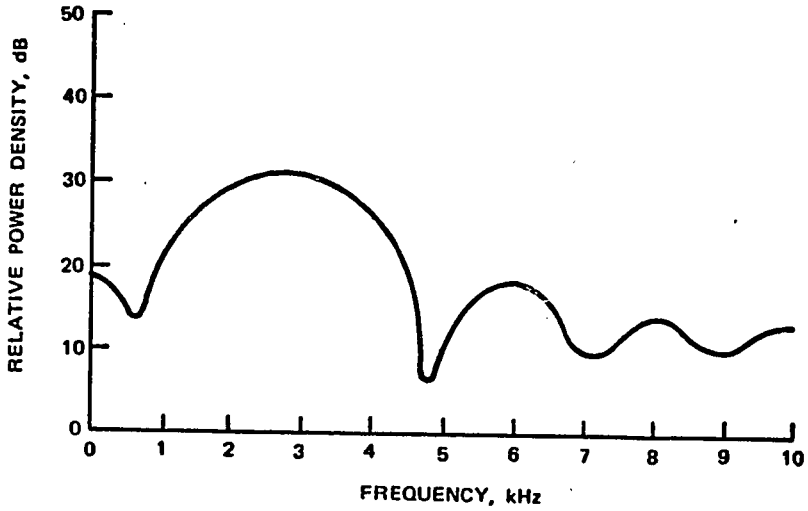

Figure 27. Spectrum of Bionic Signal.

The performance of the signal in terms of cepstral multipath detection is summarized in Figure 28 and shown in detail in Figure 29. Several differences between this and the continuous wave (Figure 15) are noticeable. The peak value of the cepstrum in the absence of multipath shows no large growth with noise as it did for the continuous wave and frequency modulation. This is partially the result of the higher values obtained for the bionic cepstrum in the low noise case. These higher values, in turn, might be expected from the low signal-to-noise ratio present over much of the spectrum.

The low noise cepstrum values with multipath are about the same magnitude as they are for the other wave types. The peak values with greater noise, however, fall off considerably faster than in the previous signal types. This is seen in the 40% multipath strength case where these peaks begin considerably above the noise induced peak values. A comparison of the spectra

from Figure 27 and that of the four millisecond linear continuous wave is shown in Figure 30. This along with the modulation coefficient

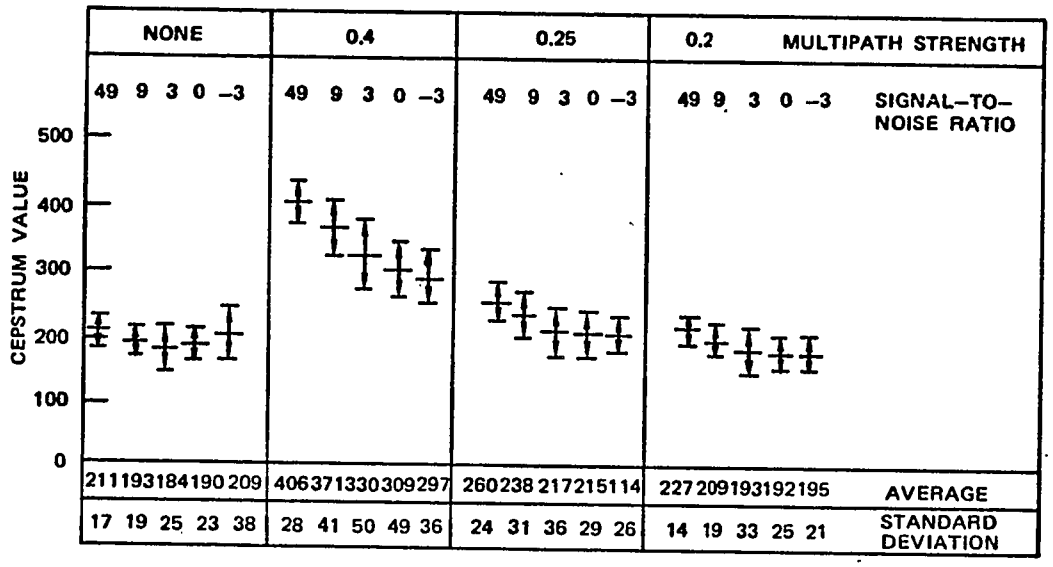

Figure 28. Performance of Bionic Signal in Noise.

$$B_N(\omega) = \frac{1}{1+\frac{\phi_n(\omega)}{\left(\sum_{j=1}^{N}\alpha_j^2\right)\Phi_x(\omega)}} \tag{89}$$

of the cosine term in equation (82) provides some insight into this more rapid decrease. Recall that $B_N(\omega)$ is a coefficient of $\cos\omega\tau$ in the logarithmic amplitude spectra before the final transformation for computing the cepstrum.

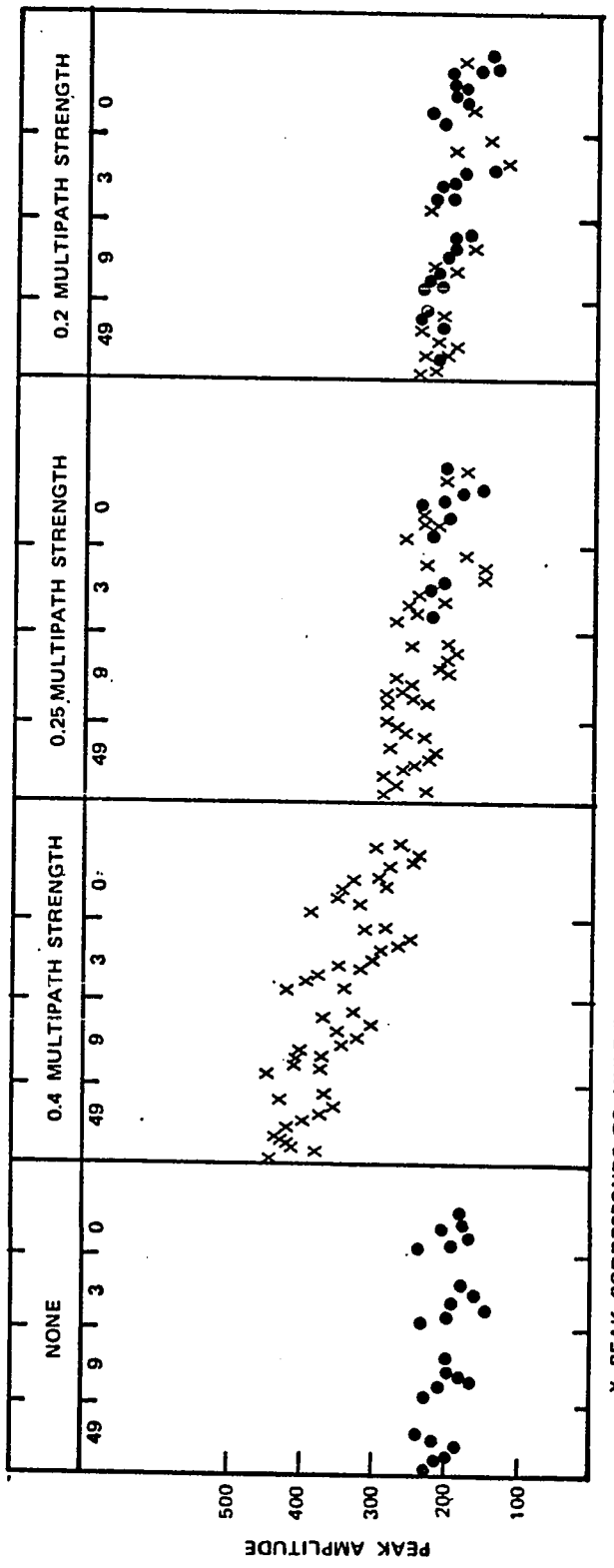

Figure 29. Peak Cepstrum for Various Targets, Multipath Strengths and Signal-to-Noise Ratios with Bionic Pulse.

The height of the cepstral peak depends on the portion of the spectrum that has a large value. The shape of the bionic spectrum, combined with its lower mean magnitude, reduce the value of $B(\omega)$. The lower magnitude of the bionic spectrum results from the shape of the bionic waveform. Whereas the other waveforms are of nominally constant amplitude over the pulse length, the bionic is not. For comparison purposes, the peak power, rather than the average power, have been kept the same for each signal type. The lower total energy of the transmitted bionic pulse is reflected in the signal-to-noise ratios listed in Figures 24 and 25.

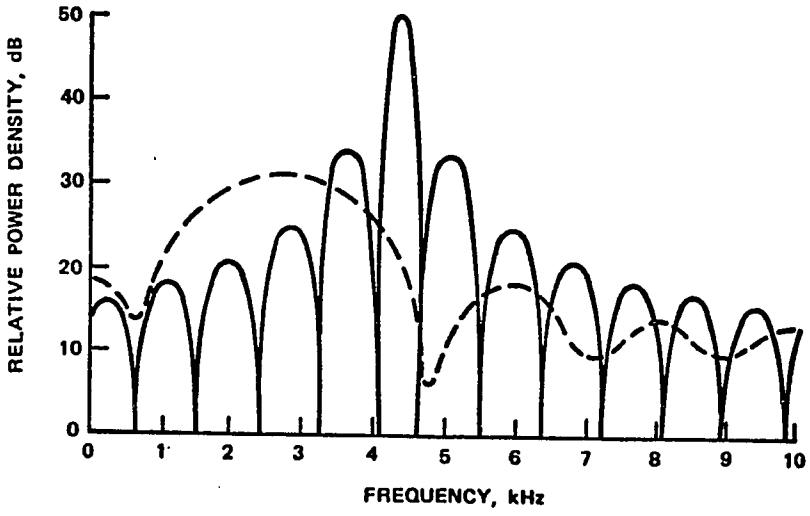

Figure 30. Bionic and Continuous Wave Spectra.

Figure 31 provides a summary of the detection probability and false alarm rate performance for multipath using the bionic signal. Note that the signal-to-noise ratios here again do not correspond to those in Figures 20 and 25.

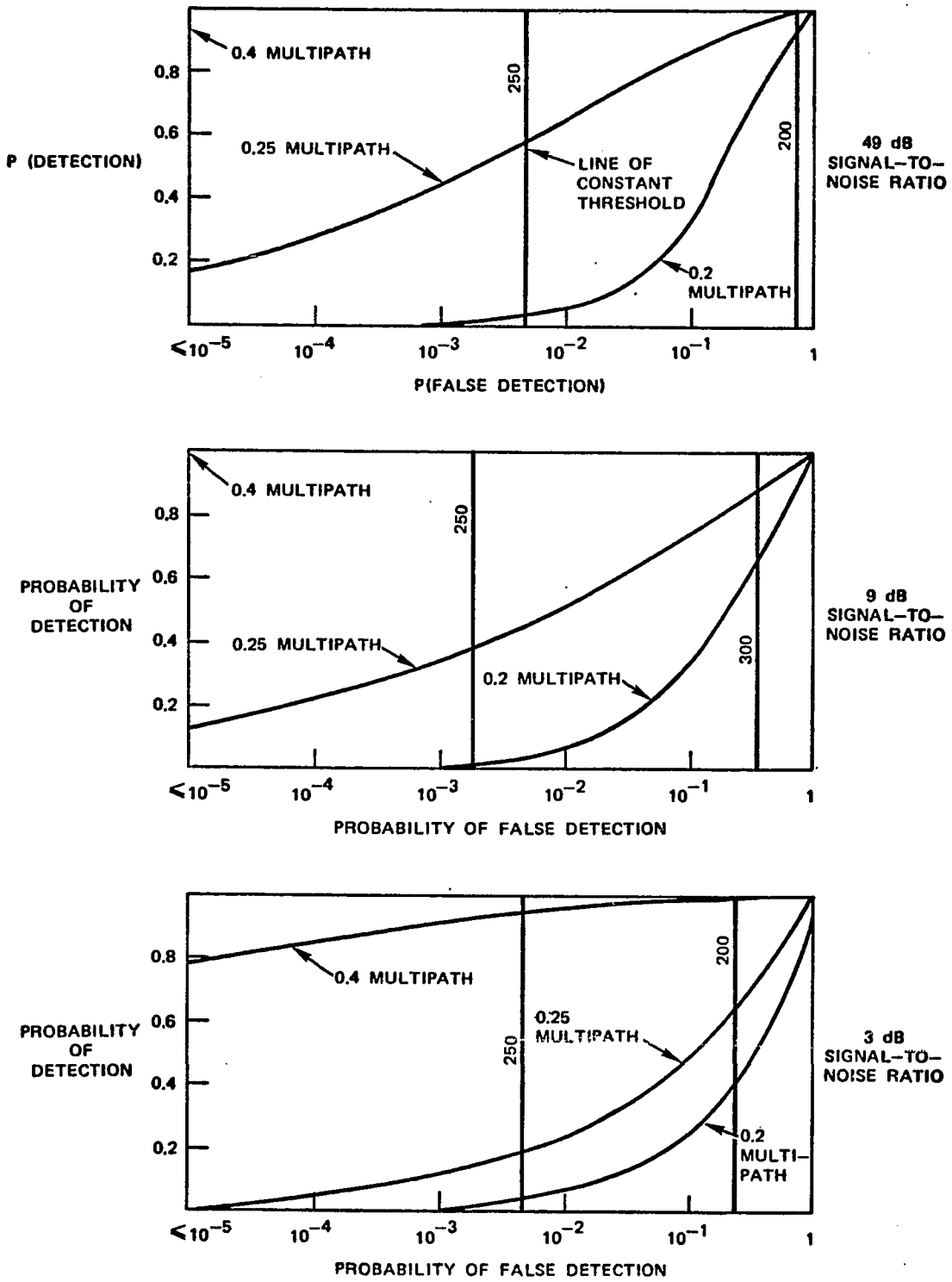

Figure 31. Detector Performance for Three Noise Levels and Three Multipath Strengths with a Bionic Waveform.

5.3 Linear Period Modulated Pulse

Like the bionic signals, a special case of linear period modulation, the linear period modulated signal is Doppler tolerant. These signals, in contrast to the linear frequency modulated signals, have a varying frequency such that the instantaneous period of the waveform changes linearly with time. The waveforms used are described by the equation

$$x(t) = \cos\left(\frac{2\pi}{b}\log\left(1+\frac{bt}{t_o}\right)\right) \tag{90}$$

The instantaneous frequency of this function is given by

$$f(t) = \frac{d}{dt}\left\{\frac{1}{b}\log\left(1+\frac{bt}{t_o}\right)\right\} = \frac{1}{t_o}\left\{\frac{1}{1+\frac{bt}{t_o}}\right\}, \tag{91}$$

so the period is

$$\tau(t) = \frac{1}{f(t)} = t_o+bt \tag{92}$$

which varies linearly with time. The particular signal used in the study is specified by

$$b = 0.00025 \qquad (93)$$
$$t_o = 0.1875$$

giving approximately the same bandwidth used for the frequency modulated

The performance at a 32 dB signal-to-noise ratio is shown in Figure 32 for a variety of multipath strengths. As expected from the similarity of their spectra, the linear period modulated signal and the linear frequency modulated signal perform almost identically, even for the small sample size obtained from the simulations.

A comparison of Figures 15, 24, and 32 provide little basis for preference of one signal type over another for the purpose of detecting multipath presence in the echo from a spatially distributed target. The bionic signal appears less desirable if the system is constrained by peak instantaneous power level.

5.4 Multiple Frequency Signatures

The multiple frequency signal provides a method for obtaining high resolution data without requiring wide instantaneous bandwidth and has received considerable attention in the military radar community in recent years.[5] The signal replaces a single wideband signal with a series of continuous wave pulses at regularly spaced frequencies. Each pulse's return is coherently sampled, phase corrected for relative target motion, and forms one complex value in the set of samples that form the signature. With the proper motion compensation, this set of values is the sampled Fourier transform of the target's time signature. The latter may then be recovered by an inverse Fourier

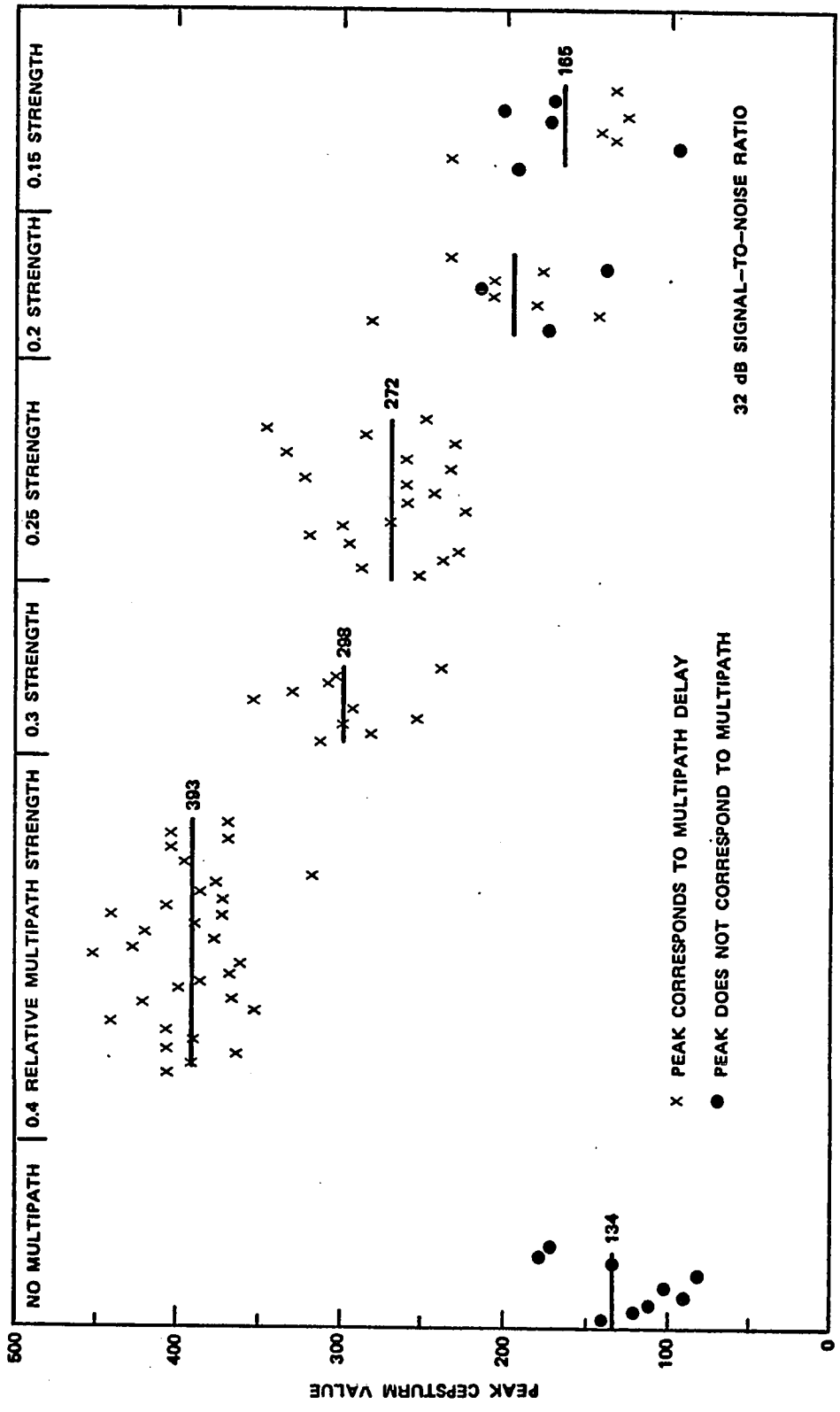

Figure 32. Peak Cepstrum Values for Various Multipath Strengths with Linear Period Modulated Pulse.

transformation. The resolution of the resultant time signature is inversely related to the total bandwidth of the series of transmitted pulses. This receiver process is then equivalent to discrete pulse compression or matched filtering. The pertinent relations are given below before discussing the cepstrum of this signal.

The group of signals, called a burst, covering the frequency range to be processed is shown schematically in Figure 32. Each pulse is of sufficient duration to illuminate an entire target at one time. For example, if targets of up to 1,000 feet in length are to be examined, the pulse length must be at least

$$\text{Pulse Length}_{\min} = \frac{2 \cdot 1000\text{ft.}}{c} \cong 2 \text{ microseconds},$$

where the radar case is considered and c is the speed of light,

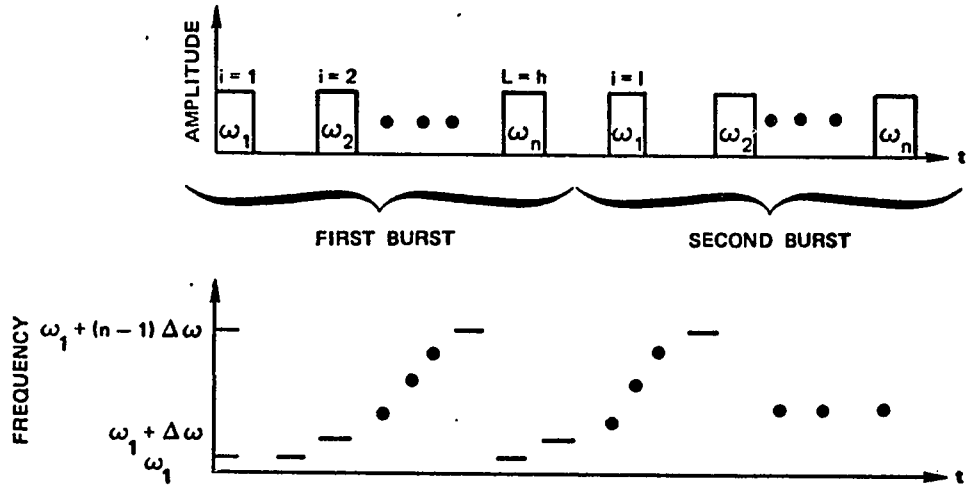

Figure 33. Amplitude and Frequency of Multiple Frequency Bursts.

The frequencies are given by

$$\omega_i = \omega_1 + (i-1)\Delta\omega \tag{94}$$

The resolultion of the resulting time signature is given by

$$r_s = \frac{\pi c}{(\omega_n - \omega_1)} \quad . \tag{95}$$

For a fixed target, the received signal at a time t_o in which a return from the entire target is present at the receiver is, using complex notation,

$$\begin{aligned} \chi_{t_o}(\omega) &= \sum_{i=1}^{N} a_i e^{j\omega\left(t_o - \frac{r_i}{c}\right)} \\ &= e^{j\omega t_c} \sum_{i=1}^{N} a_i e^{-j\omega\frac{r_i}{c}} \end{aligned} \tag{96}$$

where a_i is the cross section of the ith reflector on the target and r_i is twice the distance to that reflector. Replacing the discrete a_i by the continuous function a(t), where t = r/c, equation (96) becomes

$$X_{t_o}(\omega) = \int_o^{t_o} a(t)e^{-j\omega t}dt \quad , \tag{97}$$

or if the sampling is done after the signal has been shifted down to baseband

$$X_{1_{t_o}}(\omega') = \int_o^{t_o} a(t)e^{-j\omega t}dt \quad . \tag{98}$$

Hence the samples, x_i, $i = 1, \ldots$, approximate the Fourier transform of the high resolution time signature. This time signature may then be recovered by applying the inverse transform.

In the case of power cepstrum processing, however, the inverse transform is not required nor, for that matter, is coherent sampling. Since in cepstral processing the range profile has been used with the continuous signal only to obtain the amplitude spectrum, there is no purpose in calculating the range profile here. The measured values themselves provide the spectrum. Taking the logarithm of the sample pair's magnitude and then the transform of the resulting sequence provides the cepstrum of the corresponding profile.

The relationship corresponding to equation (2) is then

$$C_{MFS}(t) = F\{\log(G(k))\} \tag{99}$$

where

$$G(k) = |I(k)+jQ(k)| \tag{100}$$

with (I(k), Q(k)) the quadrature sample pair at the kth frequency in the burst.

A typical multiple frequency logarithmic amplitude is shown in Figure 34. Note that there is no net variation in the amplitude across the spectrum as there was due to the envelope of the pulsed signal types.

Before examining the cepstrum results, an additional processing step needs to be discussed. In the previous signal types, all multipath delays employed in the model were exact multiples of the sampling period. This was done for convenience in data reduction. If it had not been done, however, in the two multipath cases the same results could have been obtained by a very simple interpolation. When a peak in the cepstrum produces a local maximum that is spread over two adjacent delay values this interpolation must be employed. Since a rectangular window has been used throughout, the interpolation process is as follows.

If A were the height of the cepstral peak if it had coincided with a sample time, and a_1 and a_2 are the actual computed values of the cepstrum at times t_1 and t_2, as shown in Figure 35, then the values a_1, a_2, and A are related by

$$A \frac{\sin x}{x} = a_1; \; x = \frac{t-t_1}{t_2-t_1}\pi \tag{101}$$

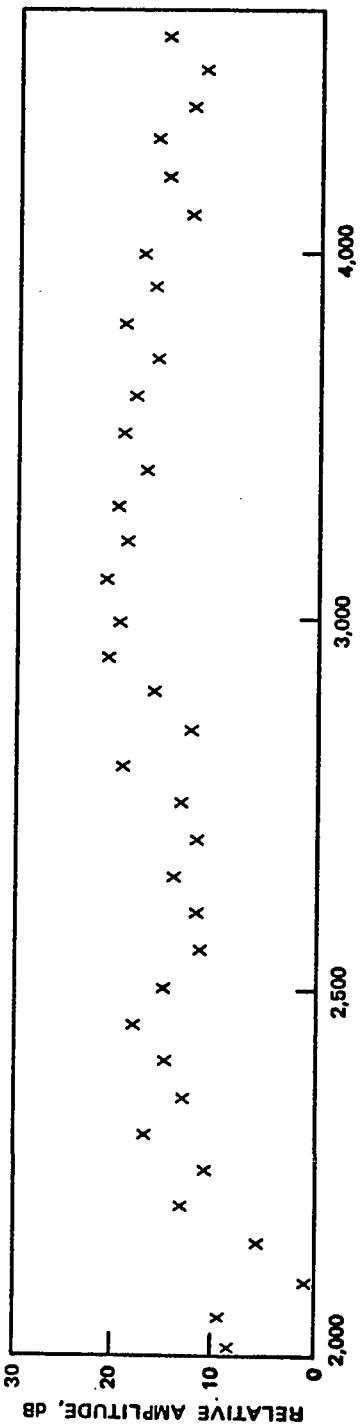

Figure 34. Typical Multiple Frequency Signature.

and

$$A\frac{\sin(\pi-x)}{(\pi-x)} = a_2 \tag{102}$$

where x is the delay of the actual peak after time t_1. Then noting that

$$\sin(\pi-x) = \sin x \tag{103}$$

equations (97) and (98) may be combined to give

$$x = \frac{\pi a_2}{a_1+a_2} \quad . \tag{104}$$

Substituting this value for x into equation (101),

$$A = \frac{x}{\sin x}a_1 = \frac{\dfrac{\pi a_1 a_2}{a_1+a_2}}{\sin\dfrac{\pi a_2}{a_1+a_2}} \quad . \tag{105}$$

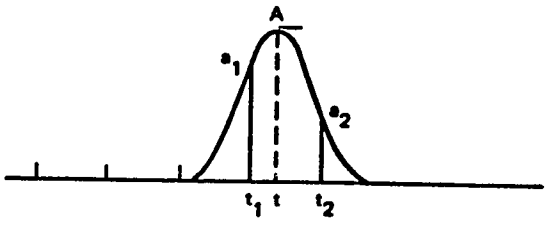

Figure 35. Sampling Off Peak Amplitude.

For computational efficiency, the interpolated value need be calculated only when the a_1 or a_2 is above some threshold.

Sampling cases with delay not coinciding with the sampling interval were computed in a variety of continuous signal cases to insure that the results obtained using equation (105) were, indeed, consistent with the more restricted delay times.

In the multiple frequency case, the cepstrum sampling interval did not coincide with multipath delays, which were kept the same as for the earlier signal types. As a consequence, the interpolation scheme has been employed to provide the peak values for the multiple frequency cepstrum results shown in Figure 36.

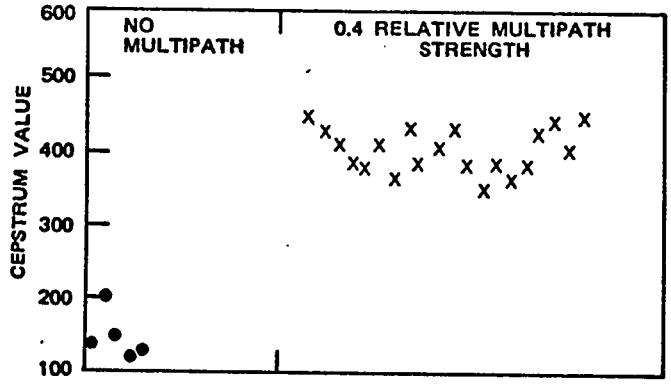

Figure 36. Peak Cepstrum Values with Multiple Frequency Signature.

The amplitudes for both the single path and the multipath cases are consistent with the continuous signal types previously examined. A straightforward advantage of the multiple frequency signature that has not been examined with simulations is its perfomance with noise.

Since the transmitted signal is longer than the target, there is a period of time during which the echo signal at the receiver is a uniform, non-varying sinusoid, the summation of the individual reflected sinusoids from each of the target reflectors. It is during this period that the quadrature pair is taken. In the absence of noise, a sample pair taken at any time during this sinusoidal return will result in the sample amplitude measurement. (Recall that phase was not used in the cepstrum calculation.) As a result, in the presence of noise, the effective signal-to-noise ratio may be improved by averaging multiple sample pairs at intervals longer than the noise decorrelation time. Thus performance may be improved by extending the pulse length without increased signal amplitude. The signal energy would be increased in this case giving, therefore, a higher signal-to-noise ratio.

It should be also noted that since each pulse is translated to baseband before sampling, a narrowband filter may be applied before samples are taken. This adds the benefits of easily implemented matched filtering. In this case, the previously suggested scheme of multiple sampling would not be required. It would be interesting, in future study, to include matched filtering with the continuous wideband signals, as well, before cepstral processing. The purpose here, however, has been to investigate the performance of the cepstral processing by itself.

5.5 Summary

The cepstrum is seen to successfully detect multipath with each of the signal types considered. As noted previously, with the constraint of peak transmitted power, the bionic signal performs most poorly. The multiple or

stepped frequency signal provides a means to use the cepstrum with less computation.

Regardless of signal type, the detectability of the multipath through the cepstrum is dependent on the strength of the multipath. The lower limit of detectability is determined by the height of target related cepstral peaks or noise depending on the noise level. It is likely that actual target signature cepstra from real targets will be lower than those computed here as a result of a much larger number of actual reflectors. A significant reduction in the maximum of actual (single path) signature cepstra would reduce the problem to one more closely paralleling previous studies with a simple signal in a one-way channel.

The varying multipath strengths detectable at different signal-to-noise ratios suggest the usefulness of using a variable detection level for multipath that is determined by the ambient noise level. This might parallel methods currently used to provide a constant false alarm rate (CFAR) in target detection problems.[6]

CHAPTER NOTES

1. D. P. Skinner, R. A. Altes, and J. D. Jones, "Broadband Target Classification Using a Bionic Sonar," JASA 62(5) (1977): 1239-1245.

2. R. A. Altes and R. A. Reese, "Doppler Tolerant Classification of Distributed Targets--a Bionic Sonar," IEEE Trans. Aerospace Electronics Systems AES-11 (1975): 708-723.

3. R. A. Altes, "Sonar for Generalized Target Location Systems," JASA 59 (1976): 97-105.

4. R. A. Altes and E. L. Titlebaum, "Bat Signals as Optimally Doppler Tolerant Waveform," JASA 48 (1970): 1014-1020.

5. M. Prickett and C. C. Chen, "Principles of Inverse Synthetic Aperture Radar (ISAR) Imaging," IEEE EASCON Record (1980).

6. Eli Brookner, Radar Technology, pp. 55-56.

CHAPTER 6

CORRECTION FOR MULTIPATH IN TARGET SPECTRAL ESTIMATES

The previous chapters have dealt with the performance of the cepstrum with various signal types in detecting multipath in the radar or sonar signature of a target. As indicated in Chapter 1, one motivation for this interest is that portions of the Fourier transforms of target echoes are being used as features upon which automatic ship classification algorithms are based. Consequently, the interest in multipath is two-fold. First, it is useful to know when multipath is present so that its effects on the performance of classification algorithms can be taken into account. Secondly, it would be extremely valuable to remove the effects of multipath on the received spectrum to reduce or eliminate its effects on classification performance.

The present chapter is devoted to the later question. First, the use of the cepstrum to obtain the spectrum of the uncorrupted target signature is discussed and examined through simulation and theory. A short discussion follows treating the more involved recovery of the spectrum of the detected signature envelope.

6.1 Effects of Multipath on Signature Spectra

The introduction of multiple, delayed replicas of a received signal such as a target signature produces considerable change in the spectrum of that signature. In particular, the differences between the spectra of signatures with

and without multipath present are often large enough to somewhat obscure the differences between the spectra of the signatures of different targets. Three cases illustrating the differences in the detected signals' spectra are shown in Figures 37 through 39. Only the first 20 values are shown since a subset of these is frequently used for automatic classification. The differences carry similarly through the entire spectrum. Note that these plots are logarithmic to allow visual comparison of the spectra across the entire band displayed.

As the cases plotted in the figures indicate, the magnitude of the multipath effects cannot be predicted from the magnitude of the multipath alone. This factor along with the delay of the multipath arrival and the characteristics of the target combine to determine this magnitude.

In the case of the undetected signal, the effects of the multipath are similar. Examples appear in the following section. Again, the differences in spectra that result from the multipath are larger than those differences existing between different targets. This provides the motivation for the signal spectra recovery method described in the next section.

6.2 Recovery of the Target Signature Spectra

Equation (5), repeated below, indicates the effect of multipath on the power spectrum of a target signature

$$\Phi_Z(\omega) = \Phi(\omega)(1+\alpha^2+2\alpha\cos\omega\tau) \tag{5}$$

where $\Phi(\omega)$ was the signature spectrum, α the multipath amplitude, and τ the multipath delay. The multipath adds sinusoidal modulation to the original spectrum.

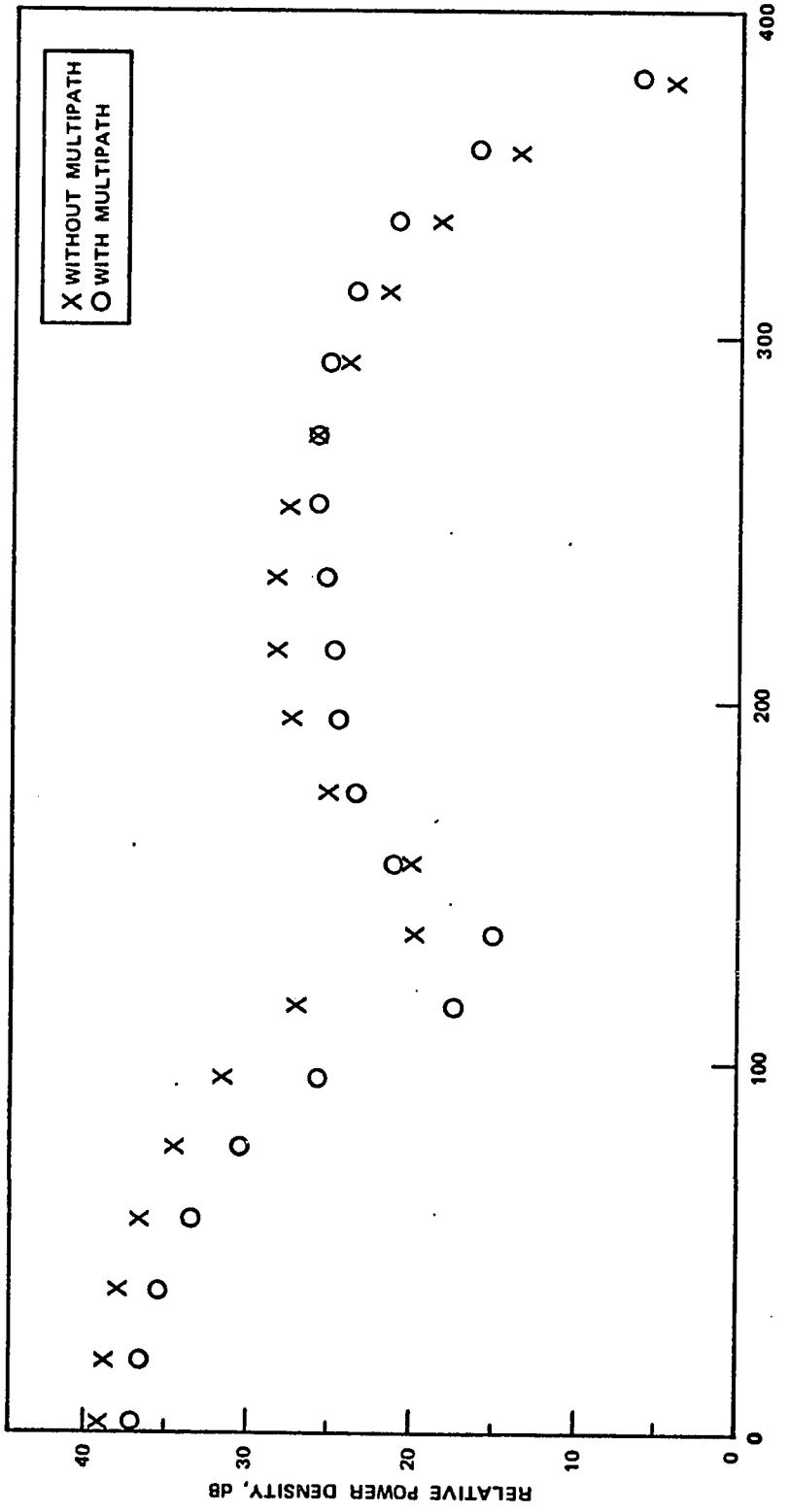

Figure 37. Example of Envelope Spectrum with and without Multipath
Multipath Strength = .4, 36 dB Signal-to-Noise Ratio.

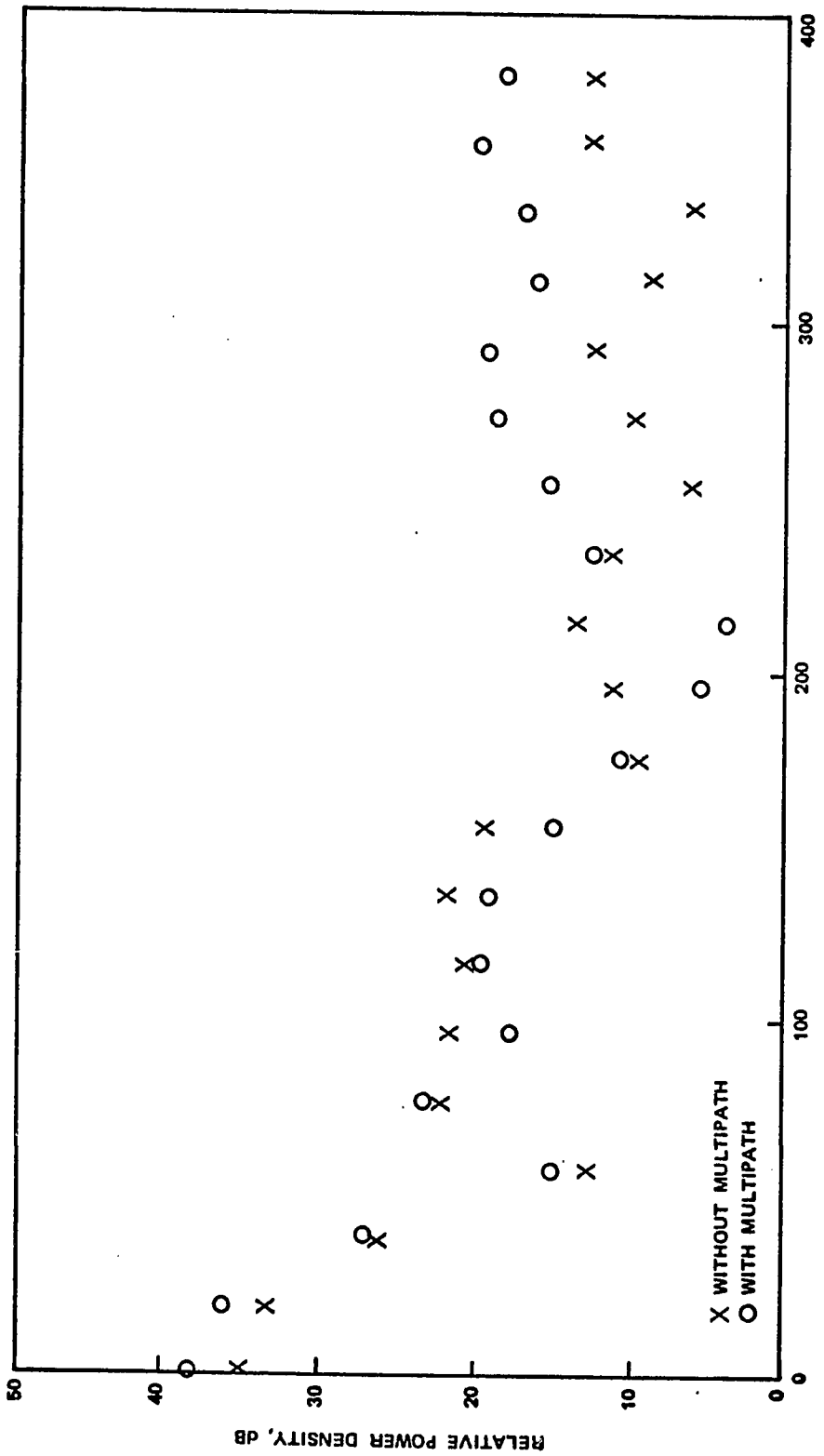

Figure 38. Second Example of Envelope Spectrum with and without Multipath
Multipath Strength = .4, 36 dB Signal-to-Noise Ratio.

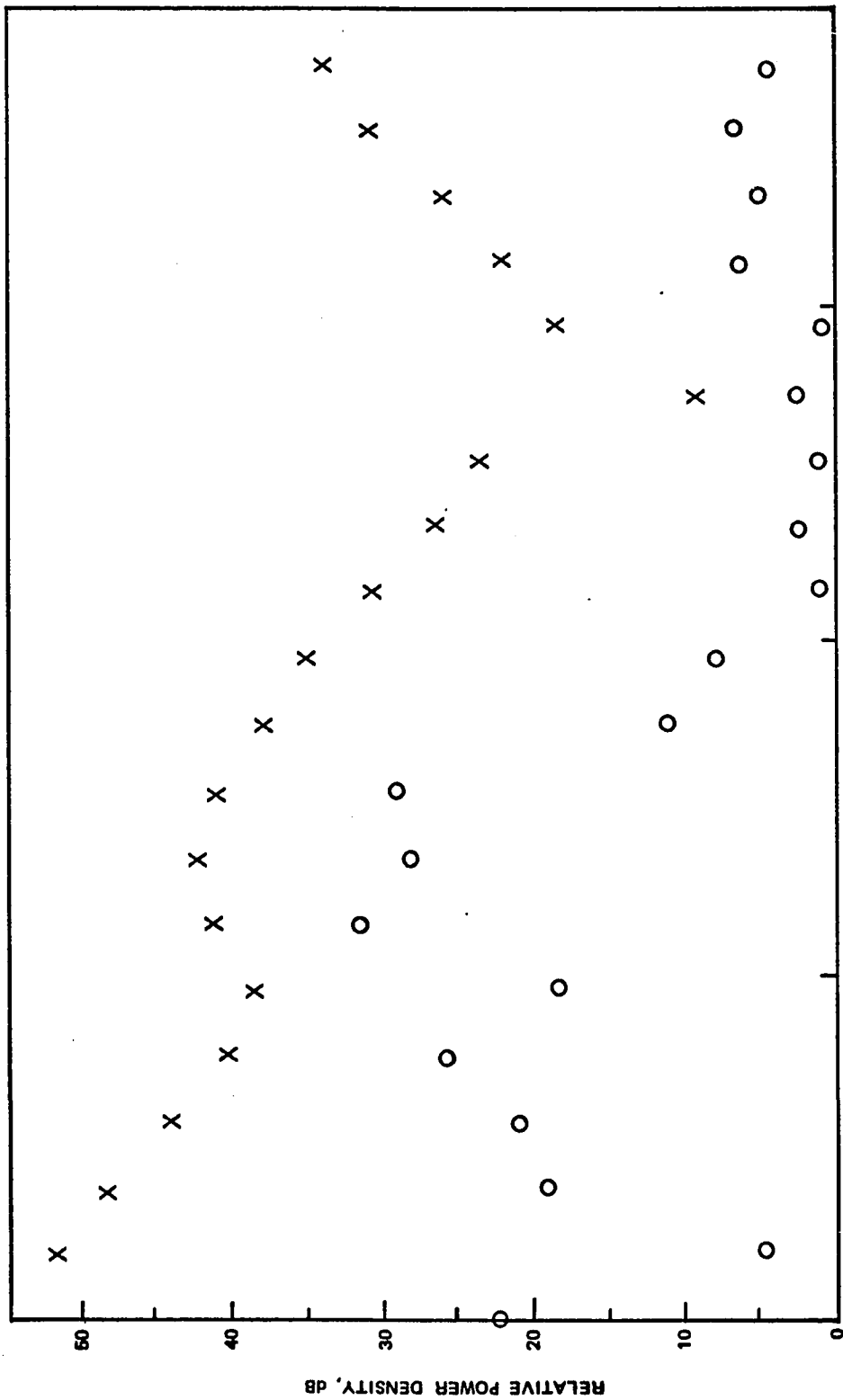

Figure 39. Third Example of Envelope Spectrum with and without Multipath
Multipath Strength = .4, 36 dB Signal-to-Noise Ratio.

In the single multipath case it was shown that there are three arrivals, so the reflected signature becomes

$$z(t) = y(t)+2\alpha y(t-\tau)+\alpha^2 y(t-2\tau) \tag{106}$$

where α is now the relative one-way signal strength via the longer path and y(t) is the basic target signature without multipath. In this case, the signature power spectrum becomes, from equation (22)

$$\begin{aligned}\Phi_z(\omega) &= \Phi(\omega)(1+4\alpha^2+\alpha^4+2\alpha\cos\omega\tau+\alpha^2\cos\omega(2\tau)+2\alpha^3\cos\omega\tau) \\ &= \Phi(\omega)(1+4\alpha^2+\alpha^4+\{2\alpha+2\alpha^3\}\cos\omega\tau+\alpha^2\cos\omega(2\tau)\end{aligned} \tag{107}$$

This provides one means of recovering the desired target signature spectrum. If the multipath parameters τ and α are estimated, $\Phi(\omega)$ can be recovered by dividing the measured spectral values, $\Phi_z(\omega)$, by the factor in equation (107) giving

$$\Phi(\omega) = \frac{\Phi_z(\omega)}{(1+4\alpha^2+\alpha^4+(2\alpha+2\alpha^3)\cos\omega\tau+\alpha^2\cos\omega\tau)} \tag{108}$$

Use of the cepstrum itself provides an alternative method of recovery. Since the knowledge of the multipath presence, amplitude, and delay comes from the peaks in the power cepstrum, removing these peaks in the cepstrum has the same effect as the direct spectrum adjustments given in equation (108). Recall,

this was one of the filtering methods discussed with the complex cepstrum in Chapter 2. Since it is only the signature power spectrum that is desired here, rather than the original signal itself, this filtering may be done with the power cepstrum.

Proceeding from equation (108), the cepstrum is calculated for this specific signal by taking the logarithm of $\Phi_z(\omega)$ and expanding the log $(1 + \alpha)$ term, where α has absolute value less than one, in the argument of the logarithm.

$$\log\Phi_z(\omega) = \log\Phi(\omega)+\log(1+4\alpha^2+\alpha^4) + \log\left[1+\frac{2\alpha^2+3\alpha^3}{1+4\alpha^2+\alpha^4}\cos\omega\tau+\frac{\alpha^2}{1+4\alpha^2+\alpha^4}\cos 2\omega\tau\right] \tag{109}$$

$$\log\Phi_z(\omega) \approx \log\Phi(\omega)+\log(1+4\alpha^2+\alpha^4) + g(\omega\tau)-\frac{1}{2}g^2(\omega\tau)+\frac{1}{3}g^3(\omega\tau)- \cdots \tag{110}$$

where

$$g(\omega\tau) = \frac{2\alpha+2\alpha^3}{1+4\alpha^2+\alpha^4}\cos\omega\tau+\frac{\alpha^2}{1+4\alpha^2+\alpha^4}\cos 2\omega\tau \quad . \tag{111}$$

Then after some manipulation and including terms only through $\cos 3\omega\tau$, equation (110) becomes

$$\log\Phi_z(\omega) \simeq \log\Phi(\omega)+\log(1+4\alpha^2+\alpha^4)+\frac{1}{2}\left\{\left(\frac{2\alpha+2\alpha^3}{1+4\alpha^2+\alpha^4}\right)^2+\left(\frac{\alpha^2}{1+4\alpha^2+\alpha^4}\right)^2\right\}$$
$$+\left\{\frac{2\alpha^3+2\alpha^5}{(1+4\alpha^2+\alpha^4)^2}+\frac{2\alpha+2\alpha^3}{1+4\alpha^2+\alpha^4}\right\}\cos\omega\tau \qquad (112)$$
$$+\left\{\frac{\alpha^2}{1+4\alpha^2+\alpha^4}-\frac{1}{2}\left(\frac{2\alpha+2\alpha^3}{1+4\alpha^2+\alpha^4}\right)^2\right\}\cos 2\omega\tau+\frac{2\alpha^3+2\alpha^5}{(1+4\alpha^2+\alpha^4)}\cos 3\omega\tau+\cdots$$

The cepstrum is then

$$C(t) = F\log\Phi(\omega)+a_o\delta(t)+a_1\delta(t-\tau)$$
$$+ a_1\delta(t+\tau)+a_2\delta(t-2\tau)+a_2\delta(t+2\tau)+\cdots \qquad (113)$$

where a_o, a_1, . . . a_n, are the coefficients of the cosine terms, cos , in equation (107).

The desired power spectrum may then be recovered by removing the peaks at zero, , and its multiples and taking the inverse transform and exponentiating yielding

$$\hat{\Phi}(\omega) \cong \Phi(\omega) \qquad (114)$$

The process actually employed was somewhat modified in that the zero peak was not adjusted. Since the target cepstrums themselves had considerable amplitude at zero, better estimates of the target spectrum were obtained leaving this value unchanged. The peaks at τ , 2τ, and 3τ were removed and replaced by the average of the adjacent values of the cepstrum.

Figure 40 shows the results obtained in one case for the central portion of the spectrum. The deviation from the single path target signature spectrum is substantially reduced. The improvement is summarized in Table 3. A .4 relative multipath strength was used in each case reported. Detection and location of the multipath arrival was included in the algorithm. The differences in the first ten spectral values, starting with the transmitted center frequency, are listed along with their average and the average differences over the entire spectrum.

	Case 1 (2.7 msec)		Case 2(5.5 msec)		Case 3 (3.6 msec)		Case 4 (3.3 ms)	
	Multipath -Single	Corrected -Single	MP- -Single	Corrected -Single	MP- -Single	Corrected -Single	MP -Single	Correct -Single
f_1	0.63	0.12	0.88	0.06	0.21	0.04	0.75	0.04
f_2	0.54	0.00	0.28	0.04	.045	0.01	0.31	0.06
f_3	0.41	0.09	0.24	0.02	0.60	0.02	0.08	0.00
f_4	0.22	0.10	0.56	0.06	0.67	0.04	0.37	0.05
f_5	0.01	0.04	0.67	0.01	0.65	0.04	0.56	0.04
f_6	0.30	0.01	0.60	0.05	0.56	0.01	0.66	0.02
f_7	0.61	0.01	0.33	0.04	0.38	0.02	0.67	0.01
f_8	0.89	0.05	0.15	0.03	0.12	0.04	0.58	0.04
f_9	1.02	0.10	0.77	0.05	0.19	0.04	0.41	0.05
f_{10}	0.92	0.06	1.00	0.07	0.61	0.10	0.13	0.00
f_1-f_{10} AVERAGE	0.55	0.058	0.38	0.04	0.42	0.04	0.45	0.03
AVERAGE (Whole Spectrum)	0.51	0.08	0.51	0.05	0.51	0.16	0.51	0.04

Table 3. Power Spectrum Correction with Power Cepstrum.

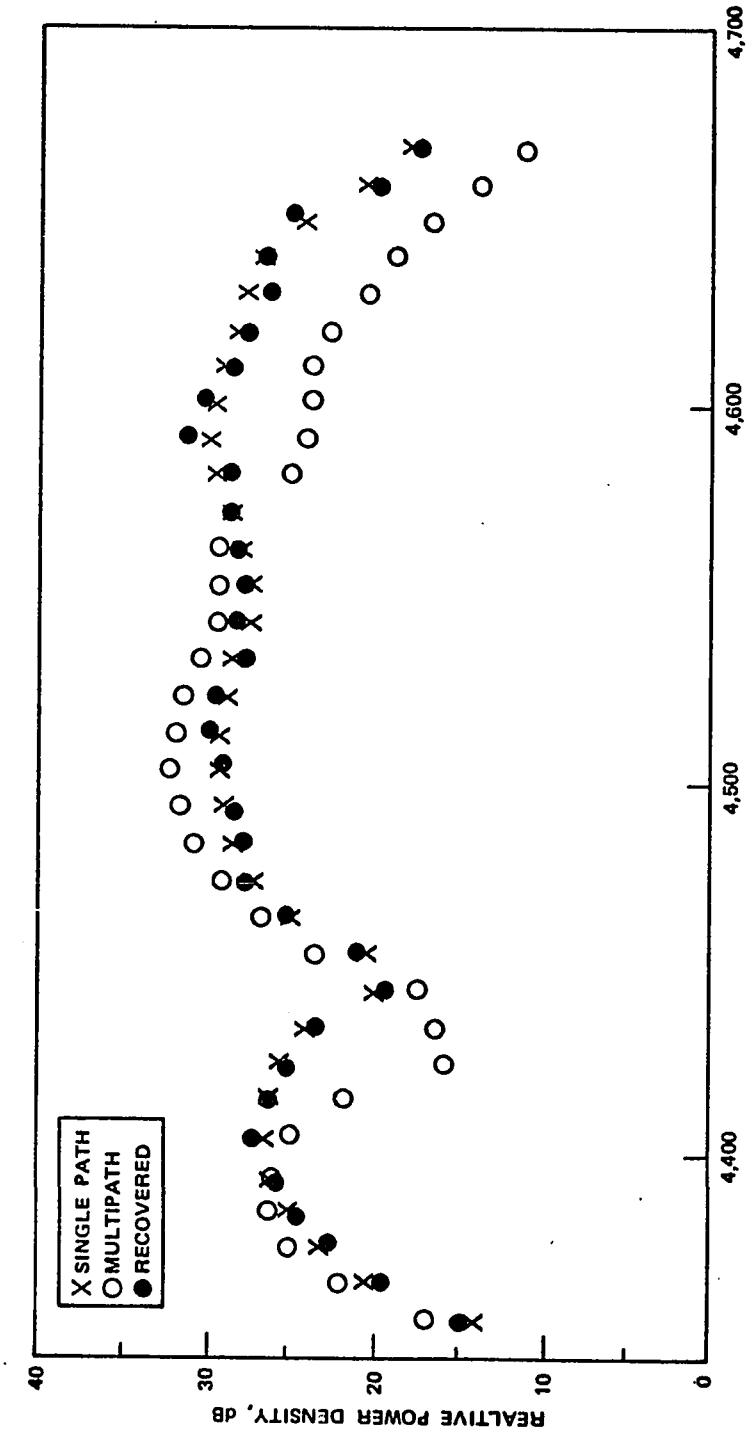

Figure 40. Signature Spectra with and without Multipath and with Multipath Corrections Applied.

The remaining differences result from several sources. First, only the first three peaks were removed. The error produced by higher multiples is probably small. This is suspected due to the lack of any high peaks in this region. The more significant error is introduced by replacing the peaks by the average of the adjacent values. Since the cepstrum of the basic signature often has appreciable value in the vicinity of the multipath spikes, there is no reason to expect the replacement value to be correct. There appears to be no simple way to estimate the correct value of the target signature cepstrum at that point. Also, it should be noted that removal of these peaks has no effect on the contributions due to noise.

One possible means of determining the correct replacement cepstrum values at the delay times is suggested by the derivation. Equation (108) provides the necessary relation between the heights of peaks at the multiples of τ. Thus the value of α in equation (112) could be estimated on the basis of this relation and the proper portion could be substracted from each τ-related peak of the cepstrum. This method was not examined in the simulation study.

6.3 Recovery of the Spectra of the Target Signature Envelopes

Recovery of the spectrum of the detected target signature is more involved and requires starting with the undetected signal. As discussed in Chapter 2, the complex cepstrum may be computed and adjusted to remove multipath contributions in the same manner described for the power cepstrum in the previous section. The procedure would then be reversed to obtain the desired time signature. The detected signature spectrum would next be obtained by standard methods.

Implementation of this technique is not straightforward, however. Recall that to obtain continuous phase in taking the complex logarithm of the transform of the original signal, it is necessary to perform phase unwrapping. In the case of a strictly time limited signal, such as considered here, there will always be zero crossings in the amplitude of the transform. These produce unremovable discontinuities in the phase of the complex logarithm. Thus, although a number of algorithms exist to calculate the complex cepstrum[1], they cannot be applied in this case because of these discontinuities in the phase. Standard techniques exist for avoiding this problem[2]. These have not been implemented in the present work, but would be expected to produce improvements comparable to those reported in section 6.2.

CHAPTER NOTES

1. J. M. Tribolet and T. F. Quatieri, "Computation of the Complex Cepstrum," Programs for Digital Signal Processing, ed. IEEE Digital Signal Processing Committee (New York: Wiley, 1979), pp. 7.1-1-7.1-11.

2. Alan V. Oppenheim and Ronald W. Schafer, Digital Signal Processing, pp. 506-507.

CHAPTER 7

CONCLUSION

7.1 Summary

This work has examined the application of the cepstrum to the particular problem of distinguishing between multiple arrivals of a known signal caused by multipath from those caused by the multiple reflector nature of a sonar or radar target. It was shown that with sufficient strength in the multipath arrival, the presence of the multipath can be reliably detected and its arrival time accurately estimated. A computationally efficient means for removing the effects of the multipath on the signature spectrum was demonstrated.

The discussion and derivations of Chapter 2 were a review of earlier work with the cepstrum and were provided as background, as well as motivation for the analysis that followed. The analysis and conclusions of Chapter 3 are new and provide one of the major contributions of this work. The derived differences in the cepstrum of the target echo and the target echo with multipath, provide the basis on which the simulations results can be interpreted. It was shown that the power spectrum provides a means for effectively making use of the differences between the effects of multiple reflectors and the effects of a small number of multipaths on the received signal. It was additionally shown how to make effective use of the known part of the signal, the transmitted waveform, in the detection process.

Chapter 4 provided simulation and theoretical results concerning the performance of the power cepstrum for multipath detection as a function of

signal parameters and noise. The basic analysis of the cepstrum performance in noise was summarized from an earlier work. The analysis was extended to cover the cepstrum application under investigation and simulation results were provided to augment the analysis.

The results concerning detection thresholds are original and demonstrate the potential usefulness of the technique in the two path case. The effects of target motion were analyzed and simulated showing that the methods described were applicable in a nonstationary scenario. The earlier analysis concerning the differences between target and multipath cepstra were shown to indicate that the methods described will not be of great use if there are many multipaths.

Chapter 5 presented entirely new results. It provided the only known comparison of cepstrum performance with this range of signal types. It was shown that the height of the cepstrum due to multipath was essentially identical regardless of the signal type employed. The main differences were found in the effects of noise on multipath detection. The greater sensitivity of the bionic signal was noted and the potential insensitivity of the multiple frequency signal was discussed.

Chapter 6 showed the usefulness of the processing in removing the multipath effects on the measured spectrum of a target reflection. This is seen as the primary immediate application of the results obtained in this work.

It is believed that the simulated results that have been presented are conservative. It is expected that the more distributed nature of actual radar and sonar targets will produce lower cepstrum values than did those modeled in this study. The results obtained here indicate, themselves, the usefulness of the methods in analyzing the spectra of target reflections.

7.2 Suggested Areas for Further Study

The question raised in the preceding paragraph provides a starting point for further investigation. It would be very informative to examine the thresholds of Chapter 4 using actual radar or sonar data. It is suggested that such an investigation start by using real data without multipath and adding the multipath artificially. This would allow positive separation of the target and multipath effects on the cepstrum.

The area of the multiple frequency signature provides another avenue for fruitful investigation. The potential insensitivity to noise and countermeasures should be further investigated. Since this signal is not time limited in the sense of a short pulse, complex cepstrum analysis may be straightforward with this signal.

The additional technique suggested in Chapter 6 for separating the portion of an individual cepstrum value due to multipath from that resulting from the target merits investigation. It suggests itself as the most promising method to improve upon the methods presented in this work.

BIBLIOGRAPHY

Altes, R. A. 1976. "Sonar for Generalized Target Description and its Similarity to Animal Echo Location Systems." JASA 59:97-105.

Altes, R. A., and Reese, R. A. 1975. "Doppler Tolerant Classification of Distributed Targets--a Bionic Sonar." IEEE Trans. Aerospace Electronics Systems AES-11: 708-723.

Altes, R. A., and Titlebaum, E. L. 1970. "Bat Signals as Optimally Doppler Tolerant Waveforms." JASA 48:1014-1020.

Bogert, B., Healy, M., and Tukey, J. 1963. "The Quefrency Alanysis of Time Series for Echoes." Spectral Analysis, ed. M. Rosenblatt, pp. 209-243. New York: Wiley.

Brookner, E. 1977. Radar Technology. Dedham, Mass.: Artech House, Inc.

Brown, W. M., and Palerno, C. J. 1969. Random Processes, Communications, and Radar. New York: McGraw-Hill.

Burinton, R. S., May, D. C. 1970. Handbook of Probability and Statistics with Tables. New York: McGraw-Hill.

Clay, C. S., and Medwin, H. 1977. Acoustical Oceanography: Principles and Applications. New York: Wiley.

Conover, W. J. 1971. Practical Nonparametric Statistics. New York: Wiley.

Cook, C. E., and Bernfeld, M. 1967. Radar Signals. New York: Academic Press.

Ehrenberg, J. E., Ewart, T. E., and Morris, R. D. 1978. "Signal-Processing Techniques for Resolving Individual Pulses in a Multipath Signal." JASA 63(6):1861-1865.

Ewart, T. E., Ehrenberg, J. E., and Reynolds, S. A. 1978. "Observation of the Phase and Amplitude of Individual Fermat Paths in a Multipath Environment." JASA 63(6):1801-1808.

Franks, L. E. 1969. Signal Theory. Englewood Cliffs, New Jersey: Prentice-Hall, Inc.

Hassab, J. C., and Boucher, R. 1976. "A Probabilistic Analysis of Time Delay Extraction by the Cepstrum in Stationary Gaussian Noise." IEEE Trans. on Information Theory 22(4):444-453.

_____. 1979. "Optimum Estimation of Time Delay by a Generalized Correlator." IEEE Trans. on Acoustics, Speech, and Signal Processing ASSP-27(4):373-388.

Hodgkiss, W. S. 1978. "Detection of LPM Signals with Estimation of their Velocity and Time of Arrival." JASA 64(1):177-180.

Jenkins, G. M., and Watts, D. G. 1968. Spectral Analysis and its Applications. San Francisco: Holden-Day.

Kadota, T. T., and Romain, D. M. 1977. "Optimum Detection of Gaussian Signal Fields in the Multipath-Anisotropic Noise Environment and Numerical Evaluation of Detection Probabilities." IEEE Trans. on Information Theory IT-23(2):167-178.

Kemerait, R. C., and Childers, P. G. 1972. "Signal Detection and Extraction by Cepstrum Techniques." IEEE Trans. on Information Theory 18(6):745-756.

Kleijnen, J. P. C. 1974. Statistical Techniques in Simulation. New York: Marcel Dekker, Inc.

Koopmans, L. H. 1974. The Spectral Analysis of Time Series. New York: Academic Press.

Kroszczynski, J. J. 1969. "Pulse Compression by Means of Linear-Period Modulation." Proceedings of IEEE 57(7):1260-1266.

Mangano, D. T. 1980. "A Comparison of Three Schemes for Filtering Signals which have Propogated through a Random Multipath Medium." JASA 67(3):842-852.

Meyer, D. P., and Mayer, H. A. 1973. Radar Target Detection. New York: Academic Press.

Mikhalevsky, P. N. 1980. "Crossing Rate Statistics for Finite Bandwidth or Modulated Multipath Signals." JASA 67(3):812-815.

Mood, A. M., Graybill, F. A., and Boes, D. C. 1974. Introduction to the Theory of Statistics. 3rd ed. New York: McGraw-Hill.

Nilsson, N. J. 1961. "On the Optimum Range Resolution of Radar Signals in Noise." IRE Trans. on Information Theory IT-11:245-253.

Oppenheim, A. V., ed. 1978. Applications of Digital Signal Processing. Englewood Cliffs, New Jersey: Prentice-Hall, Inc.

Oppenheim, A. V., and Schafer, R. W. 1975. Digital Signal Processing, Englewood Cliffs, New Jersey: Prentice-Hall, Inc.

Papoulis, A. 1965. Probability, Random Variables, and Stochastic Processes. New York: McGraw-Hill.

_____. 1977. Signal Analysis. New York: McGraw-Hill.

Prickett, M. J., and Chen, C. C. Sept., 1980. "Principles of Inverse Synthetic Aperture Radar (ISAR) Imaging." IEEE EAASCON Record, Aerospace and Electronics Systems Society.

Root, W. L. 1962. "Radar Resolution of Closely Spaced Targets." IRE Trans. on Military Electronics MIL-197-204.

Sandhu, G. S., and Audeh, N. F. 1980. "Measurement of Closely Spaced Point Targets." IEEE Trans. on Aerospace and Electronics Systems AES-16(2):138-143.

Schwartz, M. 1970. Information, Transmission, Modulation, and Noise. New York: McGraw-Hill.

Skinner, D. P., Altes, R. A., and Jones, J. D. 1977. "Broadband Target Classification Using a Bionic Sonar." JASA 62(5):1239-1245.

Skolnik, M. 1980. Introduction to Radar Systems. New York: McGraw-Hill.

Turin, G. L. 1980. "Introduction to Spread-Spectrum Antimultipath Techniques and their Application to Urban Digital Radio." Proceedings of IEEE 68(3):328-352.

Urick, R. J. 1975. Principles of Underwater Sound. New York: McGraw-Hill.

Van Trees, H. L. 1968. Detection, Estimation and Modulation Theory. Part I. New York: Wiley.

VITA

Gerard Royal Steiner was born in Hampton, Virginia on May 28, 1943, the son of Mr. and Mrs. Roy Steiner. He graduated from Hampton High School, Hampton, Virginia in 1961. He received a Bachelor of Science (1970) and Master of Science (1971) in Physical Oceanography from the University of Washington, Seattle. He is currently employed at the Naval Weapons Center, China Lake, California.